

PRELIMINARY ANALYSIS OF PHOSPHATE NODULES IN
THE WOODFORD SHALE, LATE DEVONIAN – EARLY
MISSISSIPPIAN, SOUTHERN OKLAHOMA

By

DARWIN R. BOARDMAN III

Bachelor of Science in Geology

Oklahoma State University

Stillwater, Oklahoma

2009

Submitted to the Faculty of the
Graduate College of the
Oklahoma State University
in partial fulfillment of
the requirements for
the Degree of
MASTERS IN SCIENCE
May 2012

PRELIMINARY ANALYSIS OF PHOSPHATE NODULES IN
THE WOODFORD SHALE, LATE DEVONIAN – EARLY
MISSISSIPPIAN, SOUTHERN OKLAHOMA

Thesis Approved:

Dr. James Puckette

Thesis Adviser

Dr. Darwin Boardman II

Dr. Mary Hileman

Dr. Sheryl A. Tucker

Dean of the Graduate College

TABLE OF CONTENTS

Acknowledgements.....	i
Table of Contents.....	ii
List of Figures.....	iv
Abstract.....	1
Chapter	Page
I. INTRODUCTION.....	2
1.1. Geologic Setting.....	2
1.2. Methods.....	7
1.3.1. Sampling From Outcrop.....	7
1.3.2. Total Organic Carbon.....	13
1.3.3. X-Ray Fluorescence.....	13
1.3.4. Thin-Sections.....	14
1.4. Literature Review.....	14
II. PHOSPHATE NODULES.....	17
2.1. Phosphate Occurrences in the Woodford Shale.....	17
2.2. Modern Phosphates Nodules.....	19
2.3. Interest of Phosphate Nodules.....	20
2.4. Geochemistry to Understand Nodule Formation.....	21
III. FINDINGS.....	24
IV. DISCUSSION.....	30
4.1. X Ray Fluorescence Data.....	33
4.2. Thin Sections.....	34
4.3. Phosphate Nodules.....	34
V. Conclusions.....	36
References.....	38

Appendix A.....	40
Appendix B.....	42
Appendix C.....	55

LIST OF FIGURES

Figure	Page
1 Stratigraphic Nomenclature.....	6
2 Late Devonian Reconstruction of North America.....	8
3 Geographic Location of Study Areas.....	9
4 McAlister Cemetery Locality.....	10
5 Phosphate Nodules Insitu.....	11
6 I-35 North Locality.....	12
7 Upwelling Zone Model.....	18
8 Elemental Trends of Type A Nodule.....	25
9 Elemental Trends of Type B Nodule.....	26
10 Elemental Trends of Type C Nodule.....	27
11 Thin Section of Type A Nodule.....	28
12 Thin Section of Type C Nodule.....	28
13 Morphology Summary.....	29
14 Insitu Phosphate Nodules in Host Shale.....	31
15 Upwelling Model with Interpreted Locality Environments.....	33

ABSTRACT

The Woodford Shale is an organic-rich, siliceous marine shale with cherty beds and phosphate nodules. Phosphate nodules are a well-known feature of the Woodford Shale that deserves further scrutiny to explain their source, growth and abundance. Geochemical and petrographical analysis of the interior of phosphate nodules as well as the encasing beds was conducted to provide insight into their genesis. Because phosphate nodules grow very slowly, they inherit a chemical signature that reflects the changing chemistry of the surrounding water during their formation.

Nodules from two localities were collected and analyzed using thin section microscopy, x-ray fluorescence, x-ray diffraction and coulometric titration. Nodules were chosen based on their external morphology and internal structure. In addition, host shale was analyzed to compare the composition of nodules with the encasing beds. Highly structured nodules that are laminar or circular have a higher concentration of metals with abundance increasing in darker bands. Distribution of metals is symmetrical in highly ordered nodules and predictable. Metals distribution is more random in unstructured nodules that lack symmetrical banding. The decrease of certain metals and loss of structure in nodules is interpreted as representing less favorable conditions for phosphate growth. TOC is reduced in phosphate-bearing shale compared to beds without nodules lower in the section.

Radiolarians are especially well preserved in structured phosphate nodules. The opaline biogenic silica of radiolarian tests was relatively unstable, dissolved and re-precipitated as silica minerals including chalcedony and chert.

CHAPTER 1

INTRODUCTION

The Woodford Shale has fascinated geologists for decades. It is widespread, dark colored, rich in total organic carbon, radioactive, and recognized for its phosphate nodules and chert. Many studies focused on the Woodford Shale as a source rock for petroleum, but this resource shale was re-examined to determine its origin and potential as a petroleum producer. An aspect of the Woodford Shale that deserves additional attention is the determination of the origin and abundance of phosphate nodules. This paper examines Woodford phosphate nodules geochemically and petrographically and categorizes their differences in morphology. Further, the geochemical signature of phosphate nodules was compared to their host shale to determine if they reflect genetic differences.

Geologic Setting

The lower Paleozoic section, including the Woodford Shale, formed in a broad sea along the southern margin of Laurentia. In Oklahoma, Woodford sediments were deposited in the Oklahoma Basin that formed over the Southern Oklahoma Aulocogen. The Woodford represents a change from Lower Paleozoic deposition that

was dominantly carbonates and shallow marine sandstone to shale. The Woodford Shale is an organic-rich, marine shale (Arthur and Sageman, 1994) that is characteristically gray to brown to black; finely laminated; > 1% organic material; rich in phosphate and chert in some areas and contains preserved evidence of biogenic silica. High TOC values are attributed to higher rates of bioproductivity resulting from nutrients being transported from the base of thermoclines (Arthur and Sageman, 1994).

Trace elements are important indicators of water chemistry during deposition. Trace elements whose elevated concentrations are typically indicative of marine environments are Cd, Ag, Mo, Zn, V, Cu, Ni and U (Arthur and Sageman, 1994).

Uranium and molybdenum in particular, are important since they can be used as proxies for organic-rich shale (Luning and Kolonic, 2003) and determine depositional environments (Tribovillard et al, 2006). Uranium is introduced into the system as it diffuses from seawater (Cruse and Lyons, 2004) and precipitates in the sediments (Arthur and Sageman, 1994). Uranium diffuses into pore waters, increasing the concentration in the sediment and organic matter therein (Arthur and Sageman, 1994). Molybdenum can be an indicator of paleo environment depending on the geologic setting. Organic-rich shales that form in deep-marine conditions contain high concentrations of Mo (Cruse and Lyons, 2004; Tribovillard et al, 2006). In restricted basins, Mo cannot be readily replenished due to the lack of water column circulation (Harris et al, 2009) and can help identify a rise or fall of the sea level by associating regression with lower concentrations of Mo in the shale relative to oceanic transgression. Furthermore, organic matter can scavenge Mo if HS^-

concentrations are high enough to transform the conservative element Mo into a particle-reactive species called thiomolybdate (Cruse and Lyons, 2004; Tribovillard et al, 2006).

Marine environments responsible for laminated mud, like the Woodford, have relatively low sedimentation rates compared to other depositional systems. Uranium content reflects these differing sedimentation rates. In higher energy environments, the uranium/organic carbon ratio is inversely proportional to the rate of sedimentation (Arthur and Sageman, 1994). In contrast, low energy environments, such as marine shales, have observed trends of increasing uranium with organic matter (Luning and Kolonic, 2003).

Taff, (1902) was the first person to use the name Woodford Shale in literature.

Spesshardt (1985) described the Woodford Shale as an organic-rich, marine black shale that spans from the Late Devonian to Early Mississippian interval. Spesshardt (1985) used conodonts to determine ages, observed the abundant amounts of radiolarians throughout the Woodford Shale, and described the shale as “interbedded dark shales and cherts” on the southern flank of the Arbuckle Uplift that grades into mainly “platy dark shales” to the northeast. The Woodford Shale varies in thickness from 107 to 122 meters thick in exposed sections throughout the Arbuckle Mountains; however, it thins to the northeast (Spesshardt, 1985).

The Woodford Shale is exposed in Northeast Oklahoma but is mapped as the Chattanooga Shale (an age-equivalent formation) (Andrews, 2009). The Woodford Shale equivalent in northeast Oklahoma was defined in the Ozark Uplift. In contrast the formal Chattanooga Shale was described in the Appalachian Basin (Boardman

and others, 2009). Surface and subsurface mapping shows that the Appalachian and Ozark lithologies do not physically correlate and differ, and therefore cannot be called the same formation (Boardman and others, 2009). The Woodford Shale in the northeast Oklahoma Ozarks differs from the Woodford Shale in the Arbuckle Mountains because the Ozark Woodford lacks phosphate deposits and chert beds and is much thinner than the equivalent Woodford in Southern Oklahoma (Boardman and others, 2009). Since there are discrepancies between these three outcrop areas, the name Eagles Bluff Shale is being proposed for the Woodford equivalent in the Ozarks (Boardman and others, 2009).

The Woodford was deposited after an extensive hiatus following an uplift and erosion of the Hunton Group (Tarr, 1955). In some cases, post Hunton, pre Woodford erosion removed most of the sedimentary rock column (Tarr, 1955) and as a result the Woodford can unconformably overlie Lower Devonian to Ordovician strata. This study focuses on the Woodford shale in southern Oklahoma outcrops as they contain phosphate nodules that are easily accessible for sampling. Here the Woodford normally overlies carbonates of the Hunton Group and is succeeded by Mississippian shales and carbonates.

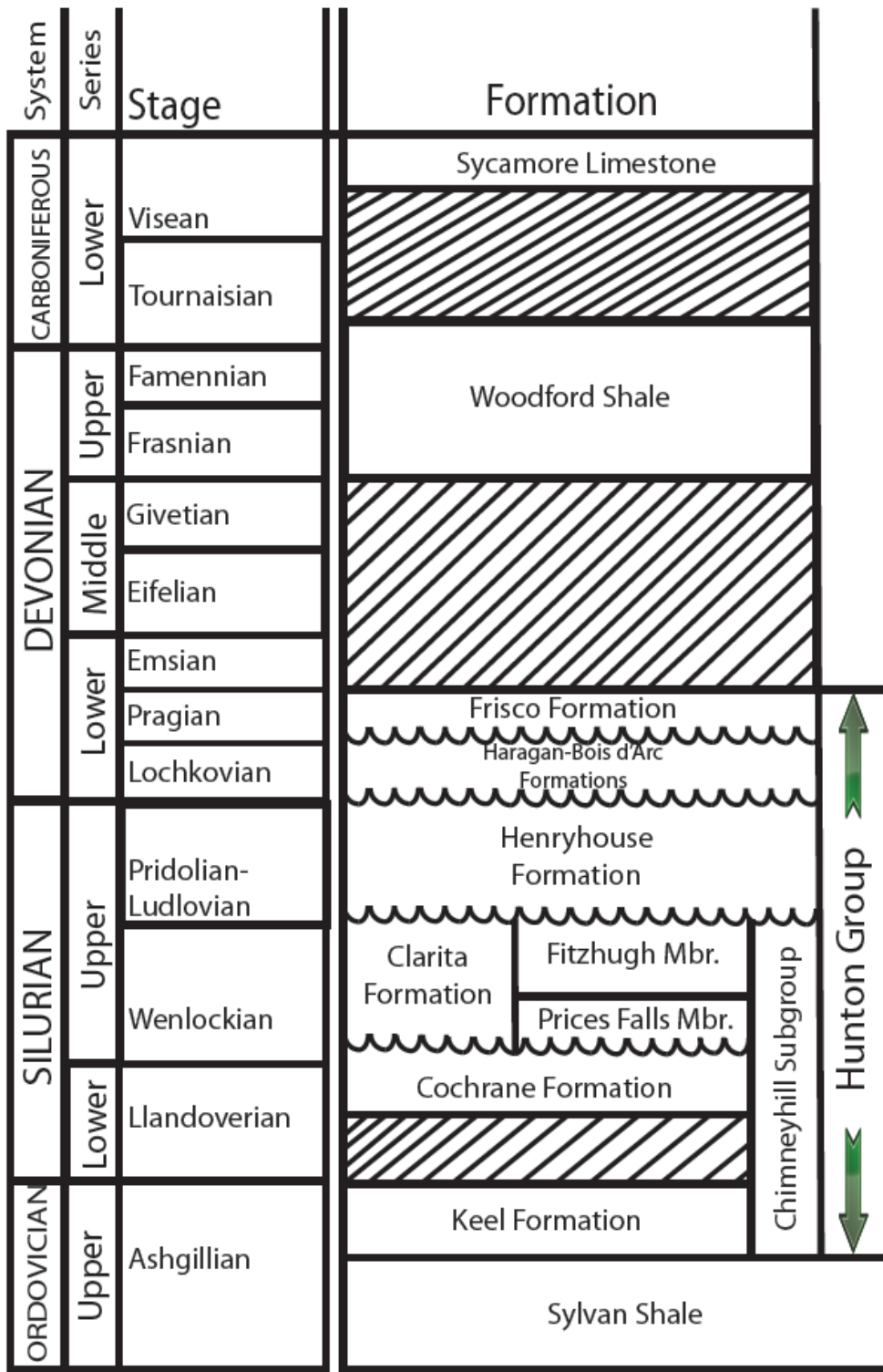


Figure 1: Stratigraphic nomenclature modified from (Barrick, Klapper and Amsden, 1990, pg. 6)

Methods

Sampling From Outcrop

Two localities were chosen for this study. The first is the McAlister Cemetery shale pit, (MSP) which is located west of Overbrook, OK and easily accessed using Exit 24 from I-35. The MSP is a mostly inactive quarry frequented by geologists, as it has a complete section of the Woodford Shale. The entrance to the quarry is located at 34°04'45.30"N/97°09'22.03"W. The second outcrop is along I-35 on the north flank of the Arbuckle Mountains. The I-35 North locality has coordinates of 34°26'49.65" N/97°07'52.87"W. Phosphate nodules are much more abundant at the McAlister Shale pit than at the I-35 N locality. The section of phosphate-bearing beds at I-35 N is only a few meters thick with nearly vertical beds and mantled by regolith (Figure 6). In contrast the phosphate-bearing beds at the MSP are fifteen meters thick and clearly exposed in the pit highwall, where the nodules are readily visible (Figures 4 and 5).

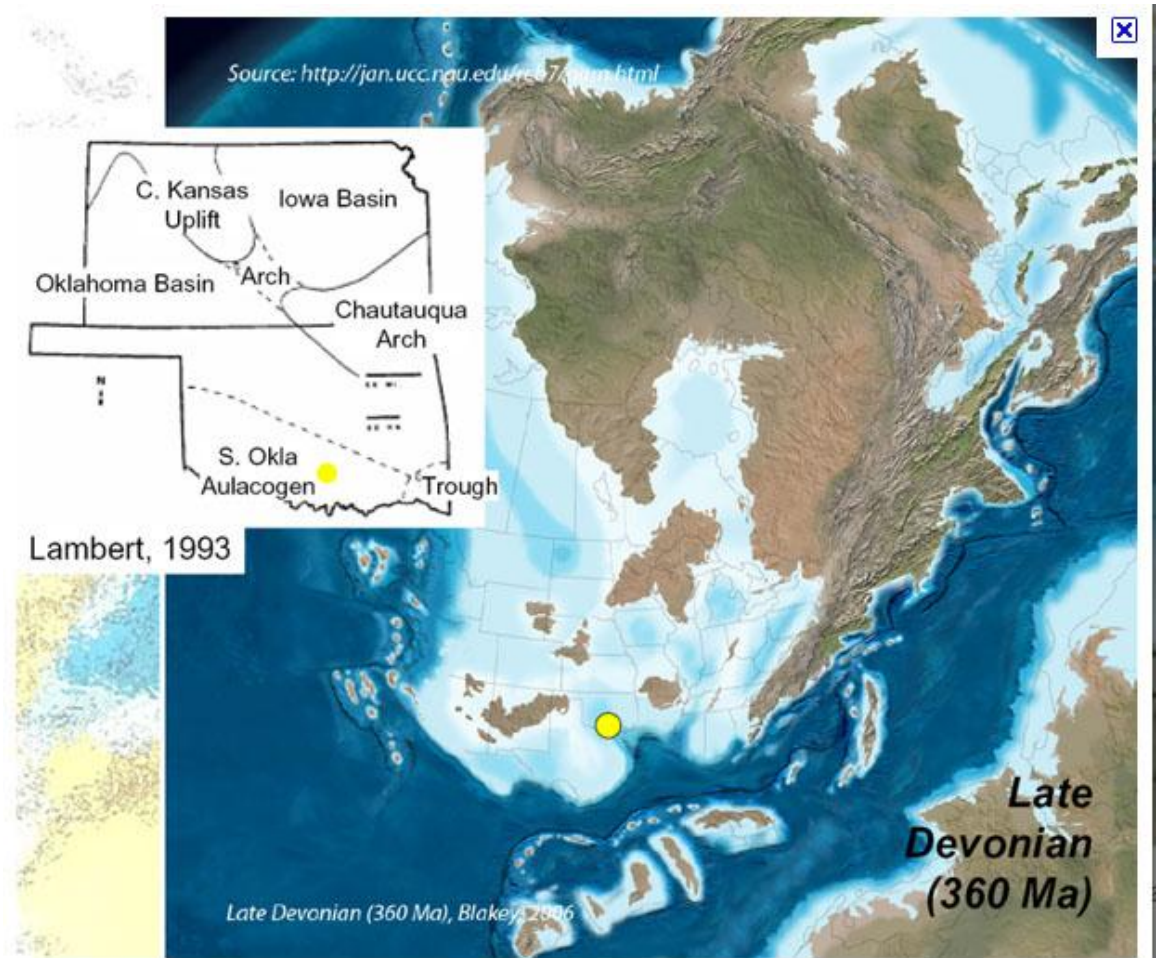


Figure 2: Late Devonian reconstruction of North America showing the positions of the study area with respect to the continent margin and the Southern Oklahoman Aulacogen.

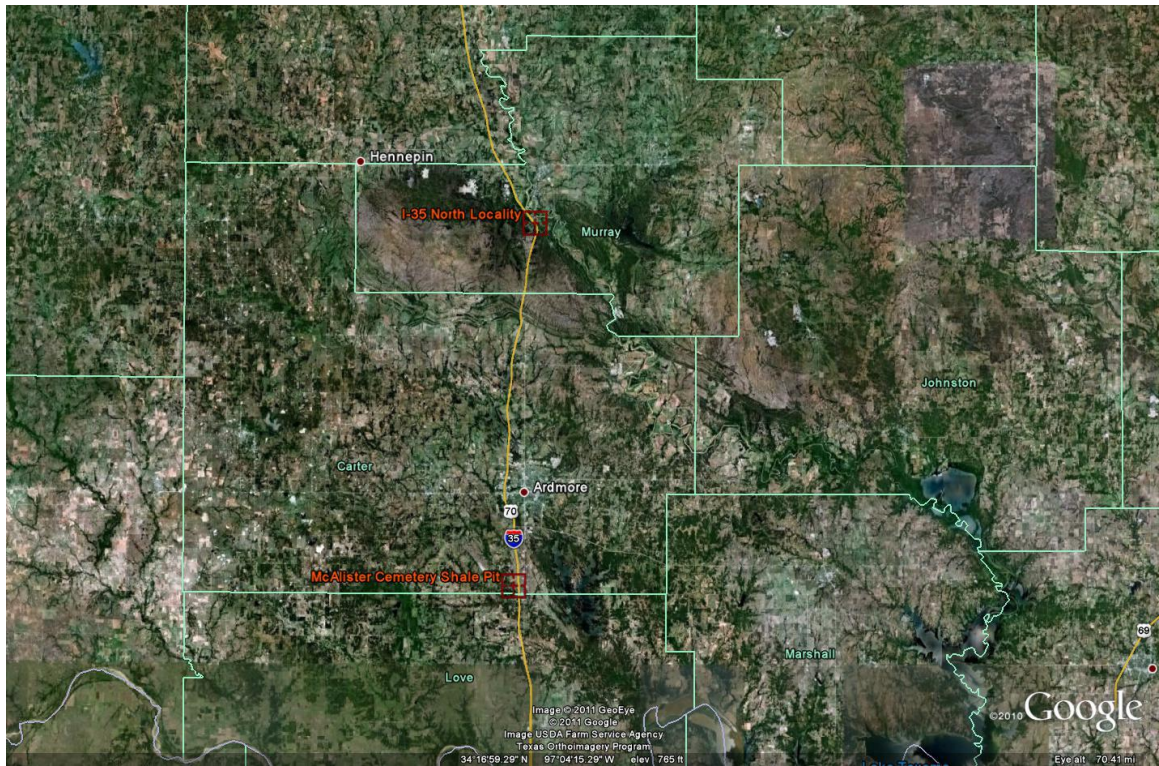


Figure 3: Geographical locations of I-35 North and McAlister Cemetery Shale pit localities (indicated in orange lettering and red markers) provided by Google Earth (2010).



Figure 4: Highwall of the McAlister Cemetery Shale pit showing the cherty and phosphate rich beds (between the arrows) that dip at 43° away from the observer.



Figure 5: Close-up picture of the high wall. Phosphate nodules are shown inbedded in their host shale with a marker for scale. This picture is provided by Dr. James Puckette.



Figure 6: Photo of the phosphate-bearing beds at the I-35 N Outcrop. Phosphate occur in the top few meters of the outcrop (between the arrows). Bedding is nearly vertical.

Twenty-two samples were collected from the upper section of the Woodford Shale at MSP, beginning one foot below the phosphatic zone and extending to one foot above the last phosphate-bearing bed. Sampling was guided by identifying changes in size and shape of phosphate nodules as well as host lithology. When changes in nodule morphology and host lithology were detected, samples were collected. Nine samples were collected from the I-35 North locality using the same methodology as employed at MSP. A total of eight additional samples were collected from both localities to corroborate measurements of TOC. This latter set of samples was analyzed using x-ray fluorescence and thin-sectioned.

Total Organic Carbon

The initial thirty-one nodules were halved using a trim saw. The second half of each sample was powdered and prepared for total organic carbon (TOC) analysis; a second aliquot was selectively analyzed using powder XRD and x-ray fluorescence. The more complete half of each sample was smoothed on a solid polishing wheel using water. All samples were thoroughly cleaned to prevent contamination. TOC was determined using a coulometric titration method provided by UIC inc. The instrument (coulometer) was attached to two separate modules: a furnace apparatus and an acidification module. The Furnace Module, MC5300 heats to 4,000 degrees Fahrenheit to liberate all carbon within the samples and gives a total carbon (TC) measurement. The second (CM5130 Acidification Module) module uses HCL acidification to generate a total inorganic carbon (TIC) value by removing carbonate. A series of blanks and calcium carbonate standards were analyzed to make certain the instrument worked properly and to calibrate results. TC and TIC for each sample were determined following the protocol established by the instrument manufacturer. TOC was determined by subtracting the TIC values from the TC values

X-Ray Fluorescence and Diffraction

Selected samples were x-rayed for bulk analysis using a Phillips Analyzer PW 1830 x-ray diffractometer. Two thin sections and six bulk powdered samples of nodules and host rock was x-rayed to determine mineralogy. Twenty-two selected samples were analyzed using the Niton XS3t x-ray fluorescence analyzer made by Thermo Scientific. In order to ensure accuracy of detecting properties for small

features on the samples, the area of exposure was reduced to 3 mm. This allowed for a high-definition examination of the characteristics within the phosphate nodules and in some cases, their surrounding shale. These measurements were taken along transects of the nodule and the host shale to establish elemental makeup and changes in metal concentration within and adjacent to each selected nodule.

Thin-Sections

Thin sections were made from eight samples, three from I-35 North and five from MSP. The thin-sections were analyzed petrographically and provided insight into the mineralogy/petrology of nodules and the diversity of micro fauna.

Literature Review

Black phosphatic shales have intrigued geologists for decades as potential source beds for petroleum. Heckel (1977) proposed that black phosphatic shale facies in Pennsylvanian cyclothems of Mid-Continent North America formed as a result of large-scale sea level changes driven by glaciation and deglaciation. During widespread inundation, thermoclines developed creating anoxic conditions that preserved organic matter. Seaward surface winds carried the surface waters to the west, which allowed colder, deeper, nutrient-rich water to cycle and replaced the upper water column. Increasing nutrients promoted planktonic blooms that enriched the water in organic matter. Once this organic matter settled to the ocean floor any remaining oxygen was consumed during biodegradation, further promoting anoxia and organic matter preservation. The

biostratigraphy, crystallography, geochemistry and petrography of phosphate nodules in Pennsylvanian cyclothems was examined by Ece (1990).

Roe et al (1982) studied Pa/U and Th/U ratios in modern phosphate nodules forming off of the Peru – Chile shelf in 250 to 500 meters deep water. These nodules are forming at an oxygen minimum zone that is not completely anoxic. Arthur and Sageman (1994) established the properties of a marine black shale and proposed that shales that are truly economic and have high TOC formed in deep oceanic basins. Spesshardt (1985) examined phosphate nodules in the Woodford and defined relationships between and differences in phosphate nodules and their host shale using stratigraphy and petrology. To ensure his lithological ties were accurate, Spesshardt used conodonts to establish the internal stratigraphy of the Woodford Shale. The ecological model for conodonts and their usefulness in biostratigraphy and interpretation of paleo environments was demonstrated by Seddon and Sweet (1971). Siy (1988) examined the distribution of La and Ce in phosphate nodules and host shales from six Woodford outcrops in Southern Oklahoma and acknowledged the role of diagenesis in altering nodule mineralogy.

The global phosphorus cycle, which includes the relationship between phosphorous and other nutrients, and accumulation, was examined by Ruttenberg (2003). Jiang et al (2007) discussed the role of phosphate as a host to rare earth elements (REEs) and the reaction of REEs with sediment. Canfield (2006) modeled changing conditions within coastal upwelling zones and the consumption of oxygen by decomposing organic matter as well as denitrification and sulfate and nitrate reduction.

Boardman and others (2009) proposed a new formation called the Eagles Bluff Shale for the Devonian black shale in the Ozarks. This change was predicated on the evidence that the Chattanooga of the Ozarks and the Appalachians are not directly correlatable and that they are lithologically different. In addition, the Woodford Shale of southern Oklahoma is different from the black shale (Chattanooga) of the formation in the Ozark Uplift because the Woodford contains phosphate deposits, chert beds and is much thicker.

Jerden Jr., and Sinha (2005) discussed the affinity of phosphorous to envelop uranium in soil and the effect of the uranium – phosphorous bond on phosphate stability. The role of metals as proxies for TOC and then accumulation in sediment is discussed by Luning and Kolonic (2003).

CHAPTER 2

PHOSPHATE NODULES

Phosphate Occurrence in Woodford Shale

Phosphate nodules occur within coastal upwelling zones where wind driven surface water moves seaward allowing the deeper water column to cycle upwards to fill in the void (Canfield, 2006). According to Heckel (1977) this process is more effective when the sea is deep enough to create a thermocline that prevents isolated cells of vertical circulation from reaching the bottom waters (Figure 7). The result is the lower water column remains oxygen deprived. However, the process of upwelling alone does not generate a fully oxygen-free environment. Many life-sustaining nutrients, such as phosphates and nitrates, flow up from the lower water column into the more oxygen-rich water above. These nutrients become engulfed by the remaining oxygen, further lowering the concentration and preventing future organic matter decomposition (Canfield, 2006).

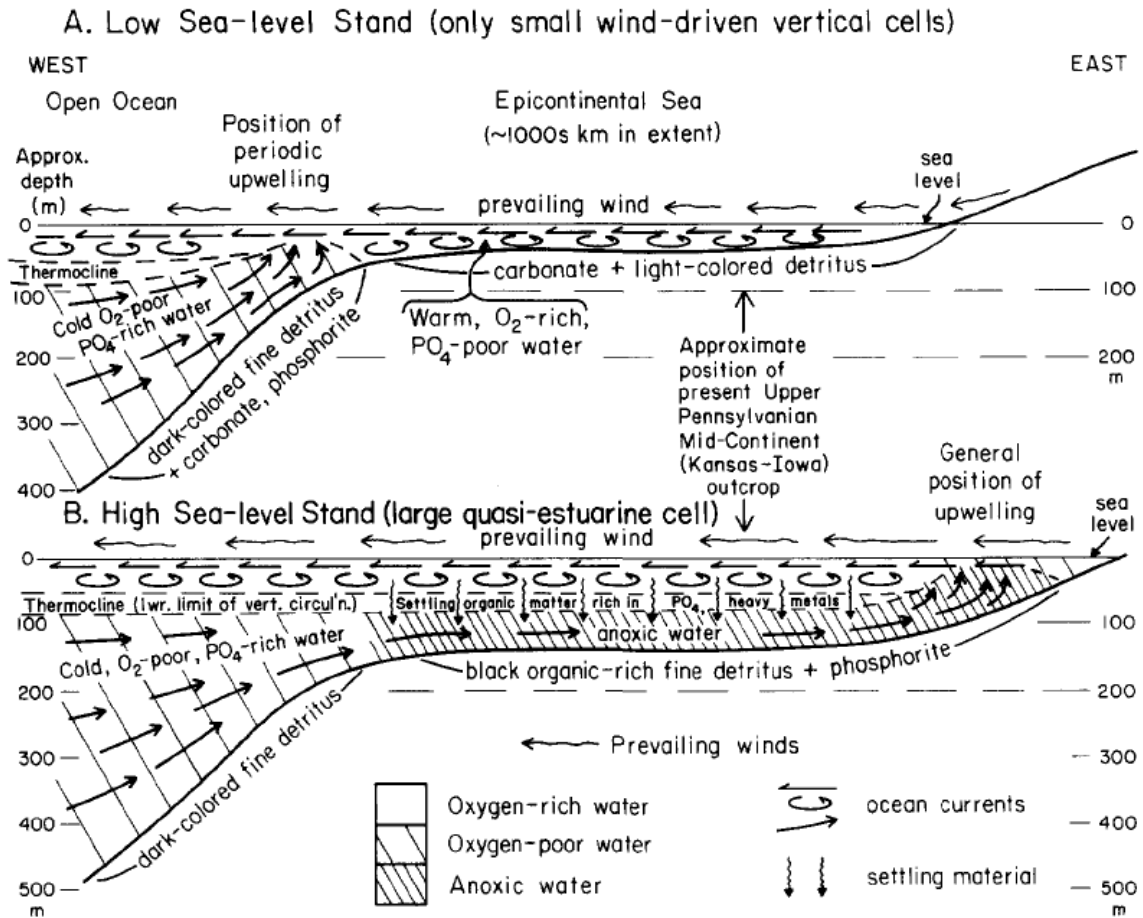


Figure 7: Heckel (1977, p.10) models upwelling zones in both low-stand and high-stand conditions.

Deposition during the Pennsylvanian was influenced by cyclothems, which are periods of repeating oceanic regression and transgression, attributed to glacial eustatic sea-level changes (Ece, 1990). At maximum transgression, these seas were deep enough to generate thermoclines that facilitated the formation and preservation of phosphate (Heckel, 1977). Though the Pennsylvanian is characterized by a series of cyclothems and multiple black phosphatic shales, the Woodford Shale only developed the correct conditions for the creation and preservation of large accumulations of phosphate nodules during the later part of

the formation's depositional history in the locations that are being studied in this discussion.

Modern Phosphate Nodules

The present model of phosphate nodule formation is based on the modern analogue from the Chile-Peru shelf (Roe, et al, 1982). Modern phosphate nodules occur at the water- sediment interfaces at depths between 250 and 550 meters deep and are around the oxygen-minimum zone (Roe, et al, 1982). The nodules themselves range in size (much like the Woodford Shale nodules) from "5-10 cm long and 2-3 cm wide" (Roe, et al, 1982, pp. 2). The nodules contain abundant carbonate fluorapatite cement, biogenic opal, marine skeletons along with other detrital constituents and are rich in uranium (Roe, et al, 1982). These nodules were radiometrically dated to give growth rates as slow as 1 to 10 millimeters per 1,000 years (Roe, et al, 1982), which provides ample time to experience extensive changes within ever-fluctuating oceanic pore water chemistry.

The modern phosphate nodules found near the Chile-Peru shelf consist mainly of quartz, feldspar, apatite, phosphate, calcite and dolomite (Kim and Burnett, 1985). Carbonate fluorapatite (CARFAP) is the main mineralogical constituent in the modern phosphate nodules. There may be a link between the amount of growth rates of the nodules and the amount of limiting CARFAP constituents within the sediment pore water, but further study on this subject is recommended (Kim and Burnett, 1985).

Interest of Phosphate Nodules

Phosphate nodules are of interest to the petroleum industry because of their association with organic-rich shales (Heckel, 1977; Ece, 1990). The Woodford Shale in the Midcontinent Region (Andrews, 2009) sourced most of the Lower Paleozoic oil and gas and is noted for its phosphate nodules (Spesshardt, 1985; Siy, 1988; Kirkland, 1992). As the Woodford developed as a resource play, interest in understanding the evolution of these hydrocarbon-rich strata increased. In the Arkoma Basin, eastern Oklahoma, the Woodford Shale produced an estimated 350 billion cubic feet of gas (BCFG), between 2000 and 2009 (Andrews, 2009). As Woodford production expands across the Midcontinent Region it is necessary to examine its evolution as a prolific source and reservoir. Phosphate nodules are not found in all sections of the Woodford Shale. Nodules are concentrated in the upper section of the Woodford in south-central Oklahoma. They become less abundant to the north and east and disappear completely in northern and eastern Oklahoma. Phosphate nodules in the Woodford Shale contain countless radiolarian skeletons. Radiolarians are dissolved in nodules to form moldic porosity; shown in Appendix B (pp. 44, 49 and 50). Upwelling zones supply nutrients like nitrates and phosphates that facilitate blooms in planktonic organisms. Flourishing numbers (along with the right environmental conditions) increase chances for preservation in the rock record. This expanded organic activity increases the amount of organic matter available, enhancing the chance for preservation and conversion to petroleum.

Geochemistry of Nodule Formation

Detailed examination of phosphate nodules is key to understand their internal composition. These nodules are riddled with trace elements and rare earth elements (REE's) (Jiang et al, 2007). The concentrations and distributions of these elements reflect the geochemistry of the oceanic water at the time of sedimentation and secretion of the nodules as well as diagenesis. For example, if the outer layer of a phosphate nodule contains higher concentrations of REE's than the middle ones, then it is likely that the pore fluids acquired greater concentration of REE from either the surrounding shale or organic matter and transferred the elements to the outer rim of the nodule during development and/or diagenesis (Jiang et al, 2007). REE's that are incorporated within phosphate nodules include La, Ce, and Pr (Jiang et al, 2007); as well as trace elements such as Ni, Cu, Pb, Mg, Cd, P and U (Ece, 1990).

A critical factor in establishing the geochemistry of phosphate nodules is determining which mechanisms could transport elements to the nodules. Coastal upwelling is important to transportation of dissolved elements in sea water. Other factors such as terrestrial sources transported by fluvial systems are considered, but the small grain sizes of the Woodford mudrocks suggests deposition was distal to a terrestrial source, thereby minimizing their influence. The preservation of organic matter can be inhibited if it is reintroduced into an oxygen-rich environment by either biological activity or ocean currents. However, phosphorus is protected through microbial activity (Ruttenberg, 2003). The mobilization of phosphorus during diagenesis allows pore waters to become super-saturated with phosphorous. High concentrations of phosphorous then precipitate to the sea floor. The large

quantities of phosphorous concentrated in one location provides better chances for preservation (Ruttenberg, 2003). Phosphorus is consumed, reworked or sorbed in the particulate phase of early diagenesis (Ruttenberg, 2003). Refractory phosphorus phases include minerals like detrital apatites that are stable and chemically unreactive when buried (Ruttenberg, 2003)

When phosphate nodules initially form, they are mostly composed of authigenic carbonate fluorapatite (CFA) (Ruttenberg 2003). This crystalline lattice contains adequate pore space to allow precipitating fluid to penetrate and influence the overall chemistry of the rock (Ruttenberg 2003). However, due to CFA's unstable nature, it recrystallizes into fluorapatite when uplifted and weathered (Ruttenberg, 2003). Most phosphate nodules in the Woodford Shale are composed of apatite (Spesshardt, 1985).

Many deeper marine source rocks (such as the Woodford Shale) accumulate uranium near or at the water/sediment interface that tends to bind with settling organic material (Luning and Kolonic, 2003). The concentrations of total organic carbon (TOC) and corresponding uranium content tend to track each other and graphically form a positive relationship (Luning and Kolonic, 2003). Using spectral gamma ray, it is possible to determine the uranium concentration of this organically rich shale (See Appendix A for uranium content in the Woodford at MSP). Black shales with high uranium concentration are coined as "hot shales" (Luning and Kolonic, 2003) due to their high gamma-ray readings that indicate higher radioactively than normal marine shales. Since this relationship has been observed

in previous studies, it is possible to treat high amounts of uranium in most marine environments as an indicator of organically rich shale (Luning and Kolonic, 2003).

Organic matter is not the only material that chemically bonds with uranium. Phosphorous is quite accepting of the uranium elemental structure. When uranium bonds with phosphorous, it stabilizes and has the potential to yield an insoluble phosphate that is significantly resistant to weathering (Jerden Jr., and Sinha, 2005). Phosphorous is so efficient at accepting and trapping uranium that it is used to clean uranium-contaminated soils (Jerden Jr., and Sinha, 2005).

Due to the low sedimentation rate in deep marine environments, phosphate nodule mineralogy is primarily determined by authigenic processes (Tribovillard et al, 2006). Elements found within phosphate nodules typically follow specific patterns due to their properties and reactions with environmental controls. For example, manganese readily engulfs molybdenum at the water-sediment interface (Tribovillard et al, 2006). So, if manganese and molybdenum are in the same system, they both should be reflecting similar patterns of distribution in the rock record. Generally speaking, nickel, cobalt, copper, zinc cadmium and molybdenum are all proxies of environmental conditions (Tribovillard et al, 2006). Elements that infer euxinic conditions at the water-sediment interface and are indicators of redox conditions include vanadium, uranium and molybdenum (Tribovillard et al, 2006). Anoxic conditions are inferred in molybdenum if absent from this list (Tribollivard et al, 2006)

CHAPTER 3

FINDINGS

Total Organic Carbon

Thirty-two samples were run for TOC values. Most of the samples contained very low amounts of TOC, especially for being a Woodford Shale deposit. There were exceptions to this and they were from I-35 North below the phosphate nodule zone. On average the TOC values were less than one tenth of one percent in the WSP locality; but the values in I-35 North were almost four times that amount on average. The two exceptions were samples I35N1 and I35N2. The corresponding TOC values of the samples are 10.6% and 8.77%. The main difference is that these samples are shale.

Five different generalized morphologies of nodules were recognized in the Woodford Shale at the sampled localities: circular with well-defined, concentric rings (Type A), elongate with well-defined, continuous rings (Type B), elongate with poorly-defined and discontinuous rings (Type C), elongate with no apparent internal ring structure (Type D) and circular with no apparent internal structure (Type E). Type A nodules were abundant at the McAlister Cemetery Shale pit (WSP) and rare at the I-35 North location. Type B nodules were similarly abundant at WSP and scarce at I-35N. In contrast, Type C nodules were abundant at I-35N, but scarce at WSP. Type D nodules were common at I-35N and scarce at WSP. Type E nodules are scarce at WSP and not found at I-35N.

The concentration of metals across the nodules was determined using the Niton XRF. Circular and elongate nodules with well-defined symmetrical ring structures have the highest concentration of metals. Measured concentration of uranium was higher in darker bands. The distribution of metals is relatively symmetrical (Figures 8 and 9).

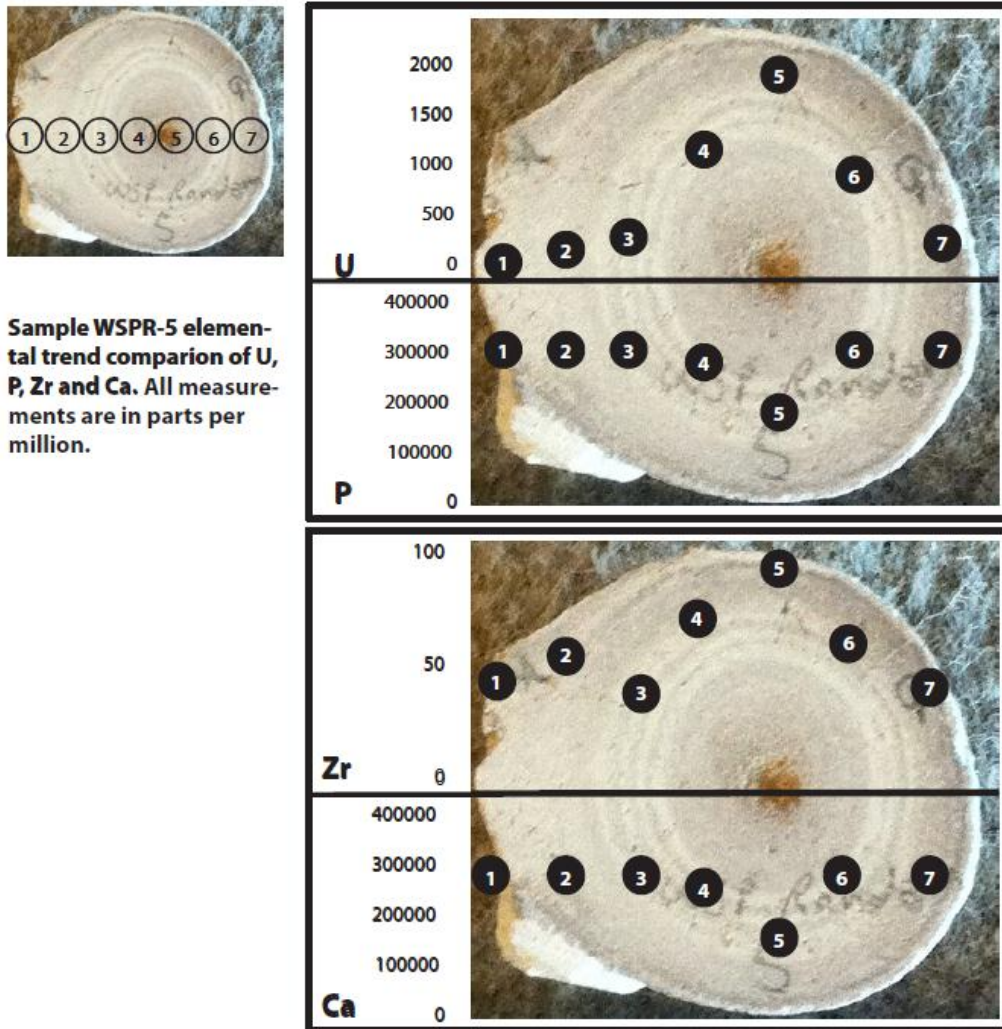
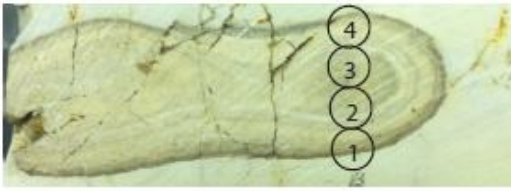


Figure 8: Trending elemental comparisons between uranium, phosphorous, zircon and calcium in nodule Type A. All measurements are in parts per million (ppm).



Sample WSPR-20
 elemental trend comparison of U and P, All measurements are in parts per million.

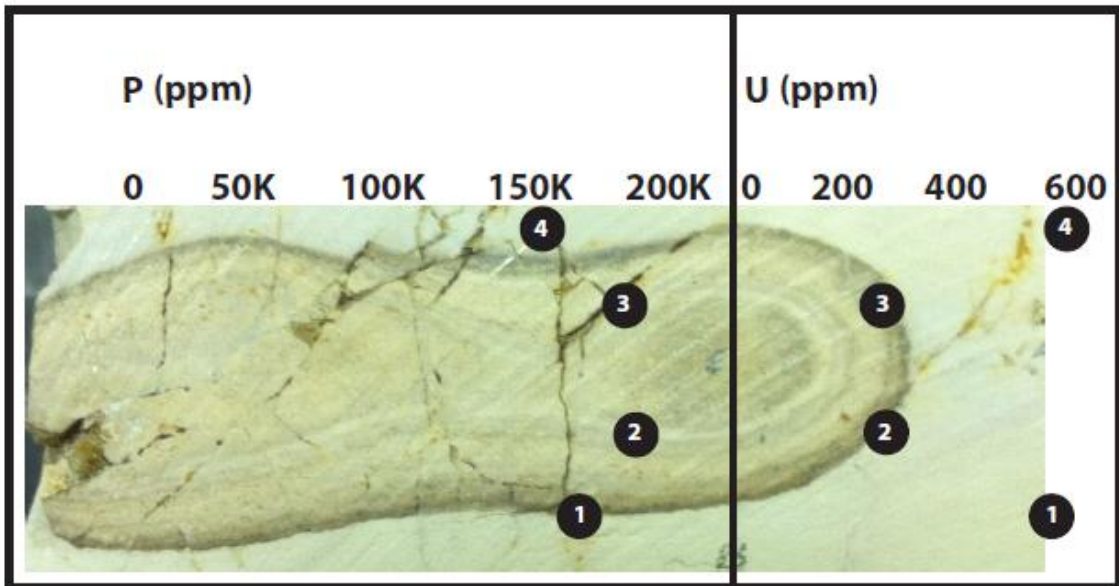


Figure 9: Trending elemental comparison between phosphorous and uranium in nodule Type B.

Type C nodules with poorly-defined discontinuous rings have lower concentrations of metals than both Type A and B. However, uranium concentrations increase in the dark rings compared to the adjacent unstructured section.



Sample 135NR-2 elemental trend comparison of U and P. All values are measured in parts per million (ppm).

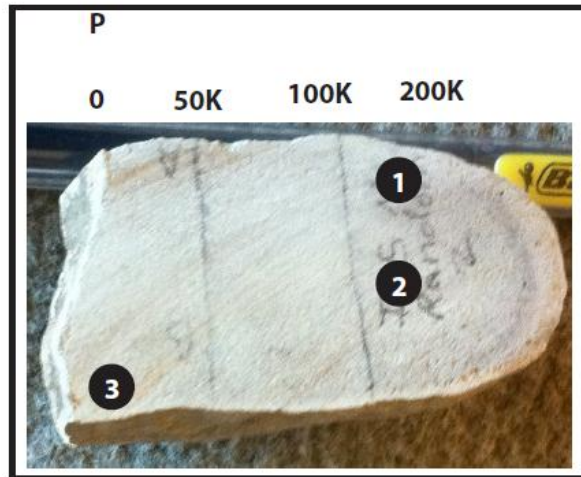
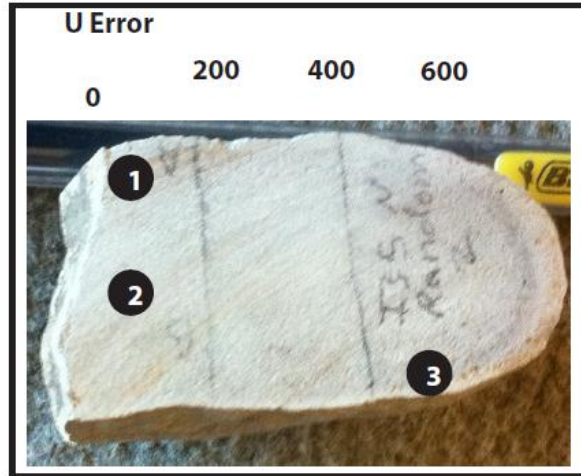


Figure 10: Trending elemental comparison between uranium and phosphorous in nodule Type C. All measurements are in parts per million (ppm).

Type A and B nodules contain pristinely-preserved radiolarians.

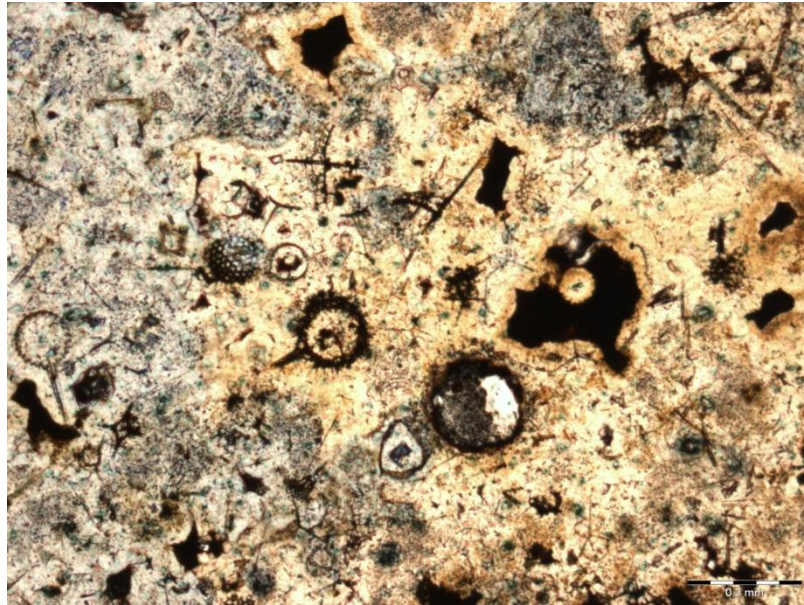


Figure 11: Photomicrograph of a Type A nodule showing diverse communities of radiolarians. Delicate structures of radiolarian tests are preserved. Plane-polarized light (PPL). Sample WSPR3-F.

Radiolarians in Type C and D are less preserved and delicate structures are often broken or missing entirely.

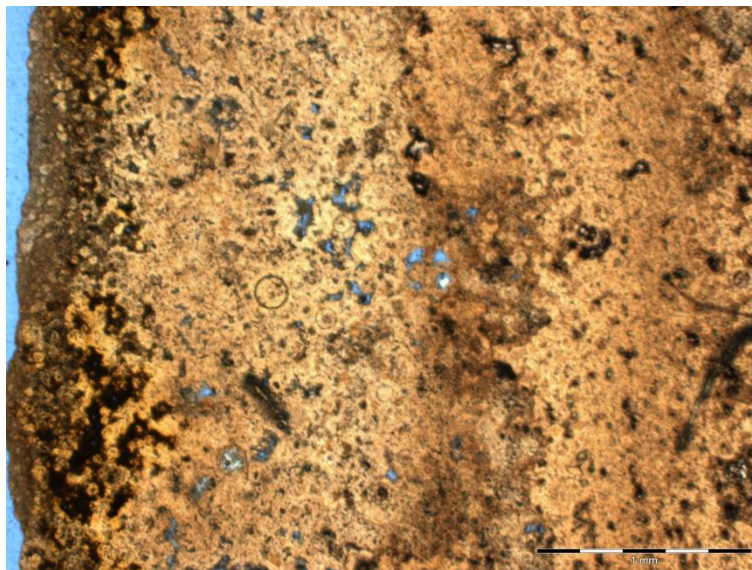


Figure 12: Photomicrograph of a Type C nodule. Preservation of radiolarian skeletons is poor and delicate features are absent. PPL. Sample I35NR-1. Porosity has formed due to dissolution of radiolarians.

The morphology and relevant characteristics of phosphate nodules are summarized in figure 13. In addition to the differences between phosphate nodules, their host shale stands out from them via lower concentrations of metals as shown in Appendix C.






MORPHOLOGY		Locality A - Abundant C - Common S - Scarce		Other Features
Type A	 <p>Circular, concentric, well-defined rings</p>	WSP (A)	Higher concentrations of uranium in dark bands and consistent, symmetrical trendology of metal distribution	Well-preserved radiolarians
Type B	 <p>Elongate, well-defined rings (continuous)</p>	WSP (A) I35N (S)	Higher concentrations of uranium in dark bands and consistent, symmetrical trendology of metal distribution Higher concentrations	Well-preserved radiolarians
Type C	 <p>Elongate, poorly-defined, discontinuous rings</p>	I35N (A) WSP (S)	Lower concentration of uranium, but uranium remains most concentrated in darker bands	Delicate structures are poorly preserved
Type D	 <p>Elongate, rings are absent</p>	I35N (C) WSP (S)	Uranium concentration is low compared to Types A and B; similar trends in certain metals exist, but symmetrical pattern is absent	Delicate structures are poorly preserved
Type E	 <p>Circular, poorly-defined to absent rings</p>	WSP (S)	Difficult to analyze because structure is not obvious	Not thin-sectioned

Figure 13: Summary of phosphate nodule morphology and important characteristics.

CHAPTER 4

DISCUSSION

It is imperative to understand the chemistry of these nodules and their host shales in order to reconstruct the paleo-geochemistry of the ocean during formation. Since these nodules formed in relatively deep environments, the sedimentation rate was adequately slow for chemical processes to take precedence over basic physical controls. However, the sediment type and make-up of the all of the physical constituents enveloped within the system played key roles in the seeding process, the pore structure and the preservation of nodules.

Phosphate in addition to uranium makes the rock more resistant to weathering (Jerden and Sinha, 2005). Higher metal concentrations and uranium in the nodules are consistent attributes of nodules with continuous and symmetrical rings. Nodules formed concurrently with deposition as evidenced by the relationships between the nodule and the enclosing beds. Beds and laminae surrounding phosphate nodules initially extend beneath the nodules (a), followed by laminar beds that terminate against or abut the nodule (b), followed by beds that onlap the nodule (c) and finally laminae that extend across the top of the nodule (d) (Figure 14).



Figure 14: In situ phosphate nodules in host shale. Laminae instantly extend beneath the nodule (a), then abut the nodule (b), lap against the nodule (c) and upper extends across the nodule (d) (arrow points to fore mentioned nodule).

Analytical transects of the shale adjacent to nodules reveal that metal concentrations in the adjacent beds are lower in the encasing shale than in the phosphate nodules. In some samples the darker colored shale adjacent to the nodule has slightly higher metal concentration than the lighter colored shale farther away from the nodule. The morphology of nodules seems to have less effect on metal concentration than internal structure.

Phosphate nodules from WSP tend to be more structured than those from I-35N. Circular and elongate nodules from WSP tend to have consistent symmetrical ring structures. In contrast, the phosphate nodules at the I-35N locality are dominantly elongate, but more importantly lack well-defined internal structure. Metal distributions from I-35 N nodules are poorly defined and overall concentrations are lower than the nodules from WSP.

These patterns are believed to reflect paleo-geographic position and depositional setting. The I-35 N locality is interpreted as shallower and as a result was less impacted by the upwelling zone than the WSP area. Uranium concentration in the nodules was higher and molybdenum concentrations lower at WSP than I-35 N. This finding is interpreted as the WSP represents water that was slightly restricted, which hinders Mo replenishment (Harris, et al, 2009); or Mo was scavenged during periods of euxinia (Cruse and Lyons, 2004; Tribovillard et al, 2006). The lower concentration of uranium at I-35N could be the result of higher oxygen levels.

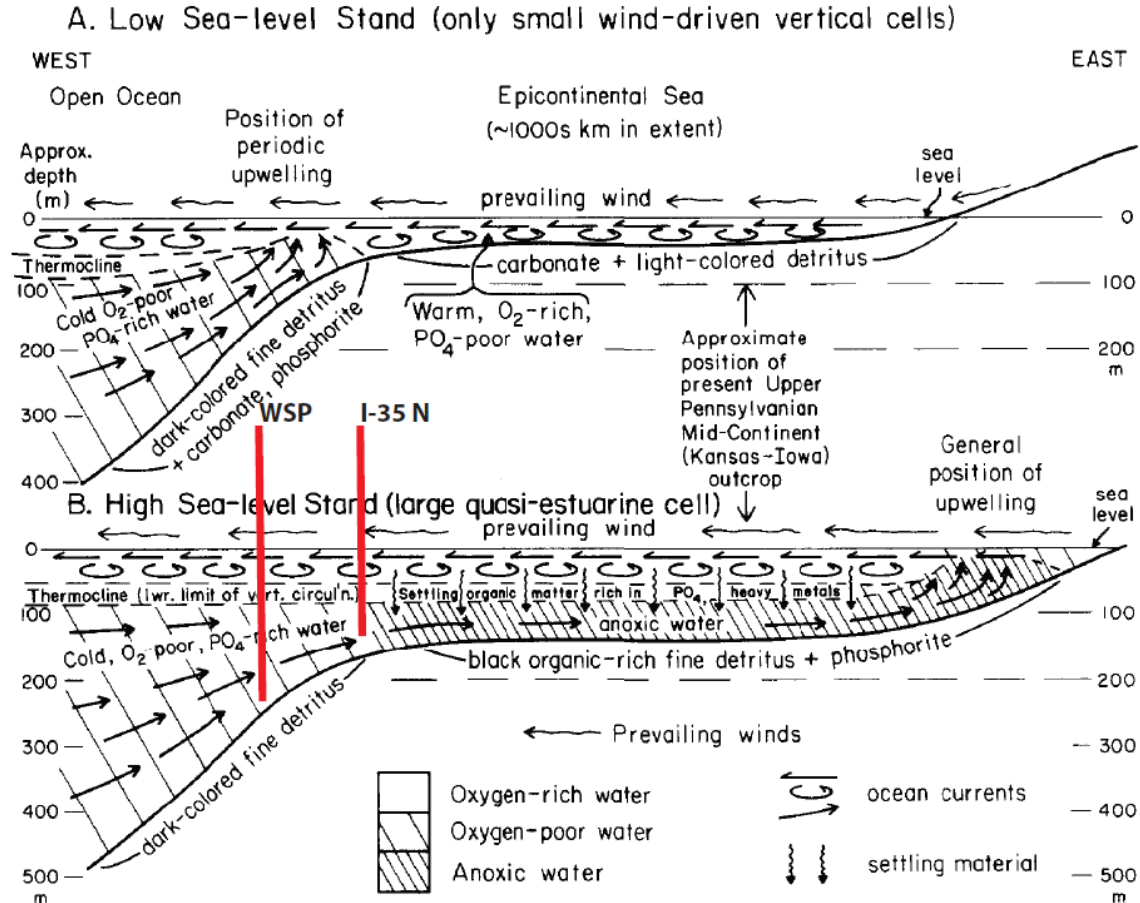


Figure 15: Heckel (1977, p.10) models upwelling zones in both low-stand and high-stand conditions. WSP and I-35N localities are positioned with respect to the model to show their proposed paleo-geographical positions along the upwelling zone.

X-Ray Fluorescence Data

The x-ray fluorescence (XRF) findings established elemental trends within the samples. Depending on the nature of the elements, positive or negative trends were observed throughout the transect of the hand samples. This is best seen in a graphical display of individual element concentrations. The elements found within these samples are both rare earth elements (REEs) and trace elements. However, some elements appear in some samples but not in others. The figures in Appendix B contain graphical representations of the sampling of the nodules and the encasing

shale. Each black dot signifies the diameter of XRF analyzer (which is 3 mm unless otherwise specified) and shows the distribution of readings.

Thin-Sections

Thin-sections show multiple levels of radiolarian preservation, porosity networks and banded structure. The less structured nodules are interpreted to represent shallow, less stable conditions. The higher concentrations of Mo in nodules from I-35 N may corroborate the suggestion that circulation provided a constant source of the metal (Harris et al, 2009). Furthermore, the poorer preservation of radiolarians at I-35N reflects less stable, higher energy conditions. The highly structured nodule from WSP with pristinely preserved radiolarians could be evidence for stable conditions during formation.

Phosphate Nodules

Phosphate nodule chemistry fluctuates throughout the nodule. The spherical nodules with concentric rings show a symmetrical profile with many of the elements. The nodules that are laminar in shape and have a massive internal structure do not show the same mirroring patterns to the degree that the spherical nodules express. Uranium is more prevalent in the nodules with darker banding and more complex internal structures. However, the elemental patterns and relationships therein remain constant. These comparisons can be reviewed in Appendix C. Shale composition reflects nodule chemistry, but metal concentrations in the shale are lower. This depletion of metals in the encasing shale is evidence that

the phosphate is trapping metals, thereby increasing their overall metal concentrations in nodules.

The elemental trends (including uranium, vanadium, molybdenum, nickel and copper) can help determine the environment that enforced the paleochemical conditions on the nodules. These elements appear throughout the phosphate nodules (as shown in the Appendix C) but express different quantities and positions. These variations can reflect a fluctuating geochemical environment between euxinic and anoxic conditions along the water-sediment interface (Tribovillard et al, 2006). The presence of U, Mo, and V in the same system provide evidence of euxinia; and if Mo is absent from this combination, the environment is interpreted to be anoxic (Tribovillard et al, 2006).

CHAPTER 5

CONCLUSIONS

Based on the analysis of phosphate nodules and their encasing shale, the following conclusions are proposed. Five phosphate nodule classifications were identified. Type A is abundant at WSP, have well-defined concentric rings, symmetrical elemental trends and well-preserved radiolarians. Type B is abundant at WSP and scarce at I-35N; these nodules are elongate with a well-defined internal structure and in all other way similar to Type A. Type C is abundant at I-35N and scarce at WSP. These nodules are elongate but have poorly defined continuous rings and contain poorly preserved radiolarians. Type D is common at WSP and scarce at I-35N. Type D nodules are elongate with massive internal structure and do not preserve delicate radiolarian structures. Type E is only found (scarcely) at WSP. These have no internal ring structures and were not thin-sectioned for this study. Nodules are inherently different than their host shale, which contains lower amounts of phosphate and transition metals. Nodules can be classified based on morphology and internal structure. Internal structures refer to intrinsic network of continuous rings. The more defined the organization of the internal rings, the higher the concentrations of most metals. Metals concentrate in the dark rings within phosphate nodules. Mo depletion relative to U is controlled by either scavenging by organic matter or environmental restriction with respect to water column circulation.

Radiolarians are well-preserved throughout the WSP locality. Delicate skeletons are more well-preserved at WSP than at I-35N. The loss of delicate features at I-35N is interpreted to be due to a shallower environment with increased water circulation. The high diversity of radiolarians at WSP suggests a deeper, more stable environment. TOC is generally lower ($\leq 1\%$) in phosphate nodule-bearing zones than in beds lower in the section ($\sim 9\%$ TOC).

Initially, phosphate nodules form concurrently with the sediment. This is evidenced by the truncation of laminae that abut the nodules. Furthermore, this supports the hypothesis that phosphate nodule growth is either \geq the sedimentation rate of the encasing shale. The phosphate nodules within WSP indicate a deeper marine environment than those at I-35N. The nodules at I-35N incorporate detritus in their outer shell because of a higher rate of sedimentation and less stable environment. Most WSP phosphate nodules have distinct internal rings that indicate oscillating water chemistry under relatively stable conditions. However, all nodules in the study areas formed by attracting elements from seawater or pore water and contain higher concentrations of metals than the encasing shale.

REFERENCES

- Andrews, Richard D., 2010, Production Decline Curves and Payout Thresholds of Horizontal Woodford Wells in the Arkoma Basin, Oklahoma, Shale Shaker (February 2010), P. 147-155.
- Arthur, Michael A. and Sageman, Bradley B., 1994, Marine Black Shales: Depositional Mechanisms and Environments of Ancient Deposits, Annual Reviews Inc., Vol. 22, p. 499-551.
- Barrick, James, E., Klapper, Gilbert, and Amsden, Thomas, 1990, Oklahoma Geologic Survey Guidebook 27 p. 5-10.
- Boardman, Darwin, Puckette; James, Watney; Lynn, Cemen, Ibrahim; Cruse, Anna; Hurst, Daniel; 2009: Abstracts with Programs- Geological Society of America, March, 2009, Vol. 41, Issue 2, p. 12.
- Brongersma – Sanders, M., 1971, Origin of major cyclicity of evaporites and bituminous rocks; an actualistic model: Marine Geology, Vol. 11, p. 123-144.
- Canfield, D.E. "Models of oxic respiration, denitrification and sulfate reduction in zones of coastal upwelling", Elsevier Inc, 2006. P. 5753-5765.
- Cruse, Anna M., and Lyons, Timothy W., 2004, Trace metal records of regional paleoenvironmental variability in Pennsylvanian (Upper Carboniferous) black shales, Chemical Geology, Vol. 206, Issues, 3-4, P. 319-345.
- Ece, Omer Isik. "Geochemistry and occurrence of authigenetic phosphate nodules from the Desmoinesian cyclic Exello epeiric sea of the Midcontinent, USA" Marine and Petroleum Geology, Vol. 7 (August 1990). P. 298-312.
- Google Earth, 2010, "Oklahoma", 34°26'49.65" N/97°07'52.87"W; 34°04'45.30"N/97°09'22.03"W. 2011. December 20, 2011.
- Harris, Nicholas; Hemmesch, Nikki; Mnich, Cheryl; Aoudia, Khodir; Miskimins, Jennifer, 2009, An Integrated and Petrophysical Study of a Shale Gas Play: Woodford Shale, Permian Basin, West Texas, The Gulf Association of Geological Societies Transactions, Vol. 59, p. 337-346.
- Heckel, Phillip. "Origin of Phosphatic Black Shale Facies in Pennsylvanian Cyclothems of Mid-Continent North America," *The American Association of Petroleum Geologists Bulletin*. Vol. 61. No. 7 (July 1977). P. 1045-1068. 7 Figs.
- Jiang, Shao-Yong; Zhao Hai-Xiang; Chen, Quan-Yong; Yang, Tao; Yang, Hong-Jing and Ling, Hong-Fei, 2007, "Trace and rare earthy element geochemistry of phosphate nodules from the lower Cambrian black shale sequence in the Mufu Mountain of Nanjing, Jiangsu province, China" Elsevier B. Vol., P. 584-604.

- Jerden Jr., James; Sinha, A.K., 2005, Geochemical coupling of uranium and phosphorous in soils overlying an unmined uranium deposit: Coles Hill, Virginia, *Journal of Geochemical Exploration*, Vol. 91, p- 56-70.
- Kirkland, D. W., Denison, R. E., Summers, D. M., and Gormly, J. R., 1992, *Geology and Organic Geochemistry of the Woodford Shale in the Criner Hills and Western Arbuckle Mountains*, Oklahoma, Oklahoma Geological Survey, Vol 93, P. 38-69.
- Luning, S. and Kolonic, S., 2003, Uranium Spectral Gamma-ray Response as a Proxy for Organic Richness in Black Shales: Applicability and Limitations, *Journal of Petroleum Geology*, Vol. 26, April 2003, p. 153-174.
- Roe, K.K., Burnett, W. C., Kim, K. H., and Beers, M. J., 1982, Excess Protactinium in phosphate nodules from a coastal upwelling zone, Elsevier Scientific Publishing Company, Vol. 60, P. 39-46.
- Ruttenberg, K. C., 2003, *The Global Phosphorous Cycle*, Elsevier Ltd., P. 585-643.
- Seddon G., and W. C. Sweet, 1971, An ecologic model for conodonts: *Jour. Paleontology*, Vol. 45, P. 869-880.
- Siy, Susan, 1988, *Geochemical and Petrophysical Study of Phosphate Nodules of the Woodford Shale (Upper Devonian- Lower Mississippian) of Southern Oklahoma*, Masters Thesis.
- Spesshardt, Scott A., 1985, *Late Devonian-Early Mississippian Phosphorite-Bearing Shales, Arbuckle Mountain Region, South-Central Oklahoma*, Masters Thesis.
- Taff, J.A., 1902, *Description of the Atoka quadrangle (Indian Territory): U.S. Geological Survey Geologic Atlas of the United States, Atoka folio, no. 79, p. 8*
- Tarr, Russel, 1955, Paleogeologic Map at Base of Woodford and Hunton Isopachous Map of Oklahoma, *Bulletin of the American Association of Petroleum Geologists*, Vol. 39, No. 9 (September 1955), P. 1851-1858.
- Tribovillard, Nicolas, Algeo, Thomas, Lyons, Timothy and Riboulleau, Armelle, 2006, Trace metals as paleoredox and paleoproductivity proxies: An update, *Chemical Geology*, Vol. 232, p 12-32.

Appendix A

Highway Interstate 35: Woodford Shale Measured Section with Gamma-ray curve (North flank, east side northbound lane)

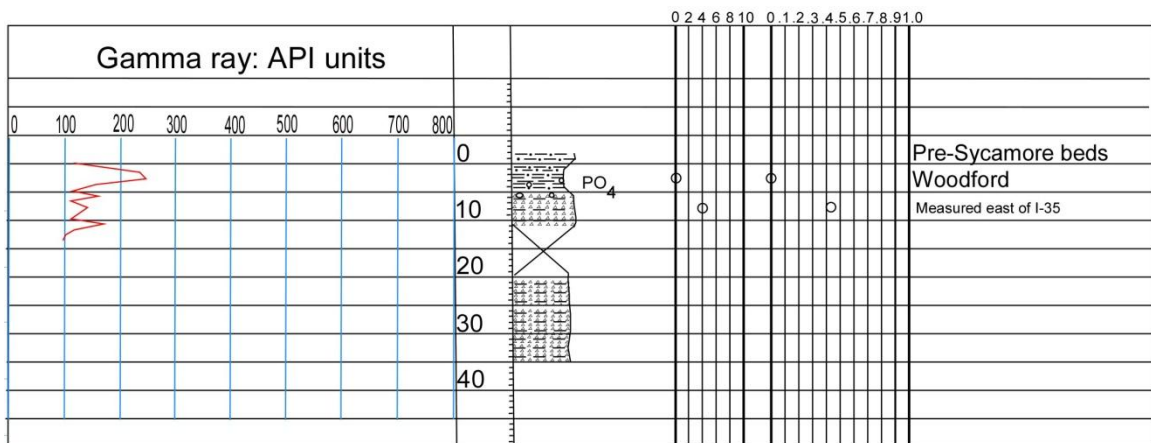


Figure A-1: Measured section with gamma-ray curve from I-35N. Provided by Dr. James Puckette

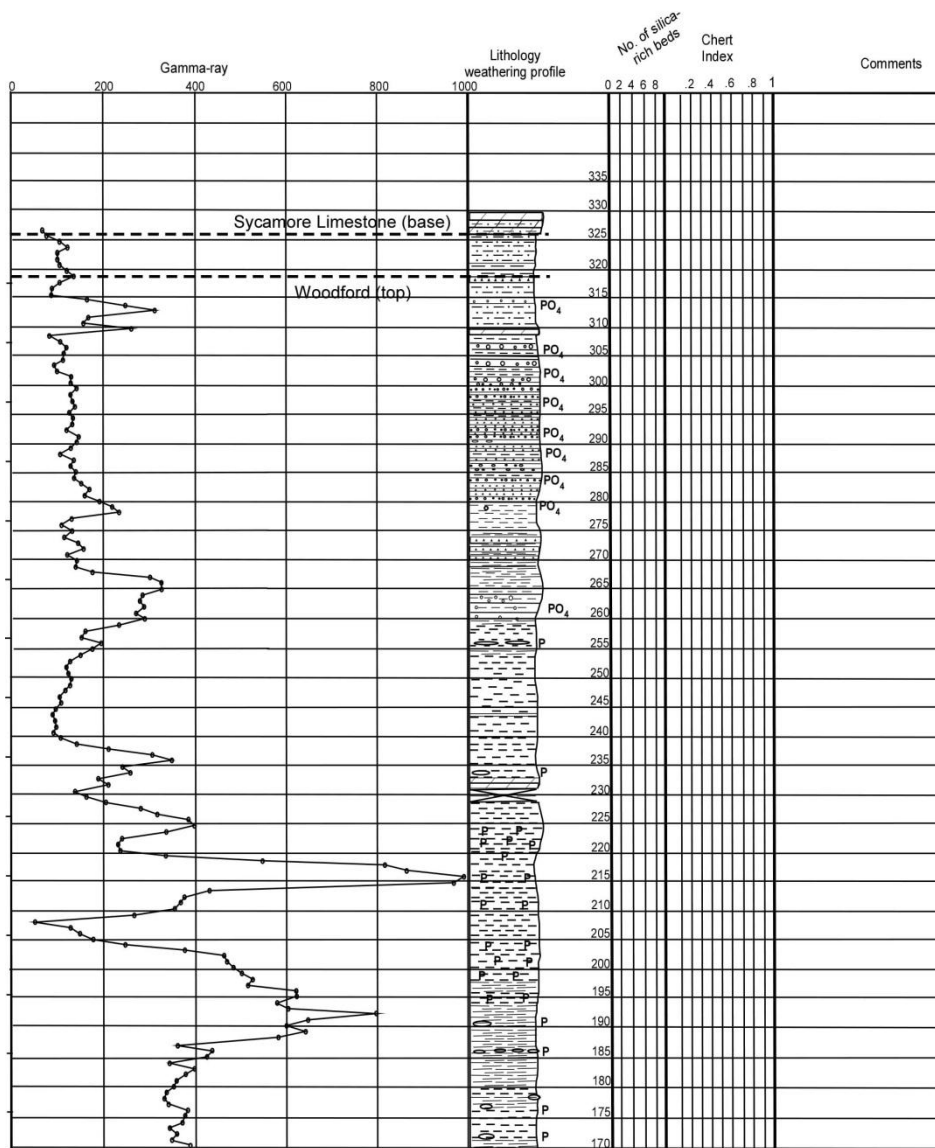


Figure A-2: Measured section and gamma-ray curve from upper half of WSP. Provided by Dr. James Puckette.

Appendix B

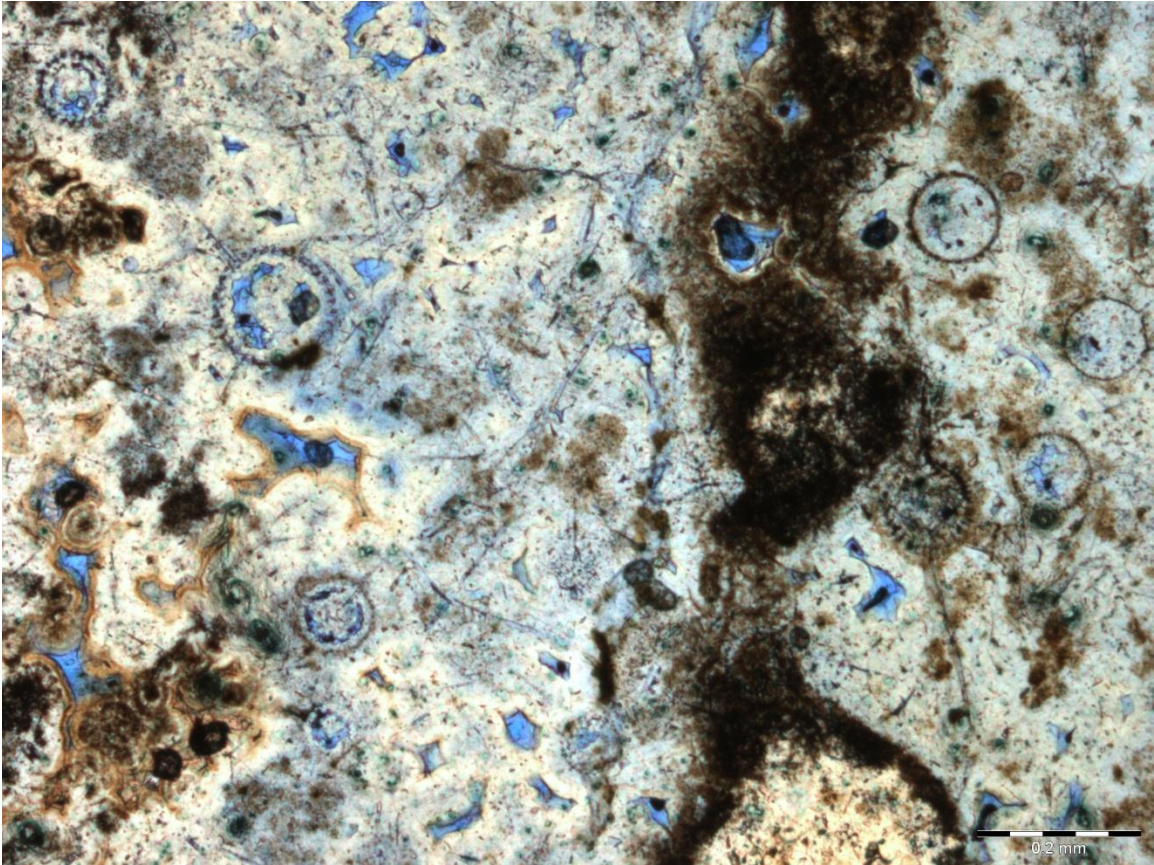


Figure B-1: I35NR-1. This sample was taken out of the WSP. Under plane polarized, it is easy to see the different kinds of radiolarians and various levels of preservation. In this picture, chalcedony cement can be observed filling in pore spaces.

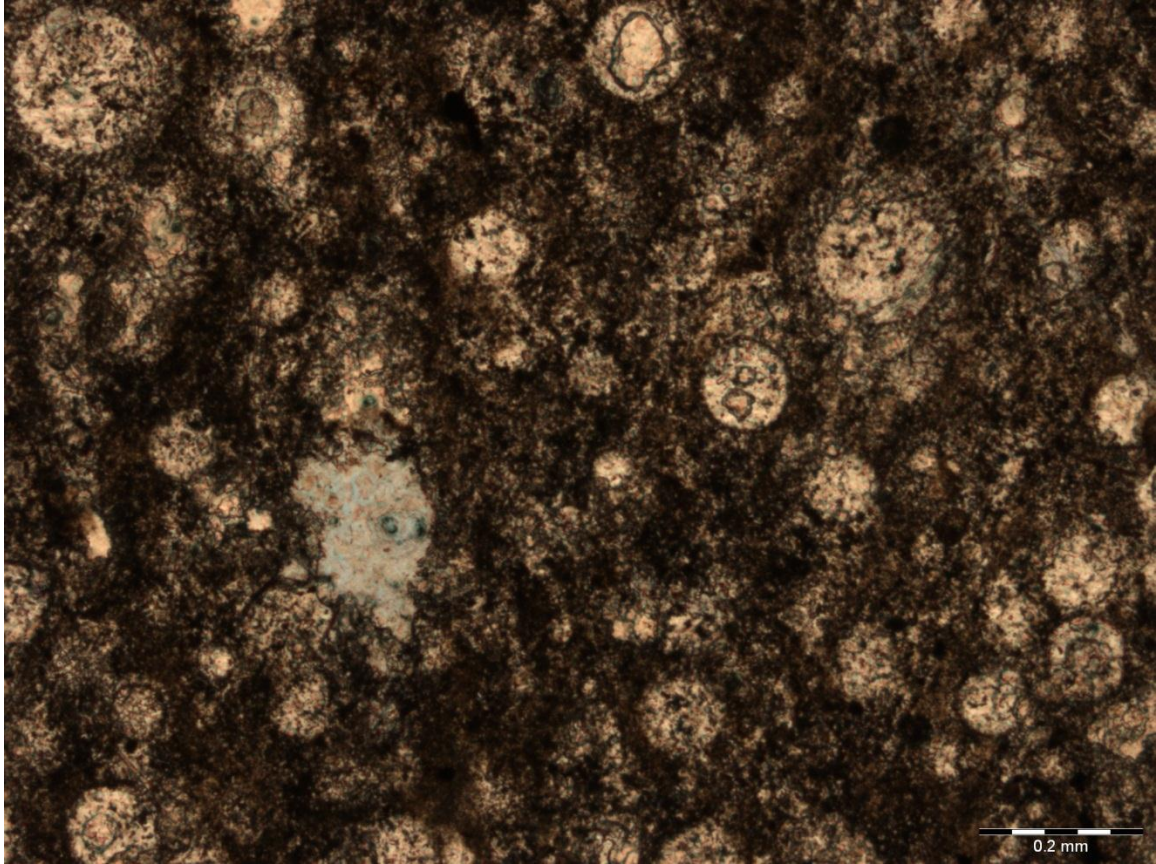


Figure B-2: MCP CON 1. This is a bouillon out of the WSP. Radiolarians are incredibly abundant as shown here. Containing mostly carbonate, there are some traces of biogenic silica from the dissolution of the original tests of the radiolarians.

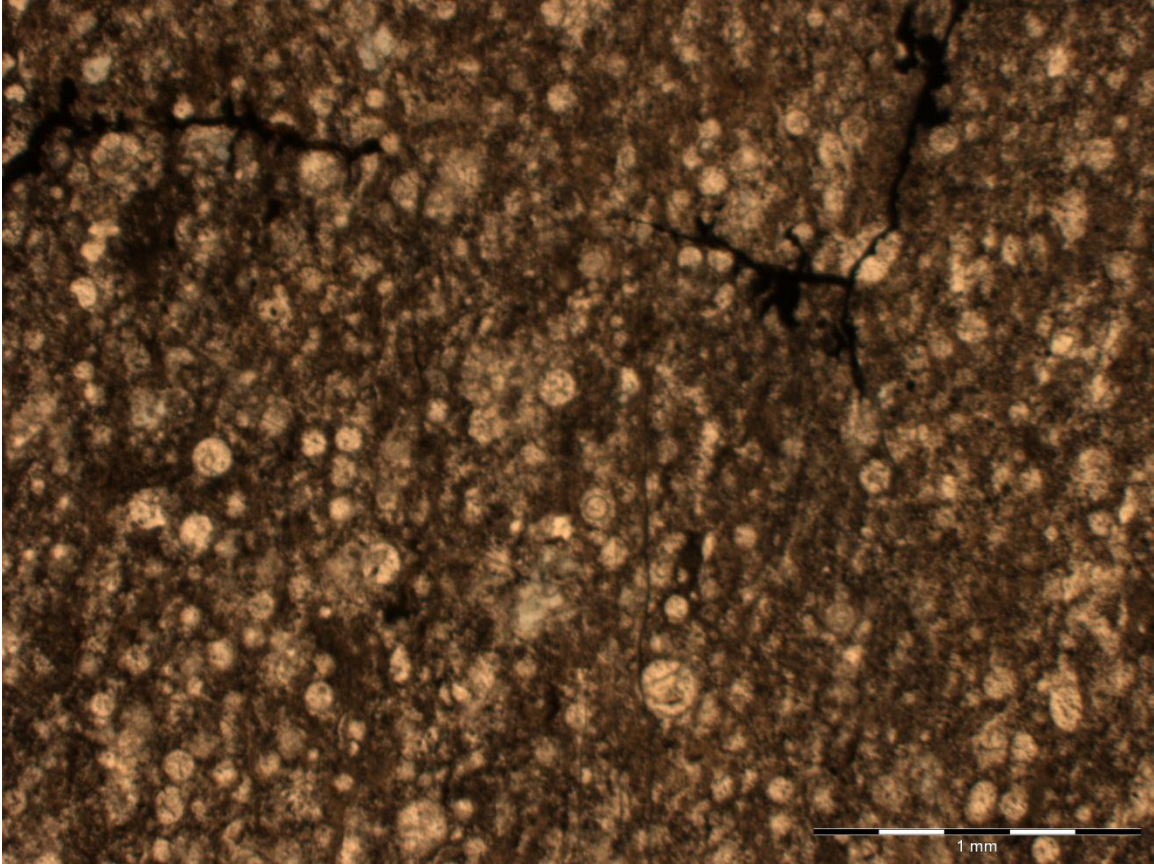


Figure B-3: MCP CON 1. This is a lower-power magnification of the previous slide to show the abundance of the radiolarians.

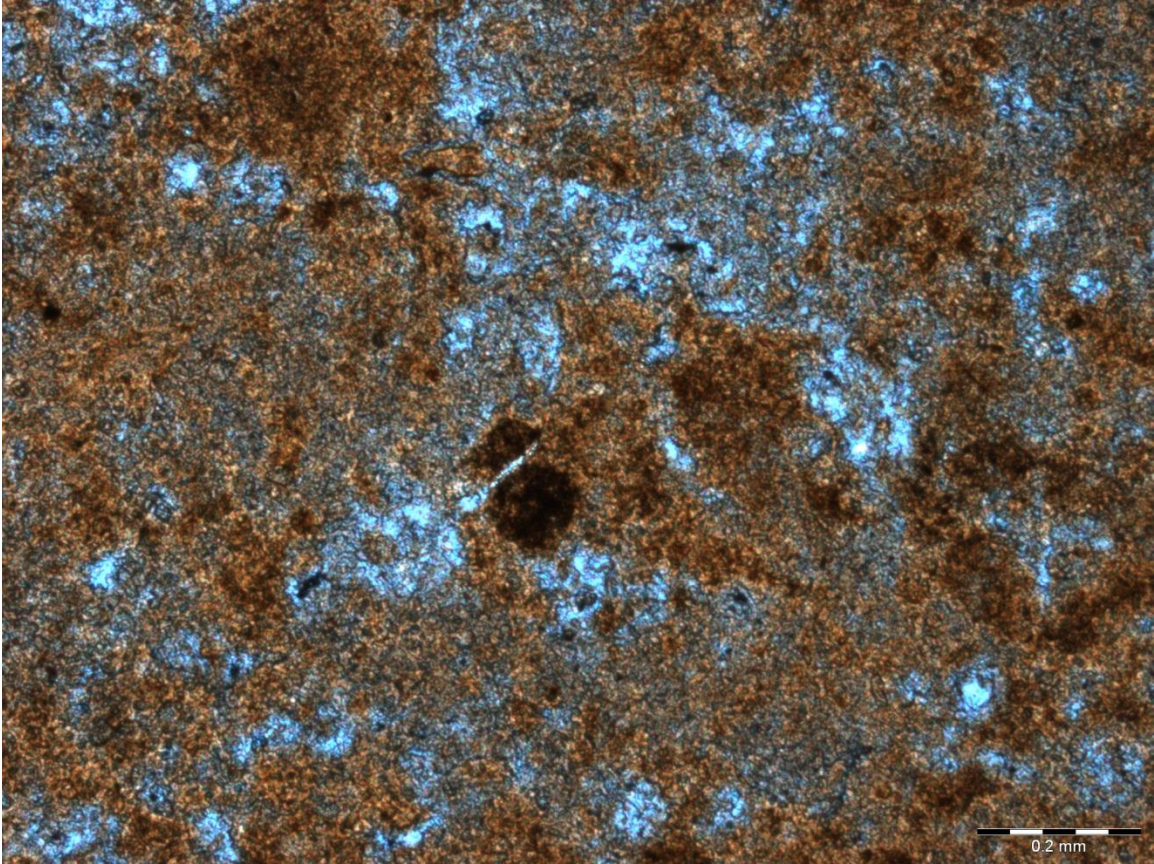


Figure B-4: WSPR2-A. WSP origin. Preferential dissolution is shown between two radiolarians in close proximity with each other. One was almost completely dissolved whereas the other one was replaced by phosphate.

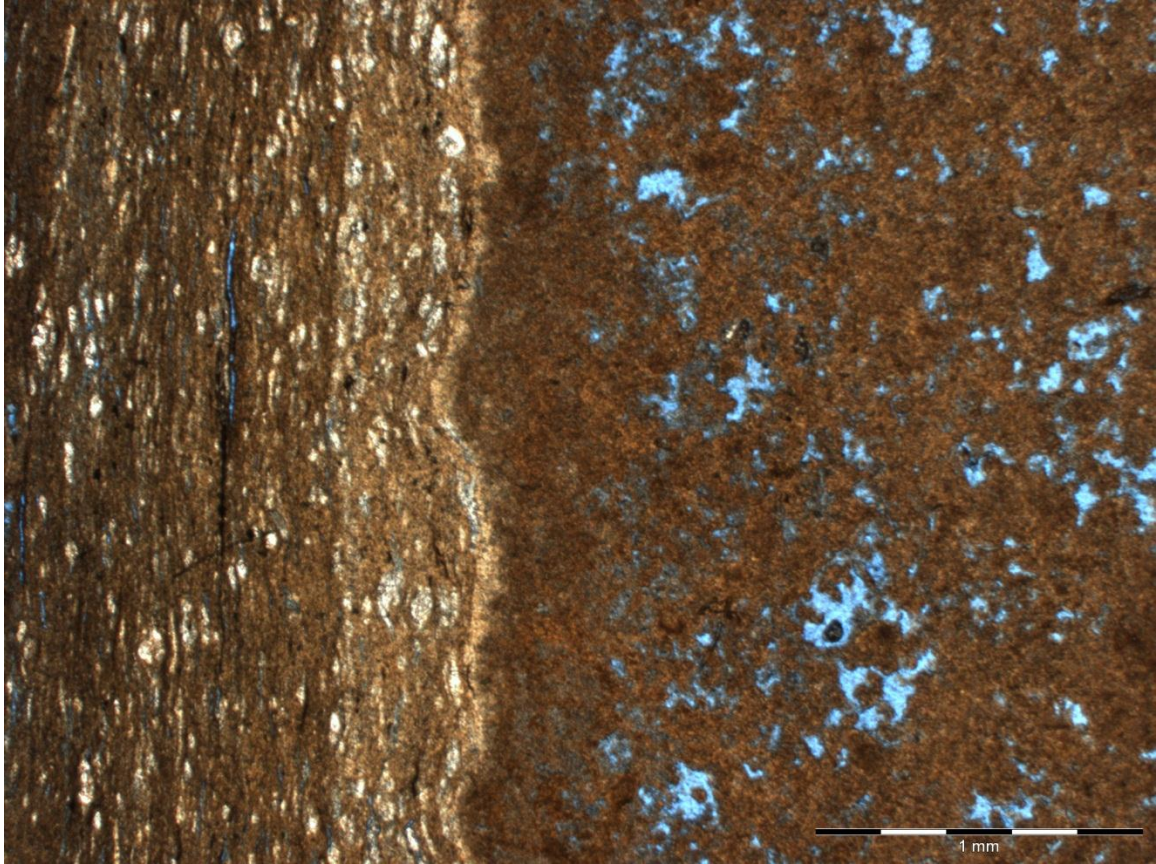


Figure B-5: WSPR2-B. The outer layer that is mud matrix has engulfed several radiolarians. The inner part of this nodule appears not to have preserved very many radiolarians and has generated significantly more porosity than the outer shell. The difference of texture of the rock between these two layers is remarkable. The outer mud shell has conformed to the more dense phosphate.

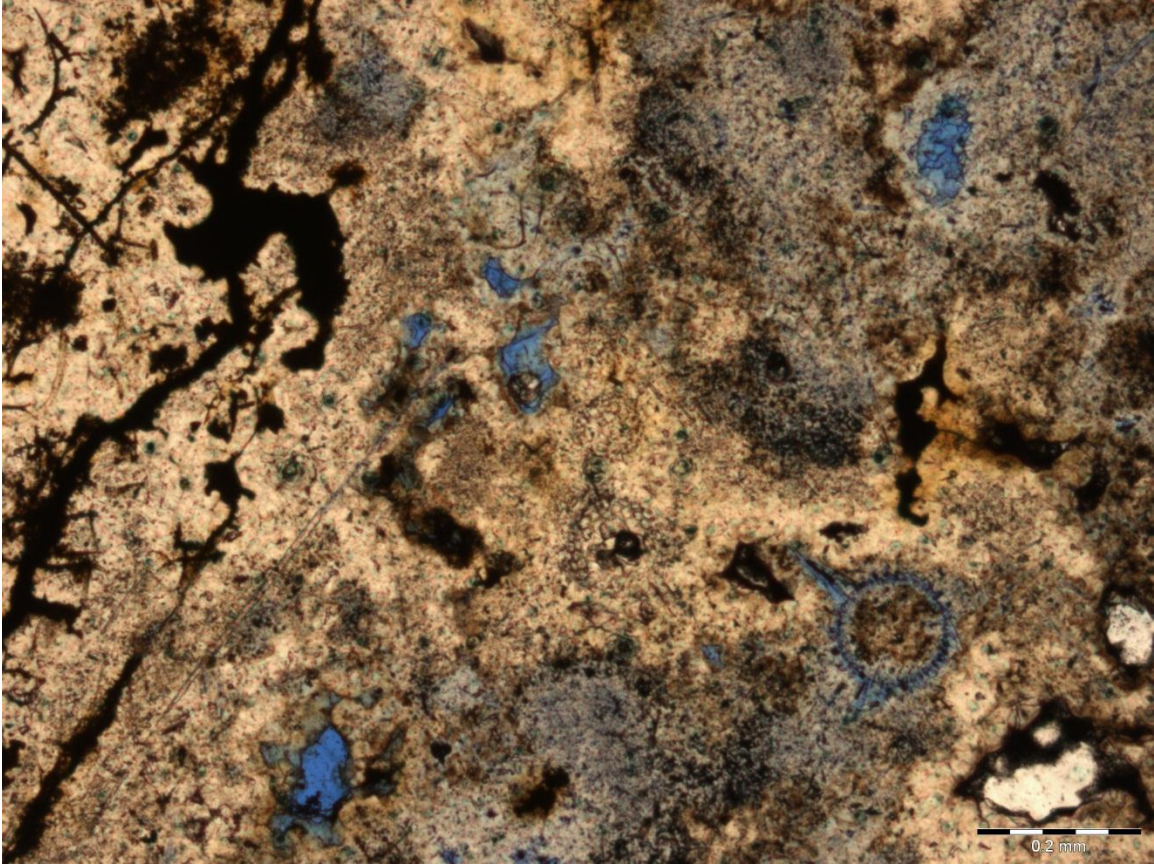
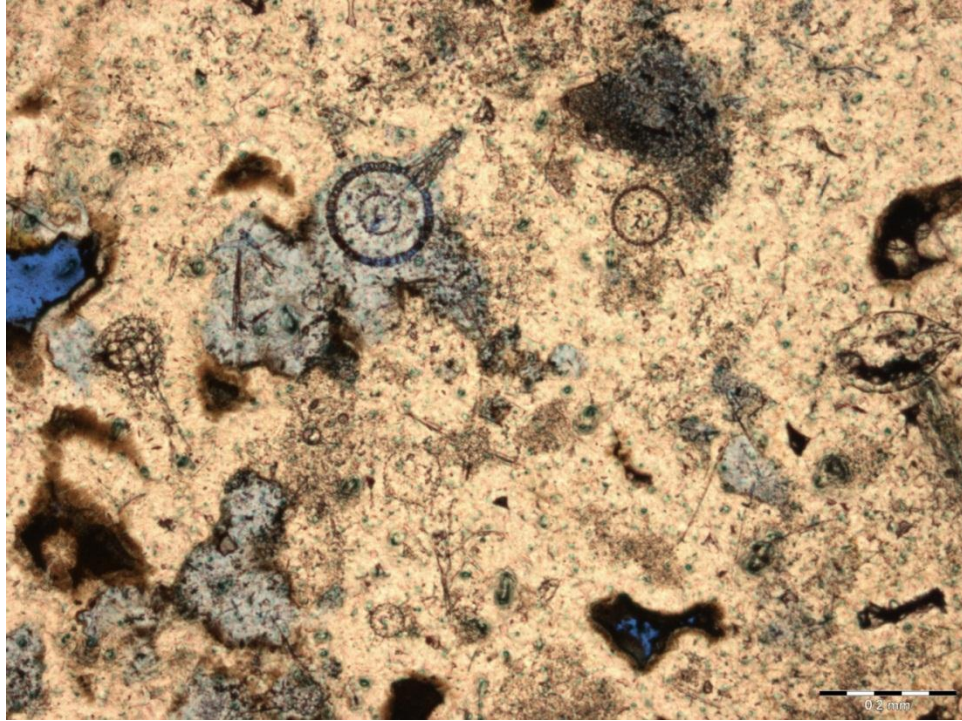


Figure B-6: WSPR3-B. From the WSP outcrop. Delicate radiolarian structures are throughout this rock. Also, a dark fluid has filled many pore spaces (likely residual oil staining).



FigureB-7: WSPR3-E in PPL. Several different kinds of radiolarians, including delicate structures are preserved. Radiolarian spines are also found here.

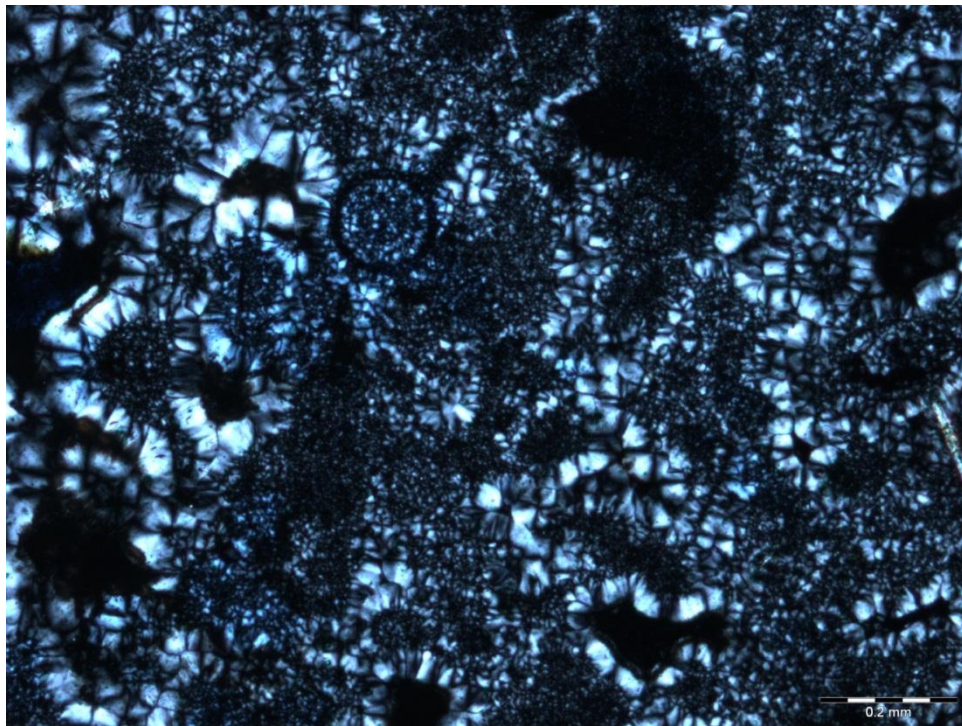
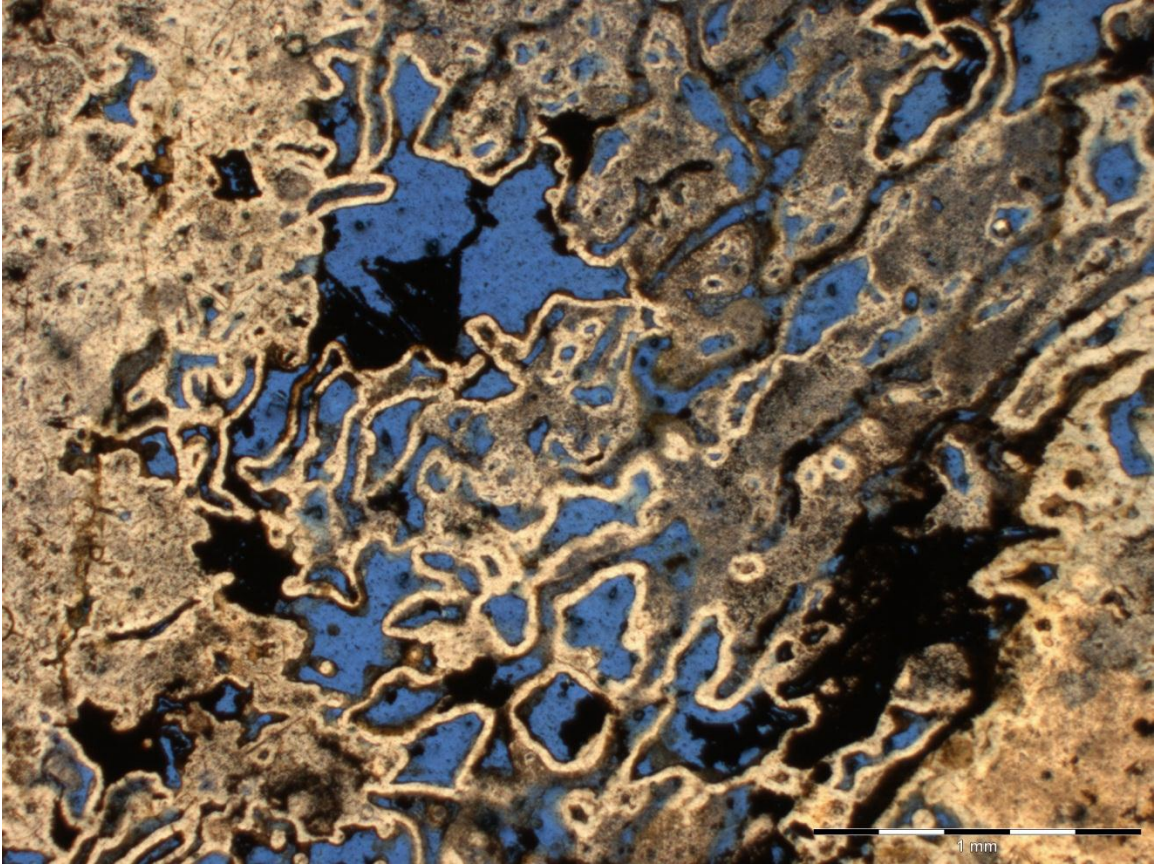


Figure B-8: WSPR3-E in CPL. Here, chert grains and chalcedony cement are highlighted. They seem to be the main contributors to this rock. Outlines of radiolarians can still be picked out in this view.



FigureB-9: WSPR3-G. At the center of the phosphate nodule this highly intricate pattern of porosity can be seen. This is likely due to mass dissolution of high numbers of radiolarians.

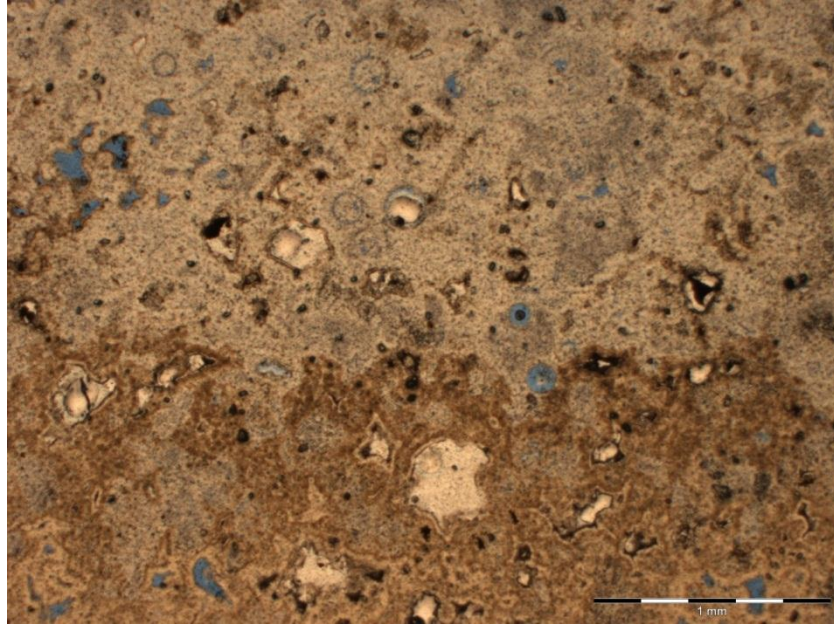


Figure B-10: WSPR4-B in PPL Out of the WSP outcrop. This slide shows preservation of a delicate radial structure and many variations of which other radiolarians have succumbed to dissolution. The darker area in the lower half of the picture is a different ring within the nodules.

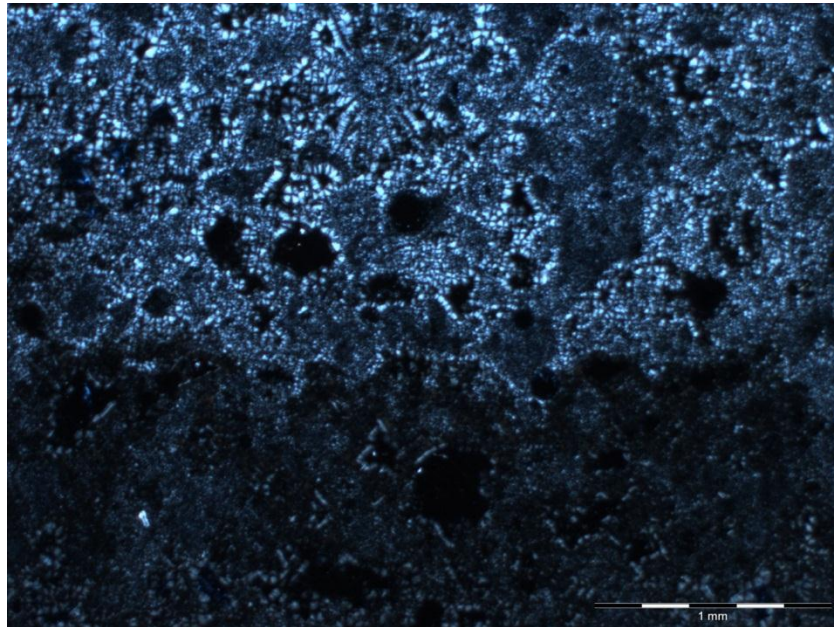


Figure B-11: WSPR4-B in CPL. The delicate radial structure can be made out easier in this view because the chalcedony cement is lighting up the pattern of the radiolarian. Another distinction is between the two bands. There appears to be a higher silica content in the upper half than in the lower half.

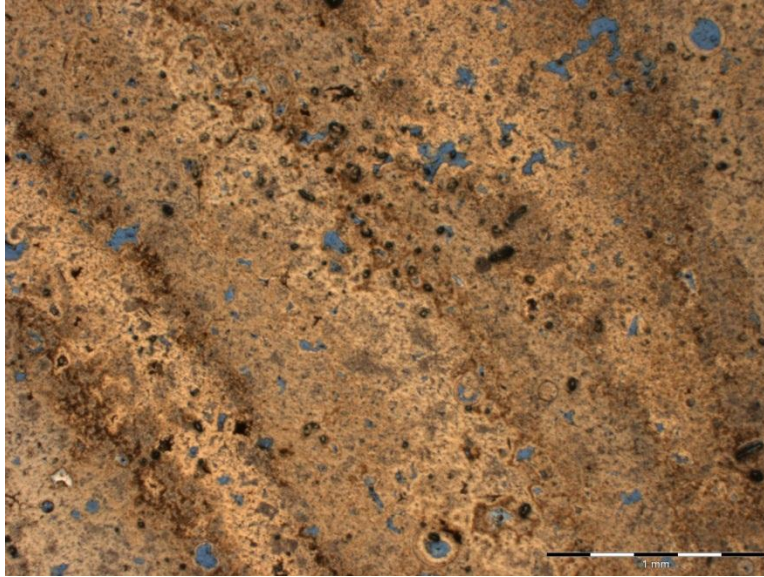


Figure B-12: WSPR5-B in PPL. This phosphate nodule is from the WSP outcrop. The internal structure of the rings is very noticeable here. Radiolarians are still found throughout the many layers of this nodule.

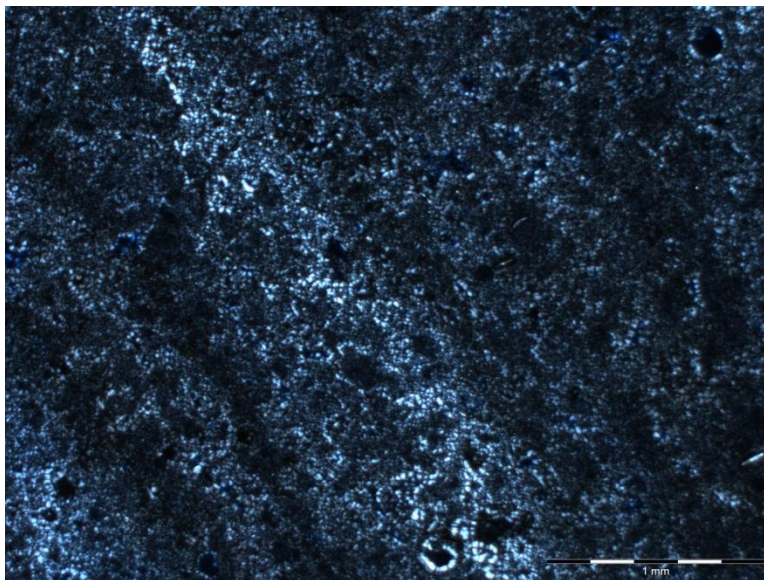


Figure B-13: WSPR5-B in CPL. The rings are still visible in this view. Silica lights up the rings and makes it easy to point out the many different rings due to silica content therein.

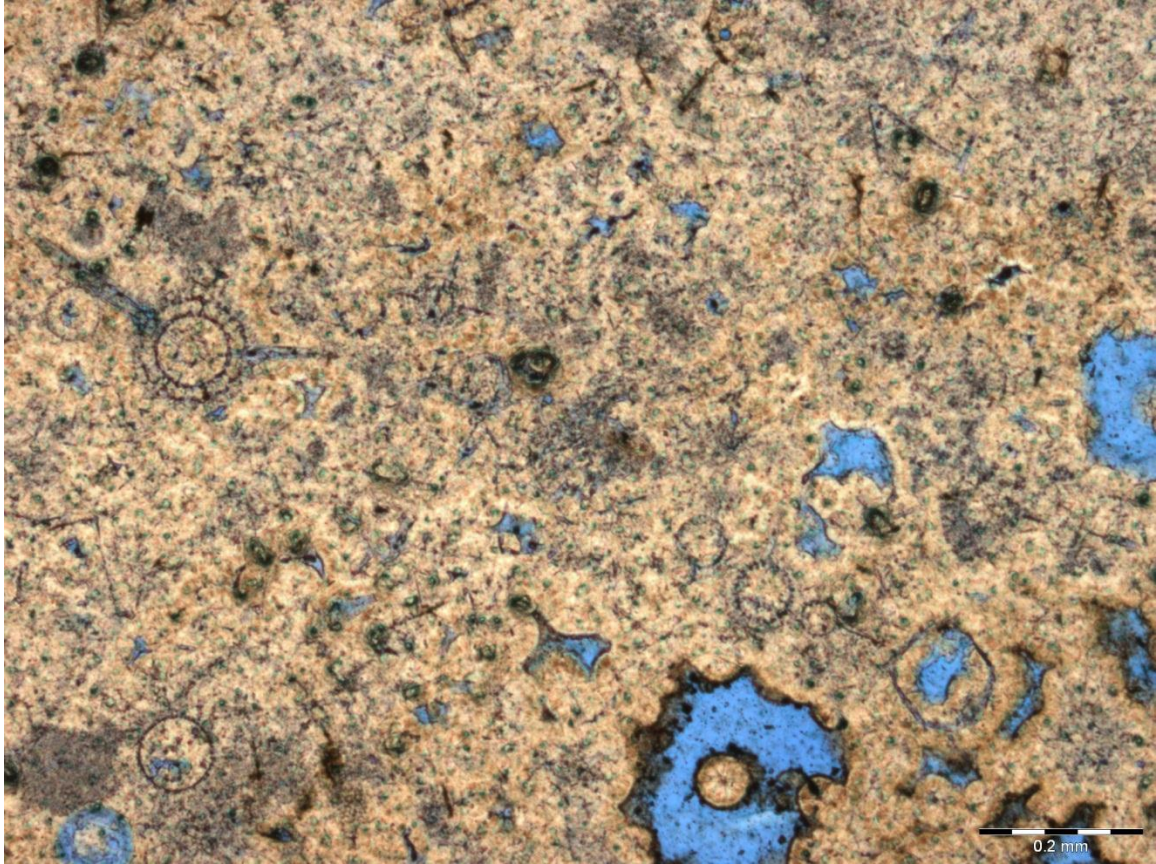


Figure B-14:WSPR5-E. Multiple delicate structures are preserved here. However, other radiolarians have gone through different phases of dissolution.



Figure B-15: WSPR7-B in PPL. This nodule is from the WSP. A large, delicate radiolarian form has been very well preserved. The spines seem to be mostly intact.

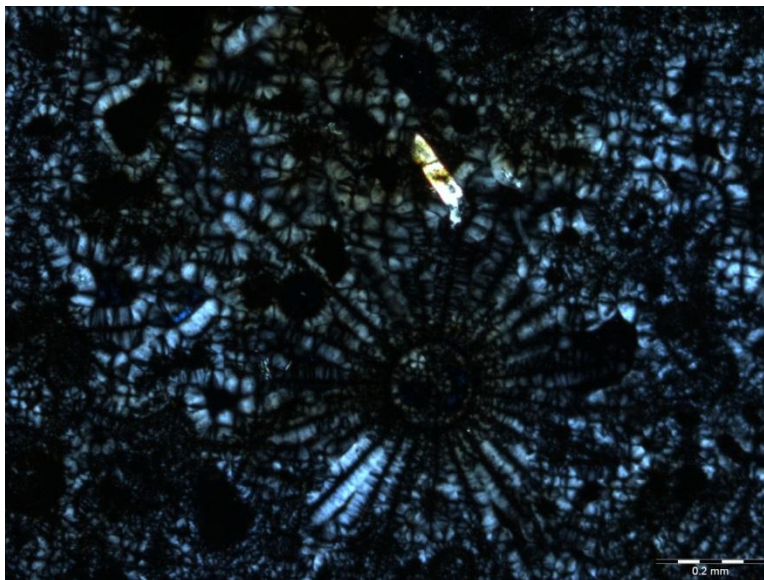


Figure B-16: WSPR7-B in CPL. The radiolarian can almost be made out easier with CPL than with PPL. Chalcedony cement is lining the spines.

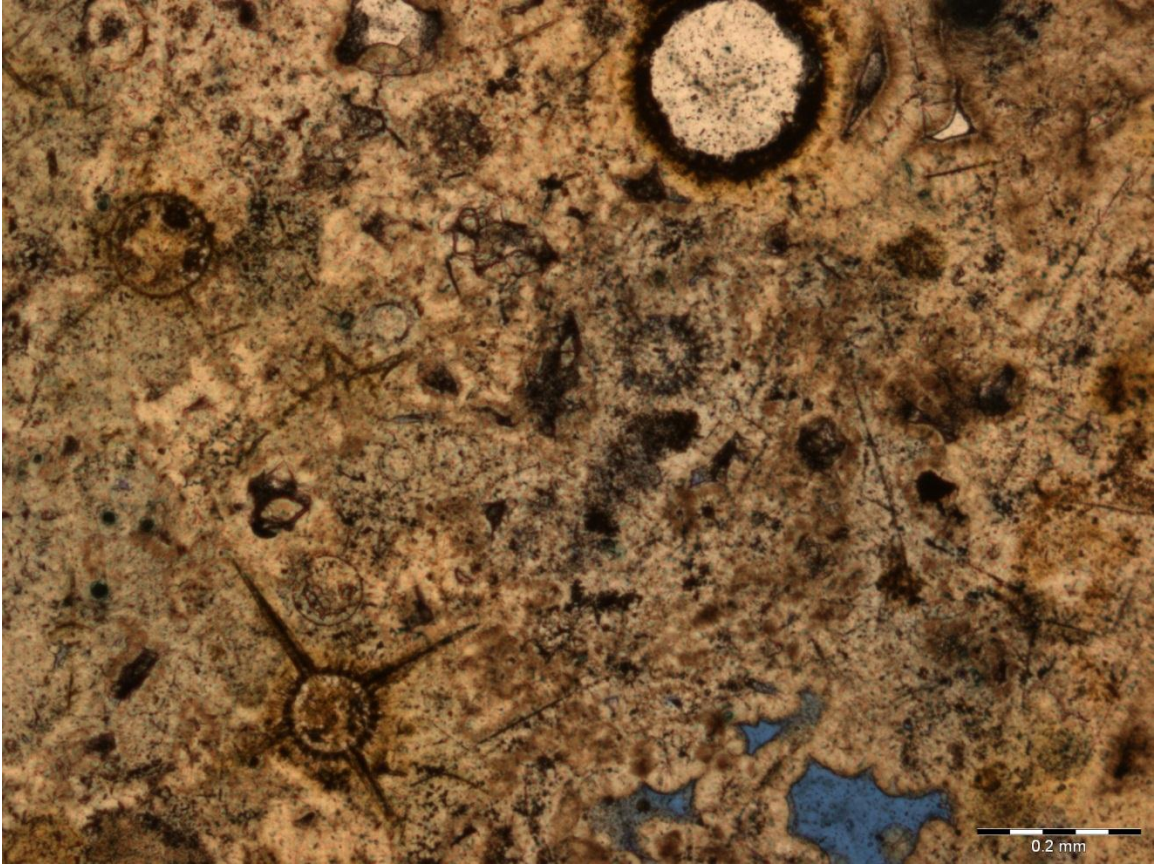


Figure B-17: WSPR7-G. This nodule is from the WSP. Different kinds of delicate radiolarian structures are preserved here.

Appendix C

TOC SUMMARY SHEET

Sample #	Adjusted Weight % TIC	Adjusted Weight % TC	TOC
WSP 1	0.334687958	0.11033583	-0.2243521
WSP 2	0.00234322	0.027834684	0.02549146
WSP 3	10.51298071	10.84013657	0.32715586
WSP 4	0.412716185	0.364979871	-0.0477363
WSP5	0.337836235	0.280487183	-0.0573491
WSP6	0.001179681	0.027553381	0.0263737
WSP7	0.000406787	0.037370433	0.03696365
WSP8	0.002431567	0.02721806	0.02478649
WSP9	0.00460279	0.027134485	0.0225317
WSP 10	0.409536711	0.342659124	-0.0668776
wsp 11	6.05126E-05	1.322574655	1.32251414
WSP 12	0.000666745	0.07267172	0.07200497
WSP 13	0.446357067	0.499637063	0.05328
WSP 14	0.428679831	0.381336619	-0.0473432
WSP 15	0.009399187	0.079104306	0.06970512
WSP 16	0.003491267	0.066908624	0.06341736
WSP 17	0.483074859	0.411823292	-0.0712516
WSP 18	0.000325127	0.036956735	0.03663161
WSP 19	0.403082475	0.57246071	0.16937824
WSP 20	0.002223834	0.037326423	0.03510259
WSP 21	0.416100786	0.315197758	-0.100903
WSP 22	0.013014303	0.030460339	0.01744604
I35N1	0.000360006	10.67227233	10.6719123
I35N2	0.000307124	8.774601233	8.77429411
I35N3	0.000679334	0.393517811	0.39283848
I35N4	0.103323785	0.193344545	0.09002076
I35N 5	0	0.412633569	0.41263357
I35N6	0	0.092246999	0.092247
I35N 7	0	0.426408278	0.42640828
I35N 8	0.220359847	0.31610932	0.09574947
I35N 9	0	0.173399281	0.17339928

Figure C-1: This table summarizes TIC, TC and TOC measurements. Measurements from I35N1 and I35N2 are representative of the underlying non-phosphate nodule-bearing shale at the I-35 North locality. All of the other measurements are from the phosphate nodule-bearing zones in both localities.

I35NR-1

S	Cl	Si	P	Ca	Ti	V	Cr	Mn	Fe	Zn	Pb	U Error	U	Zr	Nb Error	Nb	Mo	Ag
< LOD	2721.5	14726.9	276887	345682	106	137	79.9	< LOD	4545	97.52	< LOD	78.92	< LOD	< LOD	4.4	18.8	8.92	114
< LOD	2566.1	21533.1	276107	341956	117	137	< LOD	< LOD	3955	113	< LOD	81.74	< LOD	< LOD	3.85	17.2	< LOD	86.4
< LOD	2684.8	13021.8	284091	352476	102.1	101	< LOD	< LOD	1341	55.19	< LOD	77.64	< LOD	< LOD	3.47	11.7	10.3	140
< LOD	2707.5	17804.5	278437	346816	162.8	188	< LOD	< LOD	3546	134	< LOD	54.44	133.2	< LOD	4.61	19.4	9.83	115
< LOD	2812.1	20022.1	281416	344280	133.7	148	< LOD	< LOD	3539	94.17	< LOD	87.32	< LOD	< LOD	4.07	15.6	8.63	133
< LOD	2643	21602	272706	333897	202.6	305	109	< LOD	####	206.1	< LOD	50.14	114.2	< LOD	4.58	19.7	11	< LOD
< LOD	2461.7	12555.9	277881	341228	179.5	184	81	< LOD	5632	140.7	< LOD	84.76	< LOD	< LOD	4.89	22	9.67	99.5

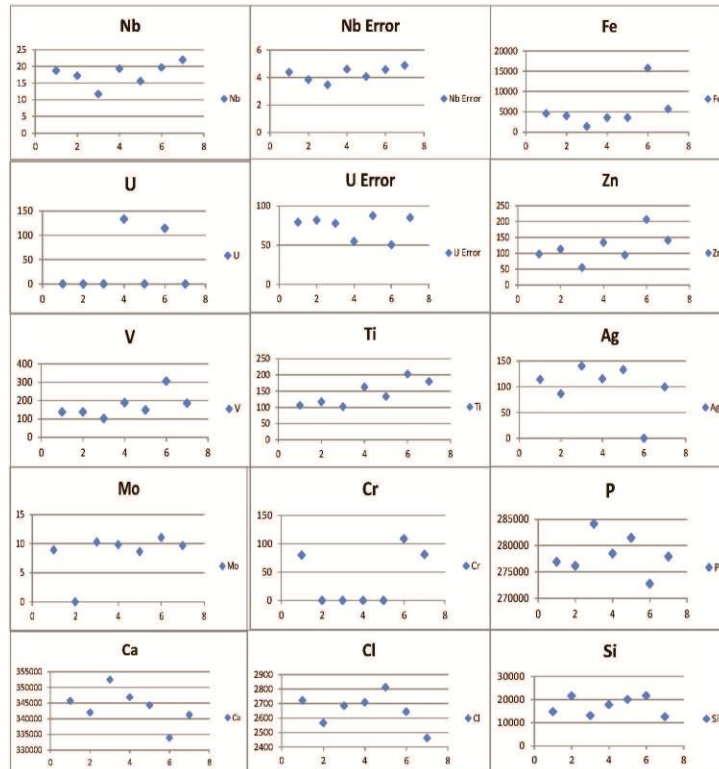


Figure C-2: Sample I35NR-1. This phosphate nodule was taken from I-35 North for statistical analysis. This nodule is flat and has almost no internal structure in the macro view.

I35NR-2

S	Cl	Si	P	Ca	Ti	V	Cr	Mn	Fe	Zn	Pb	U Error	U	Zr	Nb Error	Nb	Mo	Ag
410	< LOD	42546.8	173223	323503	128.1	101	< LOD	59.15	518	48.7	14.2	31.25	< LOD	< LOD	1.52	17.7	7.02	116
384	< LOD	52003.1	168554	325130	163.7	115	< LOD	< LOD	927	63	16.7	32.63	< LOD	< LOD	1.54	17.2	7.48	126

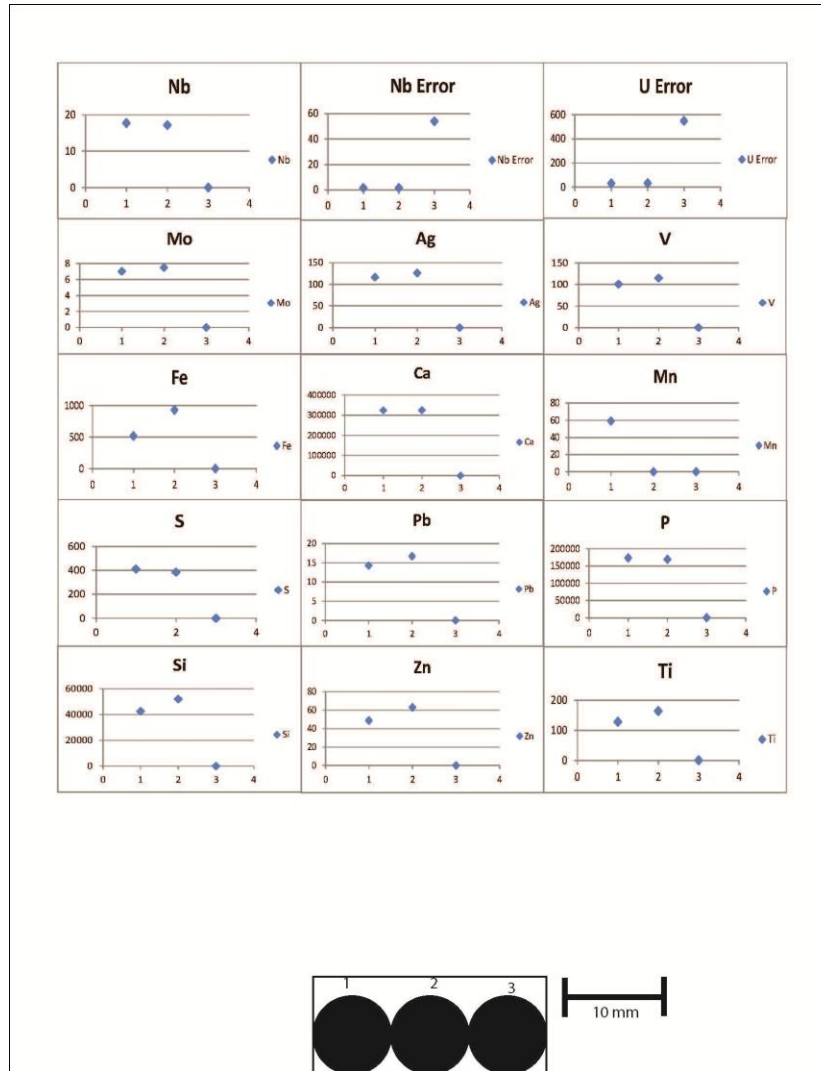


Figure C-3: Sample I35NR-2. This nodule was sampled from I-35 North. It had no internal structure and was elongate. The measurement radii of the XRF analyzer (indicated by the dark spots) were increased to eight millimeters in diameter.

I35NR-3

S	Cl	Si	P	Ca	Ti	V	Cr	Mn	Fe	Zn	Pb	U Error	U	Zr	Nb Error	Nb	Mo	Ag
2888.8	< LOD	164727.4	139323	230375	78.24	123	< LOD	< LOD	259	< LOD	11.3	24.43	< LOD	6.93	1.24	3.8	8.03	109
2667.2	< LOD	204813.9	113342	197524	154.3	156	< LOD	< LOD	544	36.13	13.9	11.63	31.61	6.12	1.21	3.34	6.83	101
2820.6	< LOD	112240.7	148634	254187	396.6	308	< LOD	< LOD	1276	15.9	17.1	15.39	274.2	17.9	1.43	9.92	< LOD	109

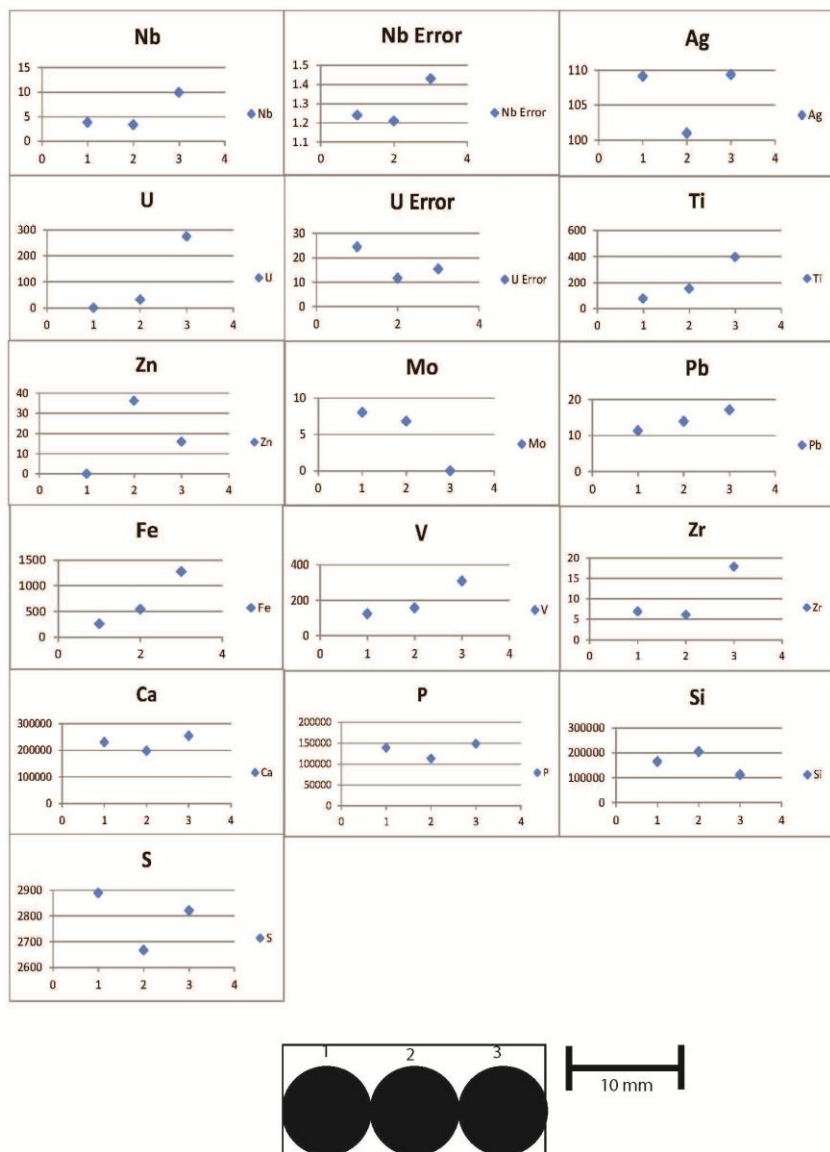


Figure C-4: Sample I35NR-3. This phosphate nodule was lacking of internal structure long and flat. The color was very dark, but this is due to detrital influx. This nodule comes from I-35 North.

1.5 Ft Below Marker

S	Cl	Si	P	Ca	Ti	V	Cr	Mn	Fe	Zn	Pb	U Error	U	Zr	Nb Error	Nb	Mo	Ag
< LOD	< LOD	407130.8	1097.3	852.05	399	217	< LOD	< LOD	1816	< LOD	12.3	9.93	< LOD	14.4	2	< LOD	< LOD	< LOD
< LOD	< LOD	416805.3	1646.2	1018.6	410.2	209	< LOD	< LOD	1529	< LOD	12.4	5.07	14.28	14.4	2	< LOD	< LOD	< LOD
605.2	< LOD	25032.33	189515	353061	140.9	89.6	< LOD	64.8	1248	95.17	20.1	17.74	214.3	17.2	1.66	21.1	8.91	125
522	< LOD	29401.5	189467	345737	167.2	140	< LOD	70.53	1427	119.9	14.7	16.65	130.2	19.9	1.6	19.6	9.19	124
504.8	< LOD	32378.12	187664	326647	176.5	115	< LOD	< LOD	1306	102.8	11.7	16.29	157.1	18.6	1.57	19.4	8.6	112
< LOD	< LOD	427404.5	938.98	197.03	316.1	166	< LOD	< LOD	1549	< LOD	13	9.83	< LOD	14.9	2	< LOD	4.46	< LOD
< LOD	< LOD	416431.6	1351.7	605.83	449.9	206	< LOD	< LOD	1031	< LOD	13.4	5.03	11	17.4	2	< LOD	< LOD	27.4
< LOD	< LOD	420125.3	1410.2	535.55	418.9	224	< LOD	< LOD	1781	< LOD	11.8	9.76	< LOD	16.6	2	< LOD	2.95	< LOD
< LOD	< LOD	423485.9	2555.1	493.67	428.8	213	< LOD	< LOD	1514	< LOD	12.5	5	10.07	15.6	2	< LOD	2.54	28
< LOD	< LOD	419823.9	3563.5	698.4	434.9	257	< LOD	< LOD	2802	< LOD	12	5.13	16.64	16.7	2	< LOD	6.34	< LOD
985	< LOD	30852.33	190768	349276	143.4	119	< LOD	70.46	1254	123.6	16.5	16.7	136.9	17.7	1.6	19	9.24	142

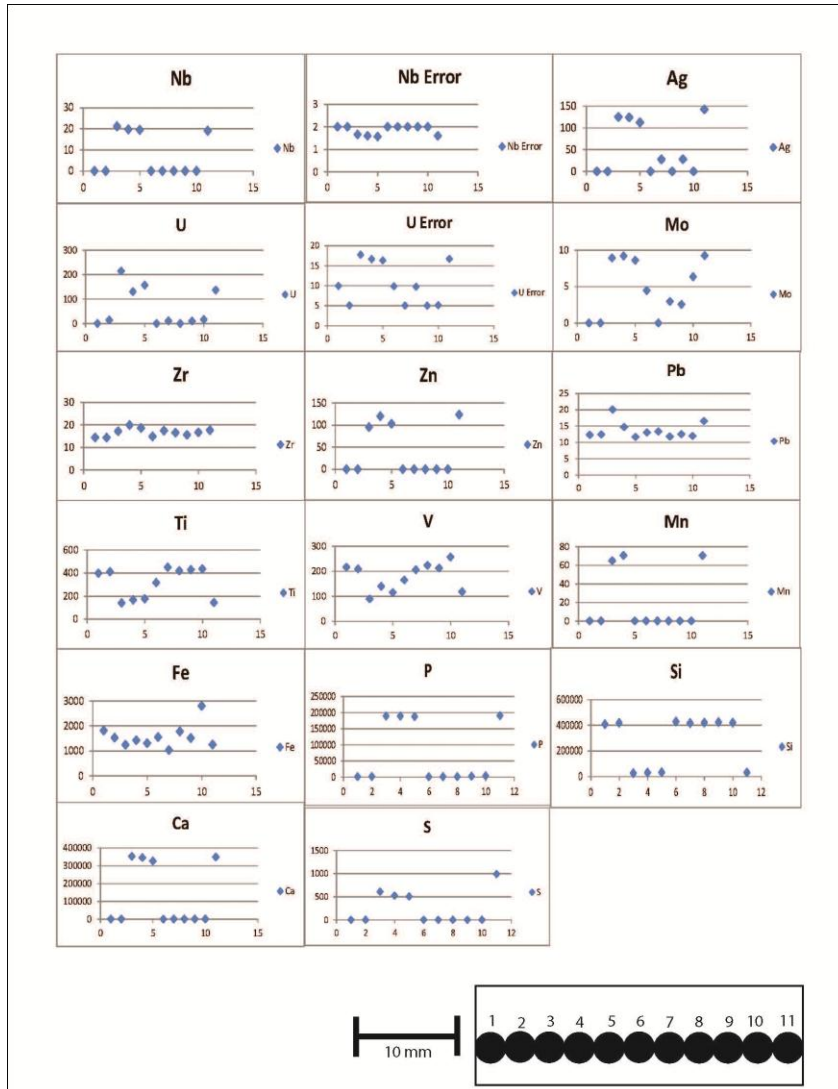


Table C-5: This sample was taken from thirty-six inches below the geologic marker at I-35 North.

4 Ft Above Marker

S	Cl	Si	P	Ca	Ti	V	Cr	Mn	Fe	Zn	Pb	U Error	U	Zr	Nb Error	Nb	Mo	Ag
24190.2	< LOD	535573.2	< LOD	253.75	1144	1796	< LOD	< LOD	4305	59.34	11.45	32.98	164.3	36	2.57	< LOD	92.1	< LOD
25709.3	< LOD	537181.3	5248	< LOD	992.5	1943	< LOD	< LOD	4067	61.07	< LOD	42.74	138.9	31	2.81	< LOD	72	< LOD
21269.9	< LOD	540096.3	6388.8	174.16	862	1672	< LOD	< LOD	4625	39.58	< LOD	37.73	118.4	28.6	3.12	< LOD	58.5	< LOD
20799.4	< LOD	539005.6	6237.2	448.49	856.4	1598	< LOD	< LOD	5306	49.17	< LOD	37.39	119.5	28.8	3.12	< LOD	60	< LOD
18877.1	< LOD	559197.5	6723.8	255.59	832.5	1272	< LOD	< LOD	3672	34.74	< LOD	32.45	98.82	24.4	2.94	< LOD	46.5	< LOD
17485.5	< LOD	552953.5	8422.8	1055.4	936.9	1419	< LOD	< LOD	3907	41.31	< LOD	37.47	111.9	22.8	3.64	< LOD	45.3	< LOD
18889.8	< LOD	542584.9	8472	667.23	958.5	1577	< LOD	< LOD	3096	37.97	< LOD	39.8	123.1	22.2	2.49	< LOD	41.5	< LOD
17809.5	< LOD	547250.4	10317	1230.4	784.7	1280	< LOD	< LOD	4460	30.3	< LOD	35.03	106.5	22.8	2.49	< LOD	52.4	< LOD
17745.4	< LOD	545338	11085	1499	785.6	1332	< LOD	< LOD	3033	33.01	< LOD	31.75	93.36	21.2	2.42	< LOD	41.4	< LOD
18066.6	< LOD	542903	11071	1638	896.9	1435	< LOD	< LOD	3755	37.03	< LOD	31.05	90.66	21.8	2.48	< LOD	47.8	< LOD
24498.9	< LOD	534474.4	10701	1076.3	1732	1566	< LOD	< LOD	2497	36.04	10.33	78.72	263.1	39.9	2.71	< LOD	82.8	< LOD
17647	< LOD	561704.4	12011	2039.6	1226	1029	< LOD	< LOD	3101	26.24	< LOD	70.15	229.3	24.9	2.7	< LOD	63.5	< LOD
17021.2	< LOD	553656.5	12962	1343.4	1833	1878	< LOD	< LOD	4641	37.15	< LOD	59.03	172.8	18	2.78	< LOD	48.8	< LOD
22682.4	< LOD	543133.8	8572.9	603.08	981.1	1692	< LOD	< LOD	3182	53.47	< LOD	44.45	144.3	31.7	2.56	< LOD	41.7	< LOD
21494.7	< LOD	532339.9	6836.7	196.38	1243	2050	< LOD	< LOD	4523	77.74	< LOD	51.7	167.4	35	2.51	< LOD	49.4	< LOD
21102.7	< LOD	533642.9	9247	< LOD	2314	2573	< LOD	< LOD	3887	55.45	< LOD	61.03	183.9	33.9	2.77	< LOD	43	< LOD
7625.31	< LOD	621233.1	13463	< LOD	3517	2397	< LOD	112.1	586	< LOD	< LOD	42.58	97.39	< LOD	2.87	< LOD	19.1	< LOD

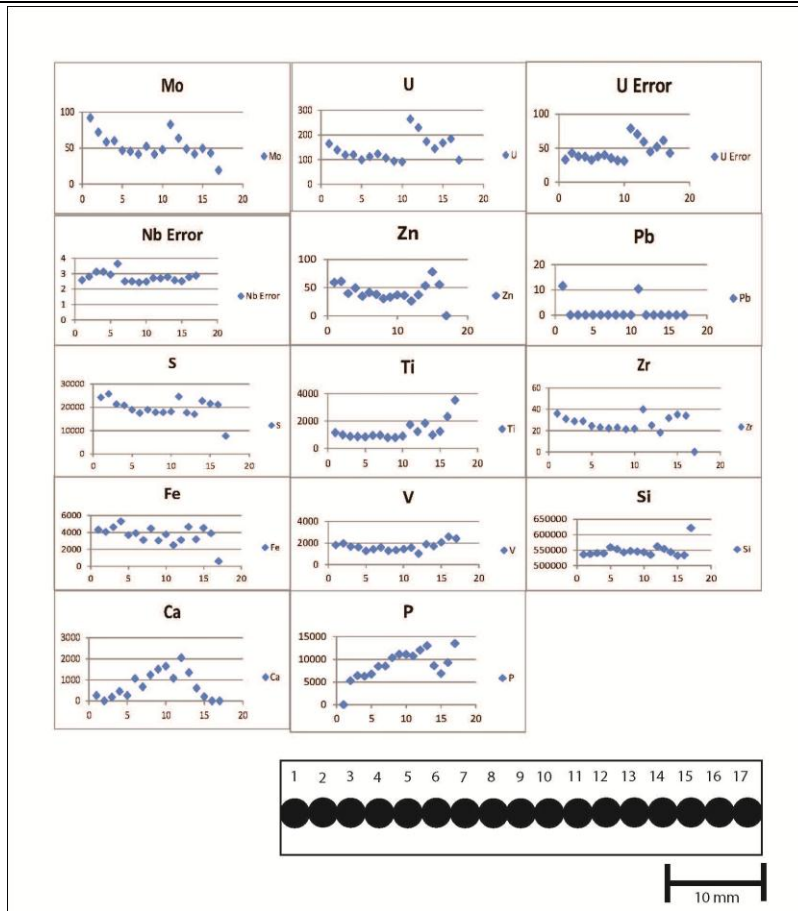


Figure: C-6: 4 feet above the geologic marker. This is a laminar nodule.

8 Ft Below Marker

S	Cl	Si	P	Ca	Ti	V	Cr	Mn	Fe	Zn	Pb	U Error	U	Zr	Nb Error	Nb	Mo	Ag
< LOD	< LOD	381736.8	< LOD	603.1	458.4	295	< LOD	< LOD	2646	< LOD	11.7	5.31	19.73	18.9	2	< LOD	< LOD	< LOD
< LOD	< LOD	385305.6	914.17	573.19	341.4	309	< LOD	< LOD	6313	< LOD	11.1	5.22	13.32	15.1	2	< LOD	7.98	31.4
< LOD	< LOD	207990	110239	195502	112.1	89.1	< LOD	< LOD	176	23.01	12.8	12.03	42.94	11.8	1.26	5.91	5.76	101
< LOD	< LOD	164433.7	132442	239770	147.7	107	< LOD	< LOD	475	43.59	16.4	14.31	161.1	15.4	1.39	10.5	4.01	93.9
< LOD	< LOD	257498.4	88010	114633	434.5	305	< LOD	< LOD	1778	12.32	13.5	10.72	205.9	21.7	1.18	7.48	< LOD	52.1

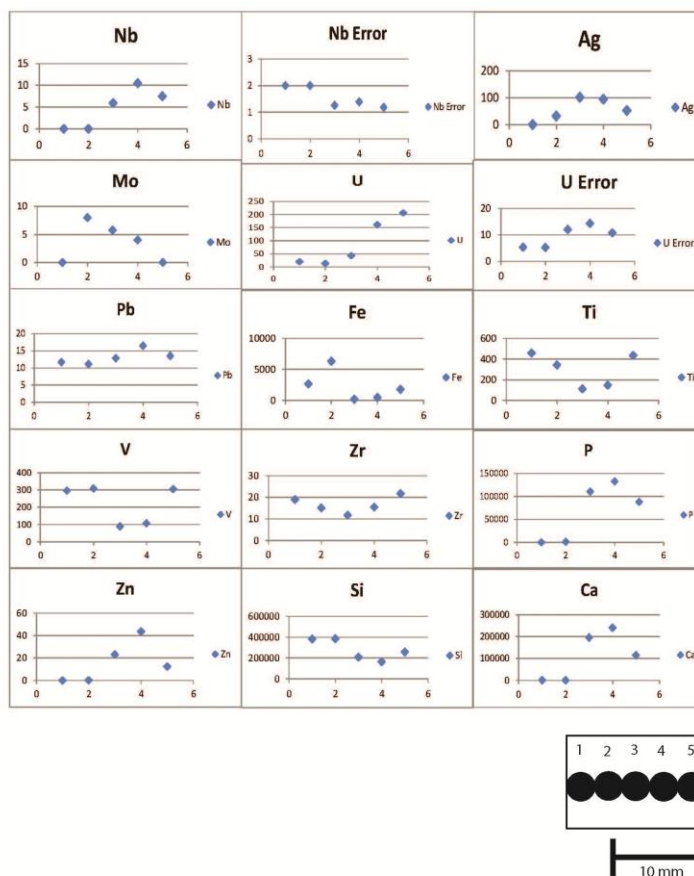


Figure C-7: Sample I35N 3. This was taken eight feet below the geologic marker at the I-35 North locality. This was a shale attached to a phosphate nodule and the nodule had a laminar morphology.

I35N Laminated Nodule 1-7

S	Cl	Si	P	Ca	Ti	V	Cr	Mn	Fe	Zn	Pb	U Error	U	Zr	Nb Error	Nb	Mo	Ag
2246.3	2887.5	63066.5	277375	335667	203.3	147	< LOD	< LOD	903	53.28	< LOD	84.45	< LOD	< LOD	3.64	14.1	12.9	108
2088.4	3134.1	31788.6	279286	343948	266.1	192	< LOD	< LOD	480	63.47	< LOD	83	< LOD	< LOD	4.23	17.2	12.7	122
1946.2	3109.8	27442.7	282308	342962	261.4	148	< LOD	< LOD	582	76.27	< LOD	78.52	< LOD	< LOD	3.37	8.79	13.7	142
7716.1	< LOD	83815.4	154203	266181	3754	2166	< LOD	414.4	####	310.3	< LOD	155.98	< LOD	< LOD	5.41	13.9	24.8	< LOD
3307.6	2596.7	27315.1	270798	318701	308.5	224	< LOD	< LOD	1535	129.3	< LOD	78.85	< LOD	25.5	6.51	< LOD	9.37	103
2251.1	2914	19960.5	287923	353995	137.9	108	< LOD	< LOD	668	68.15	< LOD	78.27	< LOD	< LOD	3.59	10.5	13.5	123
1575.8	2802.8	20799.9	286384	349085	432	249	< LOD	< LOD	495	59.93	< LOD	82.87	< LOD	< LOD	3.64	11.3	19	122

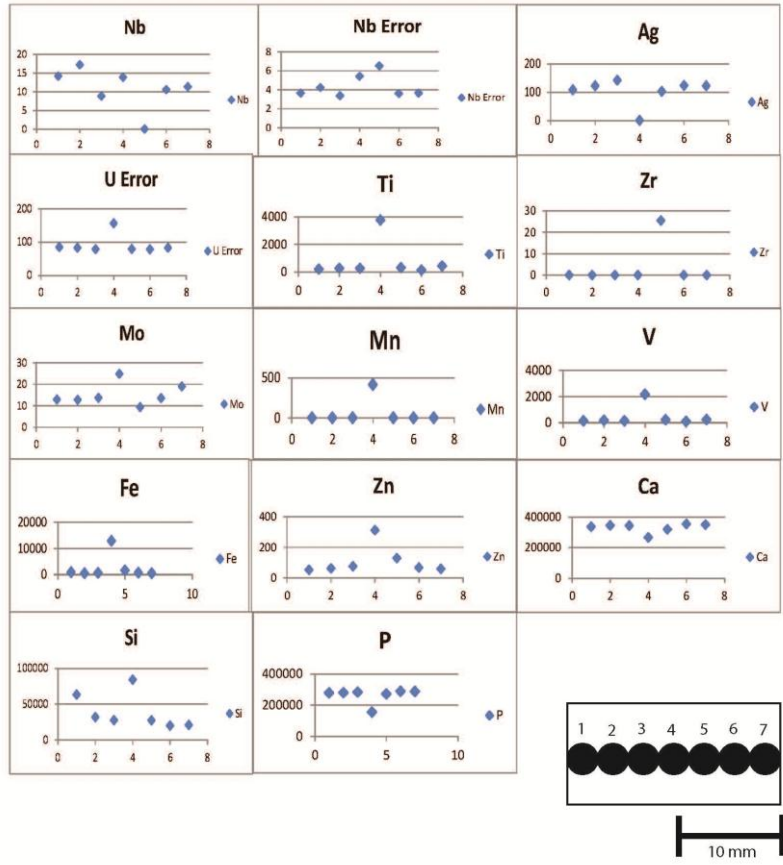


Figure C-8: Sample I35N 3. This is the same v nodule as Figure 38 however these measurements went perpendicular to the other sample. The trend here shows the center mass of the nodule.

Phosphate Couplet

S	Cl	Si	P	Ca	Ti	V	Cr	Mn	Fe	Zn	Pb	U Error	U	Zr	Nb Error	Nb	Mo	Ag
< LOD	< LOD	496162.3	129153	118113	27.2	35	< LOD	< LOD	136	21.42	< LOD	49.85	< LOD	< LOD	4.7	< LOD	< LOD	< LOD
< LOD	< LOD	526394	101557	96856	< LOD	< LOD	< LOD	< LOD	115	16.3	< LOD	40.69	< LOD	< LOD	4.47	< LOD	< LOD	73.7
< LOD	< LOD	495483.6	113946	117066	53.89	38.4	< LOD	< LOD	200	24.8	< LOD	49.66	< LOD	< LOD	4.73	< LOD	< LOD	< LOD
< LOD	500.28	446696.6	127094	132468	102.3	63.8	< LOD	< LOD	326	32.17	< LOD	48.96	< LOD	< LOD	4.73	< LOD	< LOD	70.3
2358.2	< LOD	447749.4	143109	139205	224.6	158	< LOD	< LOD	1368	64.5	< LOD	72.39	232.4	< LOD	5.45	< LOD	< LOD	122
< LOD	< LOD	571877.5	10053	5200.3	355	269	< LOD	< LOD	4071	55.81	< LOD	27.65	< LOD	19	3.92	< LOD	13.3	< LOD
2315.9	2390.1	53208.27	259943	321381	381	227	< LOD	< LOD	979	318.5	< LOD	82.27	256.5	16.8	4.18	14.1	< LOD	< LOD
< LOD	< LOD	641759.1	< LOD	888.08	82.3	81.5	< LOD	< LOD	804	< LOD	< LOD	24.38	< LOD	< LOD	2.39	< LOD	< LOD	< LOD
< LOD	3201.4	38695.98	271797	343485	148.9	105	< LOD	< LOD	893	169.7	< LOD	89.76	299.7	< LOD	4.69	19.8	< LOD	178
< LOD	3131.9	27637.14	280711	352394	224.4	120	< LOD	< LOD	437	184.6	< LOD	86.31	< LOD	< LOD	4.02	14.6	9.75	127
< LOD	2988.2	28762.72	275421	345482	133.2	83	< LOD	< LOD	458	195.8	< LOD	81.7	< LOD	< LOD	3.73	11.7	11.9	113
< LOD	3216.1	31113.29	280642	348328	182.7	130	< LOD	< LOD	650	256.2	< LOD	89.32	< LOD	< LOD	3.79	12.3	13.1	116
< LOD	2300.3	47271.53	260499	323027	309.4	188	< LOD	< LOD	853	320.6	< LOD	67.18	190.3	< LOD	4.15	14.4	13.2	< LOD
< LOD	2981	39618.6	276463	345081	216.7	132	< LOD	< LOD	405	202.5	< LOD	80.41	< LOD	< LOD	3.91	14	15.1	122
< LOD	2792.8	45184.86	277734	347760	179.8	121	< LOD	< LOD	509	221.3	< LOD	94.67	< LOD	< LOD	3.97	13.7	12.4	117
1221.3	2956.4	31556.15	277525	346484	231.8	152	< LOD	< LOD	1792	200.1	< LOD	98.27	332.9	< LOD	4.92	21.2	9.47	123

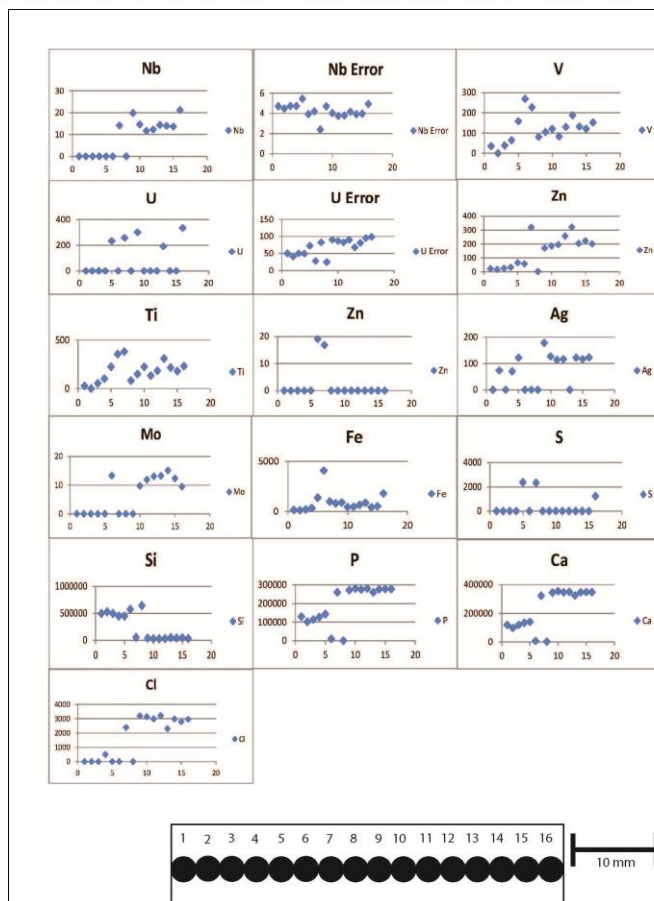


Figure C-9: Sample I35N 5. This sample is referred to as the phosphate nodule ouplet since it incorporates both laminar nodule and a concentric nodule (lowest to highest readings in that order). They are separated by a thin layer of invasive chert. This is one of two.

Phosphate Couplet 1-9

S	Cl	Si	P	Ca	Ti	V	Cr	Mn	Fe	Zn	Pb	U Error	U	Zr	Nb Error	Nb	Mo	Ag
< LOD	< LOD	491597.8	114821	113541	42.4	41.5	< LOD	< LOD	226	25.02	< LOD	48.2	< LOD	< LOD	4.69	< LOD	< LOD	90.1
< LOD	< LOD	464531.2	122897	125780	40.97	< LOD	< LOD	< LOD	197	26.23	< LOD	49.54	< LOD	< LOD	3.49	< LOD	< LOD	82.5
< LOD	355.02	494916.1	111362	110439	57.76	40.6	< LOD	< LOD	192	24.34	< LOD	45.83	< LOD	< LOD	4.16	< LOD	< LOD	73.4
< LOD	1110.5	443854.7	136449	139451	122.4	83.9	< LOD	< LOD	70.6	22.43	< LOD	53.15	< LOD	< LOD	4.82	< LOD	< LOD	84.8
< LOD	< LOD	679517.1	20762	11009	606.4	373	< LOD	< LOD	4503	92.39	< LOD	66.23	170.9	16.9	2.63	5.65	10.2	< LOD
< LOD	< LOD	645197.9	8245.3	712.65	505.3	241	< LOD	< LOD	1135	12	< LOD	28.72	< LOD	11.7	2.39	< LOD	< LOD	< LOD
< LOD	< LOD	630904.9	17585	3562.4	429.2	230	< LOD	< LOD	774	12.35	< LOD	24.17	< LOD	8.2	2.35	< LOD	< LOD	< LOD
< LOD	< LOD	663713.6	< LOD	446.87	42.89	40.5	< LOD	< LOD	185	< LOD	< LOD	20.83	< LOD	< LOD	2.27	< LOD	< LOD	< LOD
4125.3	< LOD	645903.6	8795.9	1092.3	487.9	255	< LOD	< LOD	1008	15.72	< LOD	25.47	< LOD	8.74	2.39	< LOD	< LOD	< LOD

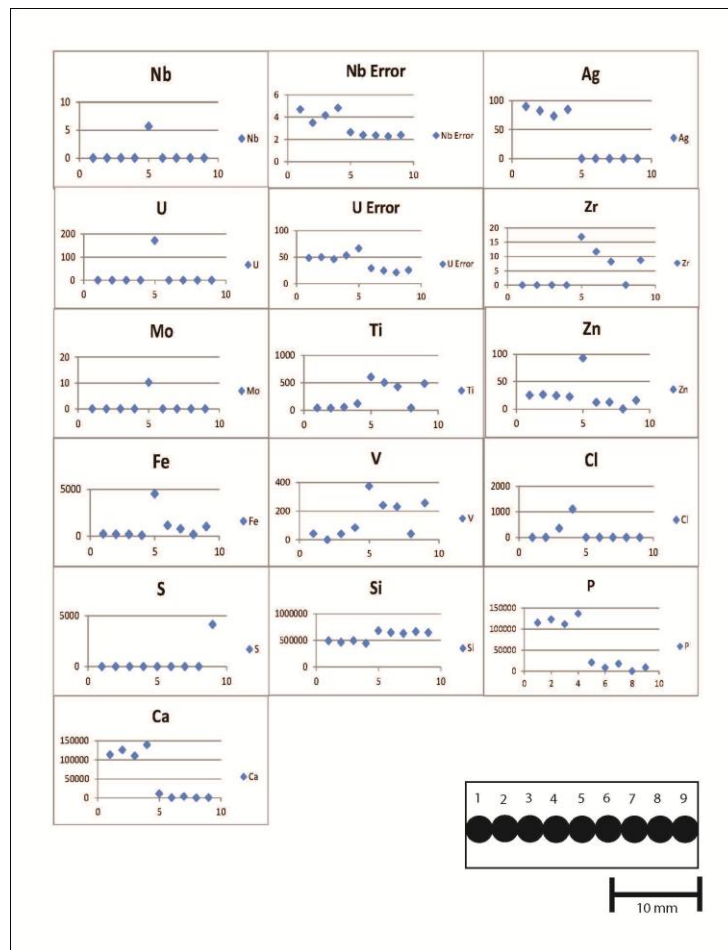


Figure C-10: Sample I35N 5. This is the same sample as Figure #. However, these measurements were taken on the opposite side of this sample; and the concentric nodule is not available to be measured. Instead, what is left of the host shale is being examined along with the laminar nodule.

MSC

S	Cl	Si	P	Ca	Ti	V	Cr	Mn	Fe	Zn	Pb	U Error	U	Zr	Nb Error	Nb	Mo	Ag
< LOD	2123	35472.6	1086	1591.7	674.5	643	103	< LOD	2797	128.8	10.9	6.55	58.2	32.2	1	2.3	< LOD	< LOD
< LOD	1623.2	34438.7	< LOD	1488.2	740.6	900	120	< LOD	####	313.4	18.7	8.04	71	25.4	2	< LOD	2.67	< LOD
< LOD	1595.8	33327.4	< LOD	2044.3	737.4	749	116	< LOD	3126	127.2	12.6	7.55	62.8	26.3	2	< LOD	< LOD	< LOD
< LOD	1608.7	33787.8	585.93	2710.9	611.6	639	79.5	< LOD	2338	85	13.4	7.25	38	14.6	2	< LOD	< LOD	< LOD
< LOD	2213.2	35221.6	582.25	657.99	596.4	582	103	< LOD	2377	98.38	12.7	7.49	61.8	24	2	< LOD	< LOD	< LOD

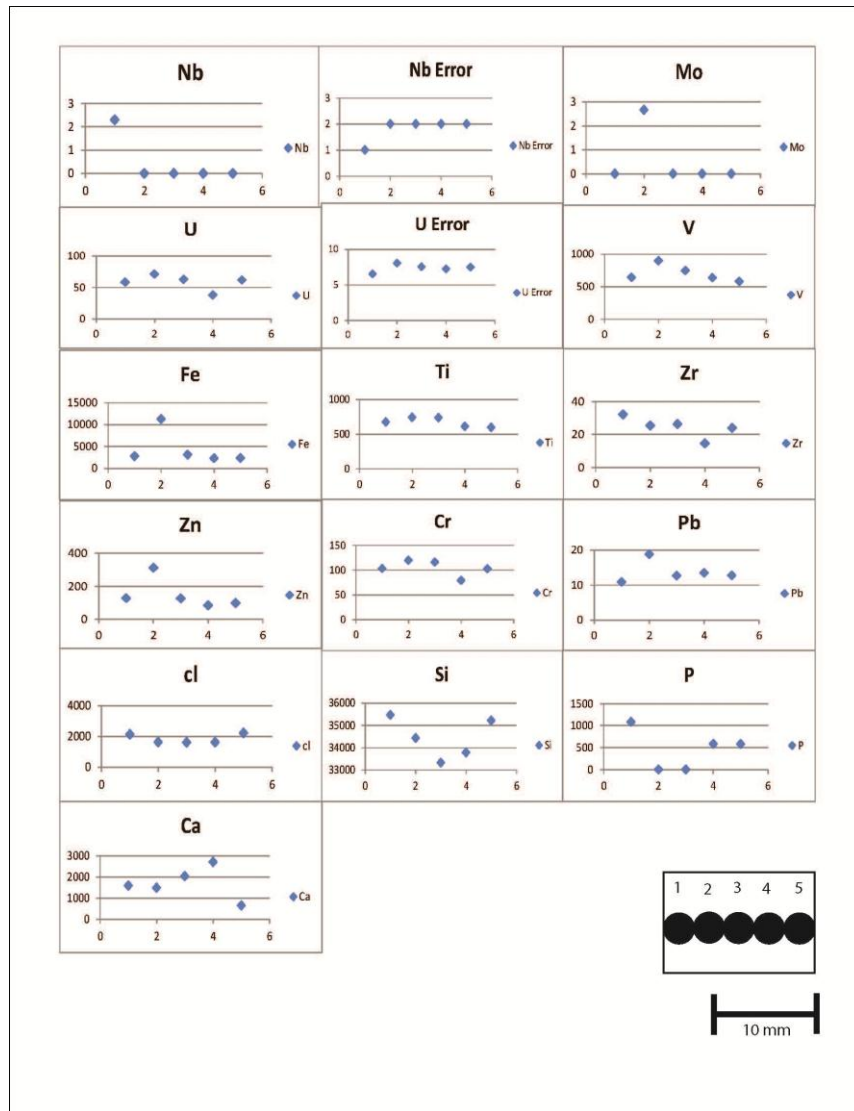


Figure C-11: Sample MSC. This sample was taken sixty feet from the dolomite bed at the WSP. This was a shale that was below a shale that had a phosphate nodule in it. This shale was bleached white, very brittle and was not. The lack of fissility of the rock makes it classified under a mud rock.

MSC PO4

S	Cl	Si	P	Ca	Ti	V	Cr	Mn	Fe	Zn	Pb	U Error	U	Zr	Nb Error	Nb	Mo	Ag
892	931.18	4567.3	33346	263239	198.1	259	< LOD	58.66	1322	919.99	30.5	21.74	305.7	45.7	1.81	20.1	12.4	109
< LOD	1103.3	9213.35	24308	196736	339.3	396	< LOD	111.7	1320	891.12	47.3	25.46	756.9	56.8	1.94	25	< LOD	120
< LOD	1203.5	11284.1	25538	226435	223.8	281	< LOD	< LOD	1191	586.41	22.5	17.98	197.4	55.7	1.69	21.5	8.81	141
525.3	1061.9	4310.42	32297	261861	194.3	256	< LOD	57.46	1901	1176.2	32	23.15	423.2	57.3	1.98	33.3	13.2	83.7

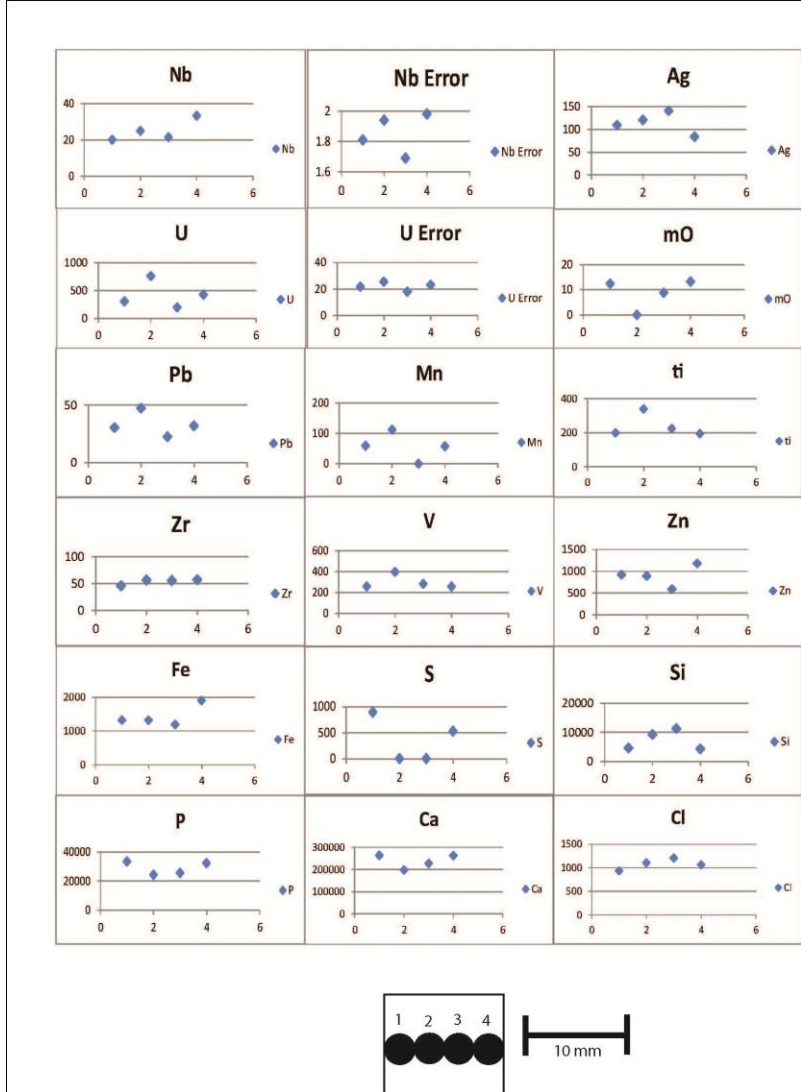


Figure C-12: Sample MSC. This is another part of the package mentioned in Figure 43. This is a concentric phosphate nodule that has very dark bands within it.

MS2

S	Cl	Si	P	Ca	Ti	V	Cr	Mn	Fe	Zn	Pb	U Error	U	Zr	Nb Error	Nb	Mo	Ag
935.9	< LOD	159848.3	122049	268378	409.2	382	< LOD63.27	2182	725.07	24.3	16.63	209.5	27.4	1.6	20.2	7.26	136	
1383	< LOD	100175.3	152206	299062	274.8	285	< LOD77.56	1151	692.88	27.1	18.99	253.8	43.6	1.7	24.3	9.38	156	
< LOD	211.6	385291.5	1470.6	743.98	778	776	54.3	< LOD	6249	208.42	20.8	7.86	69.71	27	2	< LOD	< LOD	< LOD
< LOD	< LOD	396305.3	2554.5	2023.3	957.9	991	79.8	< LOD	6466	243.96	29.7	8.79	83.53	26.9	1.03	2.43	25.1	41.5
< LOD	197	358417.5	2620.6	2192.9	896.5	2124	179	75.2	#####	1344.7	35	8.88	78.8	25.9	2.23	< LOD	71.7	50.9
< LOD	453	373014.4	2596.7	2031.4	812.2	824	66.2	< LOD	6045	250.78	19.2	7.57	60.17	19.8	2	< LOD	< LOD	< LOD
< LOD	408.8	327605	3224	2235.4	948.8	1900	134	67.41	#####	922	19.6	8.74	80.84	30.3	2	< LOD	39.5	< LOD
< LOD	315	382886.7	1875.2	1592.5	773.1	727	48.9	< LOD	2940	118.02	14.5	7.38	62.26	20.3	2	< LOD	< LOD	< LOD
< LOD	403.9	382759.5	1806.6	1008.4	799.9	720	47.2	< LOD	3040	132.23	14.5	7.54	64.82	19.2	2	< LOD	< LOD	< LOD
< LOD	< LOD	384164.6	1021.2	1228.3	749.4	696	61.7	< LOD	3097	140.94	13.9	6.96	59.23	25.1	2	< LOD	< LOD	< LOD

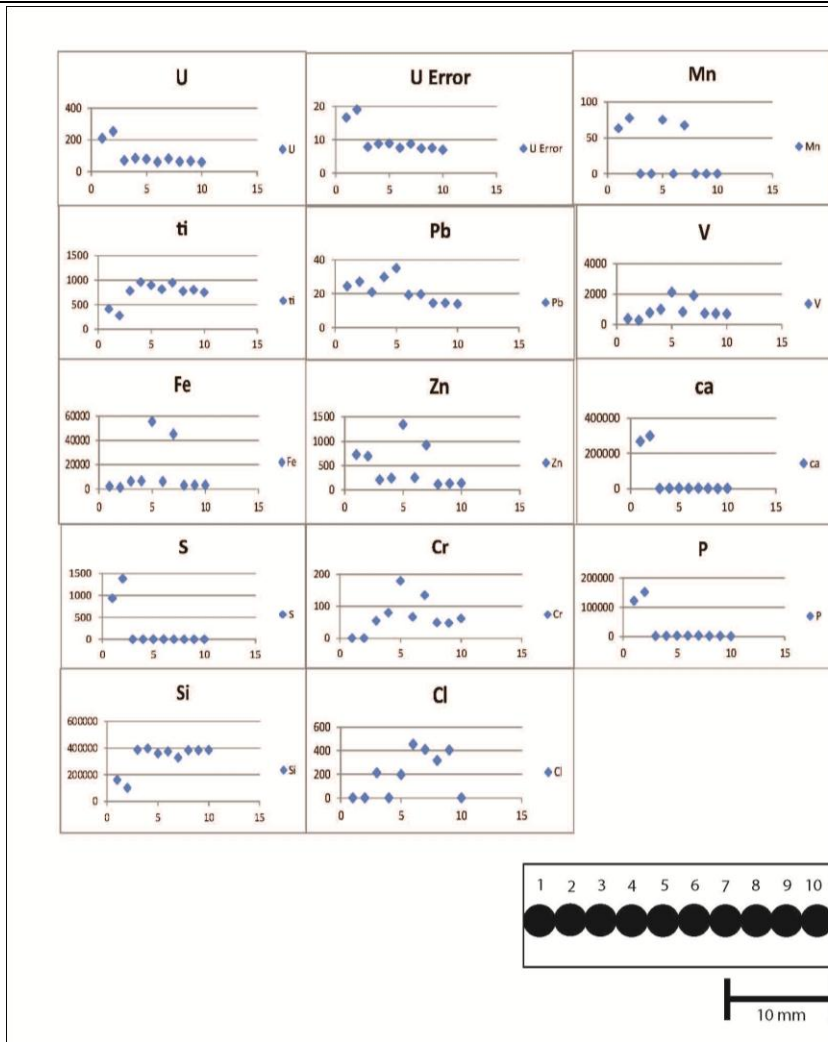


Figure C-13: Sample MS2. This was taken fifty-five feet from the dolomite ledge at the WSP. This sample has a misshaped phosphate nodule at the base of it. The nodule does not have banding, however it is highly irregular in shape and is dark in color. The rest of the rock is the host shale.

WSPR-2

S	Cl	Si	P	Ca	Ti	V	Cr	Mn	Fe	Zn	Pb	U Error	U	Zr	Nb Error	Nb	Mo	Ag
2615.1	653.96	179449.8	188255	222962	420.6	222	< LOD	< LOD	2066	56.6	< LOD	69.83	257.5	17	3.31	11.1	< LOD	< LOD
2674.8	2006.9	31656.86	267490	330059	368.1	232	< LOD	< LOD	890	40.4	< LOD	78.43	242.2	< LOD	4.44	17.3	9.14	88.2
2988.7	1754.4	88305.35	256662	318525	489.5	281	< LOD	< LOD	1030	46.3	< LOD	73.58	222.8	< LOD	5.14	23.5	8.69	128
1902.4	1979.5	70550.26	258222	323121	219.9	146	< LOD	< LOD	993	40.9	< LOD	85.34	272.2	< LOD	4.68	19.2	< LOD	< LOD
1348.6	2093.4	39186.9	264382	332732	196.8	148	115	< LOD	970	33.2	< LOD	66.47	260.3	< LOD	4.16	19.6	9.13	98.7
4370.6	735.67	187155.5	210630	201064	841.9	526	92.1	< LOD	9262	62.9	51.91	80.28	263.7	37.7	3.73	12.7	24	< LOD

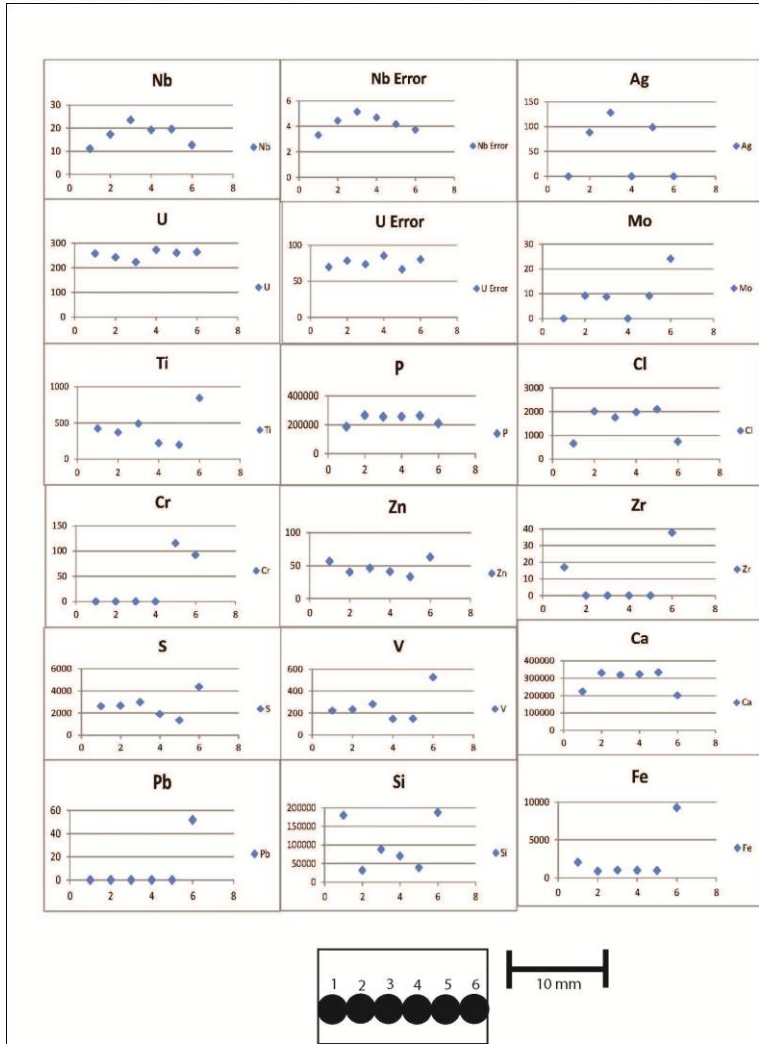


Figure C-14. Sample WSPR-2. This phosphate nodule was taken from WSP for statistical analysis. This nodule was round with concentric rings within it.

WSPR-5

S	Cl	Si	P	Ca	Ti	V	Cr	Mn	Fe	Zn	Pb	U Error	U	Zr	Nb Error	Nb	Mo	Ag
2184.7	2648.4	46058.8	285430	342765	119.3	138	< LOD<	LOD 512	622.14	< LOD 80.08	< LOD	36.3	3.49	12.3	11.7	119		
2673.3	2634.7	71722.7	281978	327346	105.2	131	< LOD<	LOD 702	1068.4	< LOD 60.47	226.92	47.7	3.79	15.4	< LOD147			
3453.3	2961.7	26996.2	285948	346401	125.8	154	< LOD<	LOD 1067	1206.5	< LOD 72.53	301.66	35.8	4.38	22.3	11.5	131		
2759.8	2691.4	79050.3	272373	316560	210.7	325	< LOD<	LOD 3565	1529.4	20.1	284.38	1074.5	66.6	7.76	41.7	< LOD162		
1710.9	541.78	91169.7	173129	236616	1070	2095	222	< LOD	#####	3287.2	46.05	299.78	1884.4	87	7.72	60.8	< LOD101	
2743	2684.4	64956.1	276140	324848	186.9	190	< LOD<	LOD 948	1434.8	15.58	176.97	918.95	59.3	5.76	36.6	< LOD98.2		
3399.6	2900.1	69566.6	277558	323205	143.8	186	< LOD<	LOD 1799	1143	< LOD 94.64	311.2	38.3	4.95	22	10.8	124		

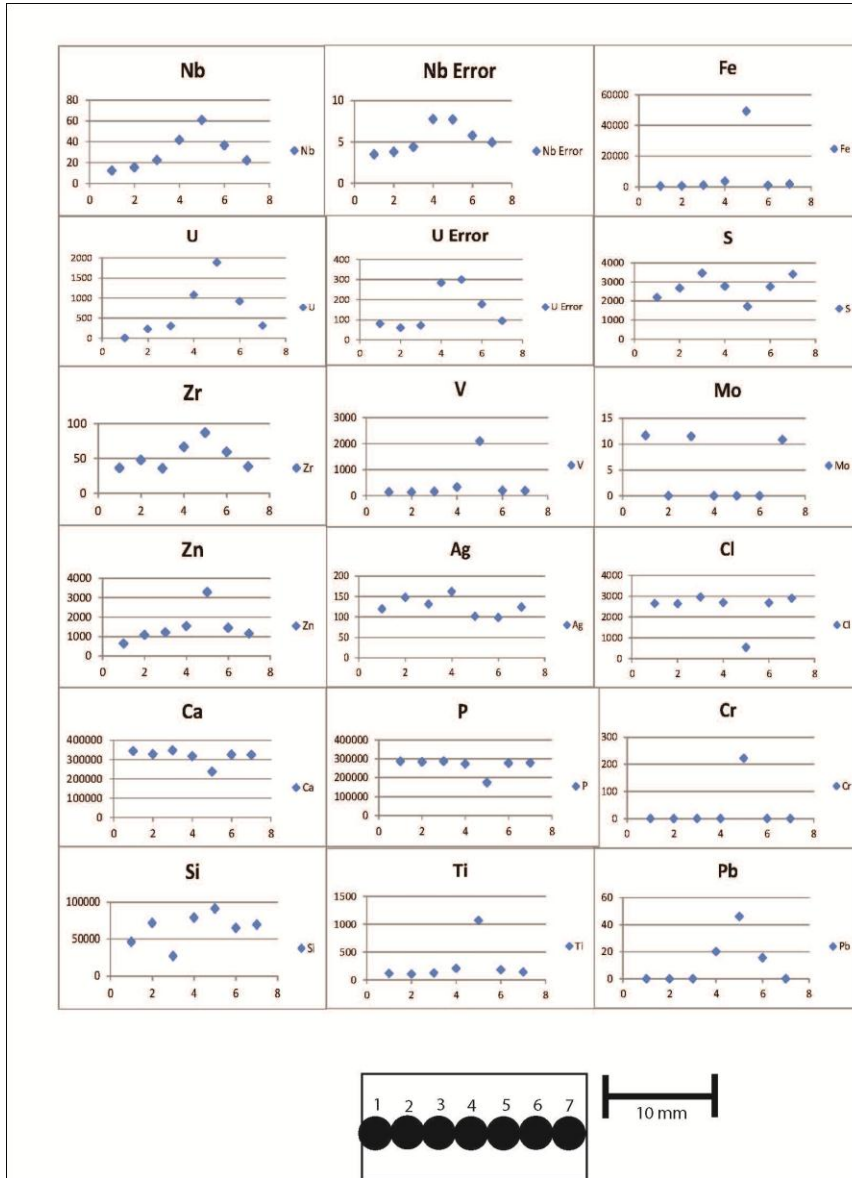


Figure C-15: Sample WSPR-5. This phosphate nodule from WSP has intense internal structure, and has an intricate mass of porosity network towards the center of it.

WSPR-6

S	Cl	Si	P	Ca	Ti	V	Cr	Mn	Fe	Zn	Pb	U Error	U	Zr	Nb Error	Nb	Mo	Ag
2609.4	< LOD	87719.38	151599	275971	125.6	111	< LOD	< LOD	707	352.2	25.1	14.95	119.3	36.5	1.52	16.5	8.33	110
803.69	< LOD	142500.3	122234	222621	53.55	82.3	< LOD	< LOD	775	279.2	19.7	12.17	40.38	18.6	1.3	3.77	5.08	113
2019.3	< LOD	126940	124789	193988	110.8	129	< LOD	< LOD	1120	174.7	23.9	13.76	117.5	23.8	1.41	9.18	4.71	59.4

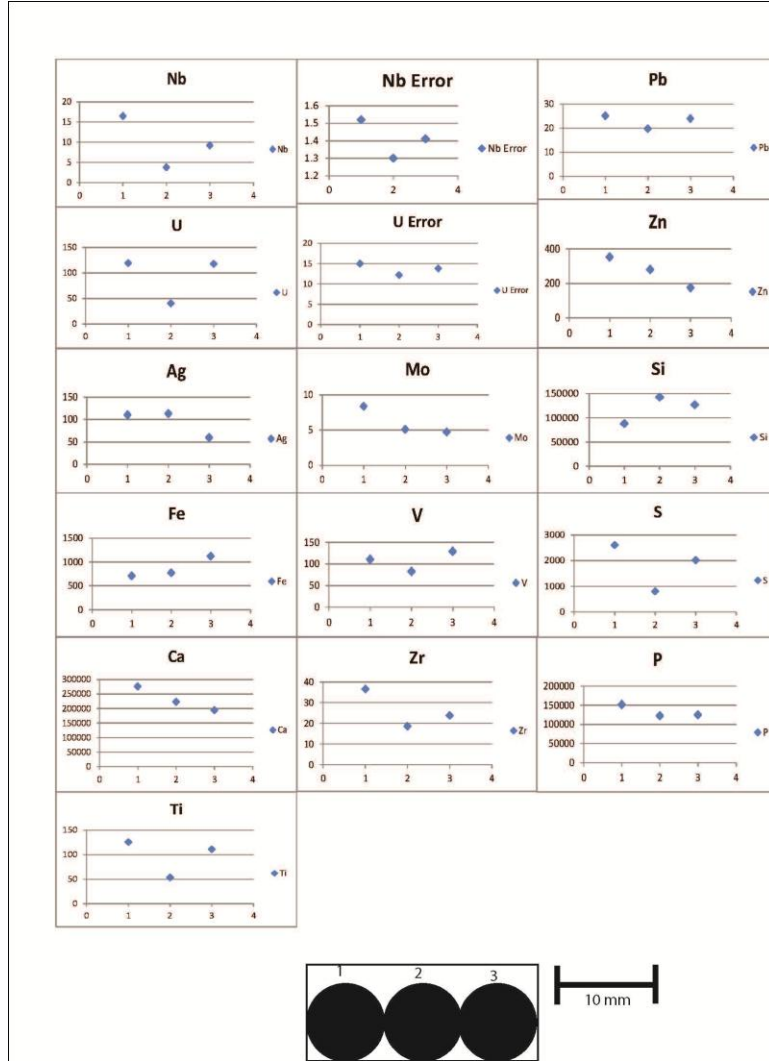


Figure C-16: Sample WSPR-6. This phosphate nodule is massive in internal structure. WSPR-6 comes from the WSP locality. The XRF diameter was increased to eight millimeters.

WSPR-7

S	Cl	Si	P	Ca	Ti	V	Cr	Mn	Fe	Zn	Pb	U Error	U	Zr	Nb Error	Nb	Mo	Ag
2324.3	2310.8	45090.41	269364	333041	128.8	193	< LOD	< LOD	2652	786.93	48.21	68.47	171.4	34.9	4.66	19.3	12.7	110
2356.6	2344.4	13095.27	271610	342040	101.5	172	90	< LOD	3182	992.8	< LOD	109.99	< LOD	37.8	4.57	17.9	16.2	107
2763.5	2249.1	14667.96	270822	338309	98.31	228	95.4	< LOD	7706	1020.2	< LOD	48.83	106.6	20.7	3.95	16.3	19.8	85.9
2119.8	1337.5	61911.36	255024	311399	198.9	227	< LOD	< LOD	7084	1179.9	< LOD	77.69	295.1	37.3	4.41	17.8	14.3	< LOD
2676.4	1412.8	192679	226282	254534	114.1	135	< LOD	< LOD	1878	584.49	< LOD	44.87	154.6	21.2	3.37	12.6	8.72	114
2605.6	2190	77095.09	270105	316763	96.58	155	86	< LOD	3803	1011.8	< LOD	60.36	231.4	33.8	3.82	15.6	10.4	119
3349.2	2538.1	6247.9	284494	348561	57.72	155	< LOD	< LOD	1150	683.06	< LOD	45.75	111	18	3.53	11.1	17.9	109
1515.5	2647.4	8265.34	279396	348897	86.1	111	< LOD	< LOD	1966	777.5	< LOD	54.93	167.1	34.7	4.05	18	12.5	141
2691.9	1993.5	155764.5	253640	262448	284.5	325	< LOD	< LOD	8364	669.61	38.63	206.04	734.6	56.2	6.03	28.3	< LOD	117

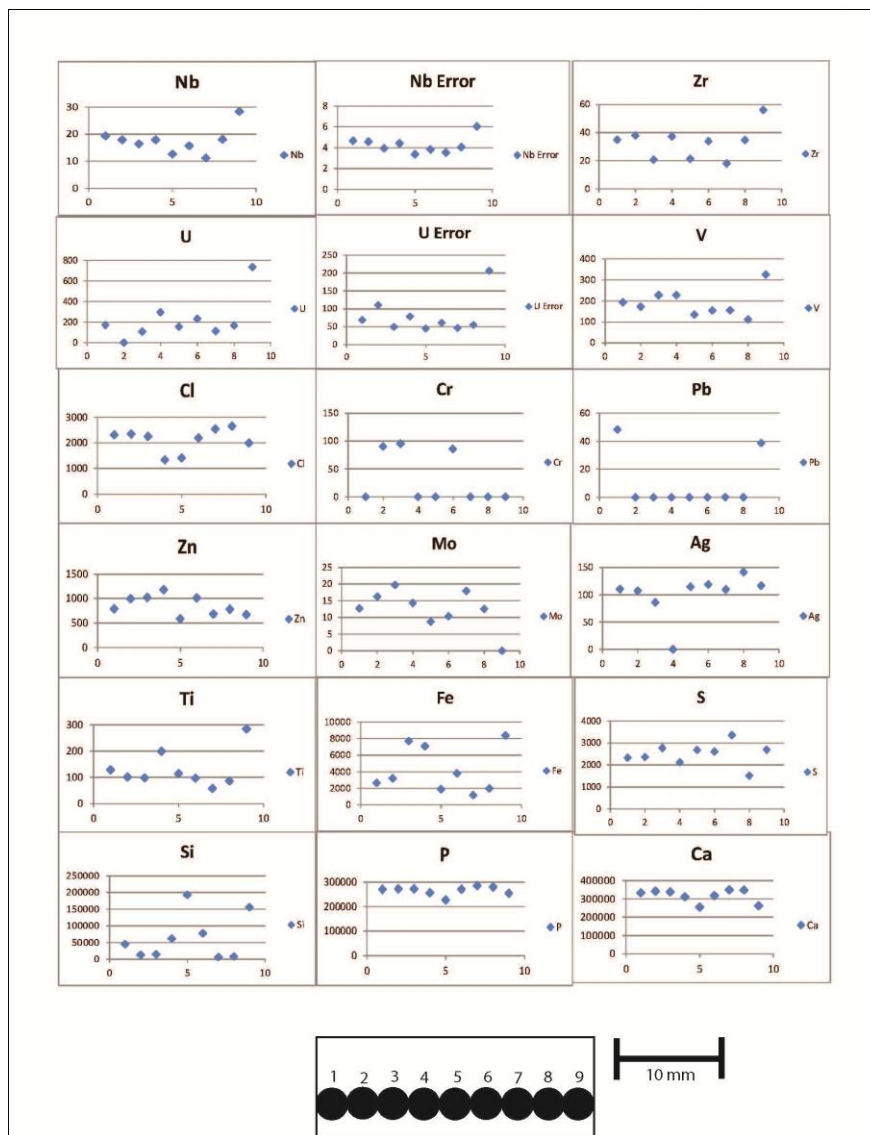


Figure C-17: Sample WSPR-7. This phosphate nodule is not perfectly circular, but still has a very well defined internal structure. This nodule has also undergone post-depositional fracturing. It comes from WSP.

WSPR-1

S	Cl	Si	P	Ca	Ti	V	Cr	Mn	Fe	Zn	Pb	U Error	U	Zr	Nb Error	Nb	Mo	Ag
2609.6	1610.2	147131.7	240311	293821	151.2	177	< LOD	< LOD	1757	826.5	22.9	82.98	283.7	38	5.11	24.4	< LOD	108
2789.4	1479.5	44620.54	244043	321869	222.9	183	< LOD	< LOD	1698	838.9	< LOD	95.97	461	35.6	4.9	27.9	< LOD	113
2771.9	2229.4	82878.4	257069	319912	238.4	270	104	< LOD	2814	988.7	16.42	108.31	387.7	34.3	4.45	18	< LOD	150
2316.4	2363.2	56788.02	265447	338764	195.5	168	< LOD	< LOD	1166	878.5	< LOD	52.22	177.5	22.8	4.23	21.2	9.37	94.1
2582.3	2114.4	57922.48	258701	338425	246.1	142	< LOD	< LOD	790	573	< LOD	50.75	173.1	29.7	3.72	14.5	< LOD	123
1684.9	1680.2	211667.6	233256	265957	161.5	126	< LOD	< LOD	911	412.6	< LOD	59.03	240.2	27	3.76	16.5	< LOD	90.2
2158.7	1636.8	188395.1	241675	269247	265.2	311	< LOD	< LOD	2425	594.6	25.16	94.28	432.4	52.8	5.35	33	< LOD	108

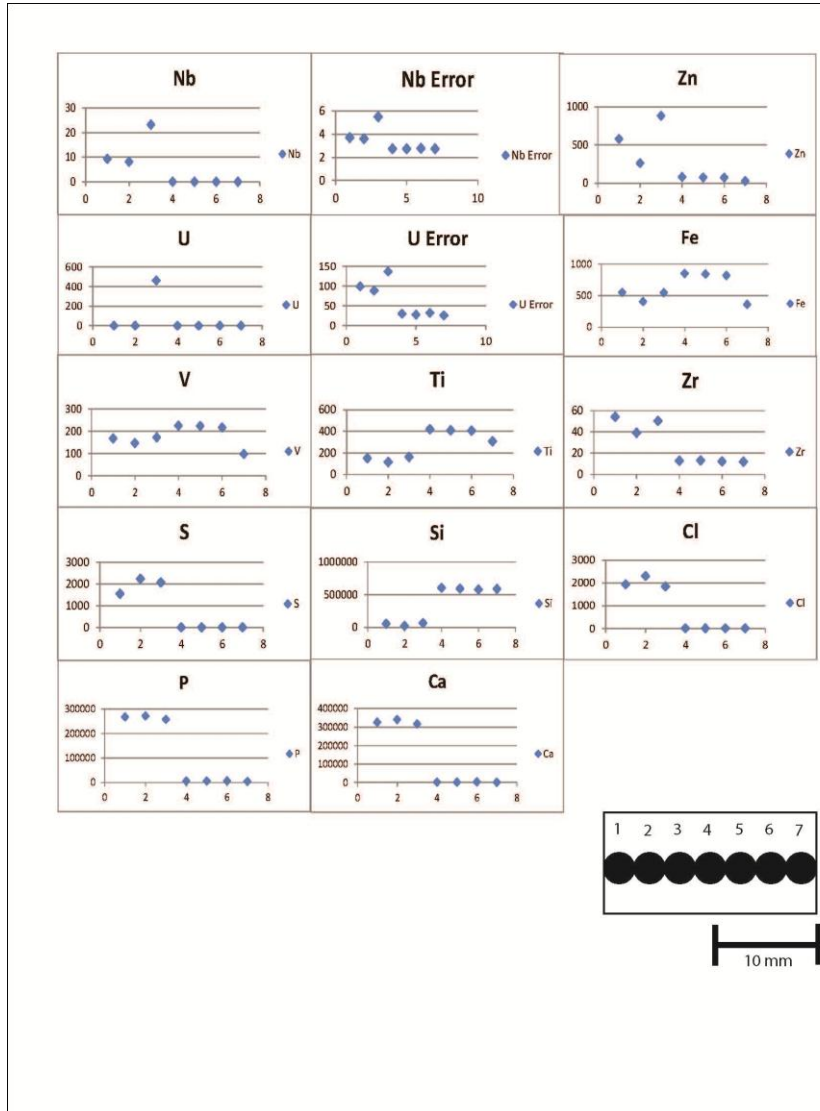


Figure C-18: Sample WSP 1. This sample was taken one foot below the dolomite bed at the WSP. This is another sample with shale attached to a nodule. Look at phosphorous for indicator of nodule.

2' Below Dolomite

S	Cl	Si	P	Ca	Ti	V	Cr	Mn	Fe	Zn	Pb	U Error	U	Zr	Nb Error	Ni	Mo	Ag
< LOD	392.74	628108.9	< LOD	2336.96	223.7	92.3	< l	< LOD	358	23.08	< LOD	23.58	< LOD	8.83	2.39	< l	< LOD	< LOD
2137.1	< LOD	636820.1	< LOD	923.78	247.8	79.04	< l	< LOD	248	15.71	< LOD	24.73	< LOD	9.31	2.37	< l	< LOD	< LOD
< LOD	< LOD	628909.3	< LOD	1039.68	374.7	176.9	< l	< LOD	384	33.32	< LOD	35.46	< LOD	9.11	2.5	< l	< LOD	< LOD
< LOD	< LOD	630314.1	< LOD	1057.98	303.3	136.5	< l	< LOD	367	29.46	< LOD	24.95	< LOD	8.93	2.41	< l	< LOD	< LOD
< LOD	< LOD	635003.5	< LOD	1095.71	254.9	84.78	< l	< LOD	269	25.88	< LOD	24.48	< LOD	13.98	2.37	< l	< LOD	< LOD
< LOD	< LOD	532808.6	50331.38	46177.51	207.6	107.4	< l	< LOD	238	81.14	< LOD	41.47	207.4	11.2	4.19	< l	< LOD	< LOD
1896.2	1120.5	250172.4	211746.2	242163.1	98.44	122.5	< l	< LOD	215	145.5	< LOD	73.94	< LOD	< LOD	3.12	7	14.77	104.4
1738.5	1128.2	312382.5	183034.4	201987.9	89.67	86.9	< l	< LOD	242	111.7	< LOD	63.59	< LOD	< LOD	5.58	< l	19.63	100.5
1231	2197.1	133955	245962	302088.5	120.3	150.2	< l	< LOD	249	125.6	< LOD	73.45	< LOD	< LOD	6.05	< l	12.95	124
1716.2	2547.9	129456	243449.4	302039.3	119.7	145.9	< l	< LOD	370	164.1	< LOD	80.58	< LOD	22.45	3.46	9	12.87	130.8
3994.9	2685.3	176033.1	230252.3	276362.5	179.1	222.5	< l	< LOD	606	214.5	22.52	62.46	152.1	23.69	3.84	#	14.67	98.78

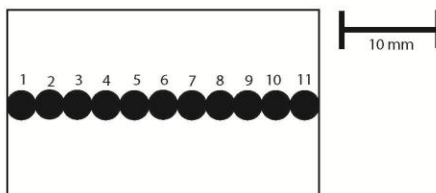
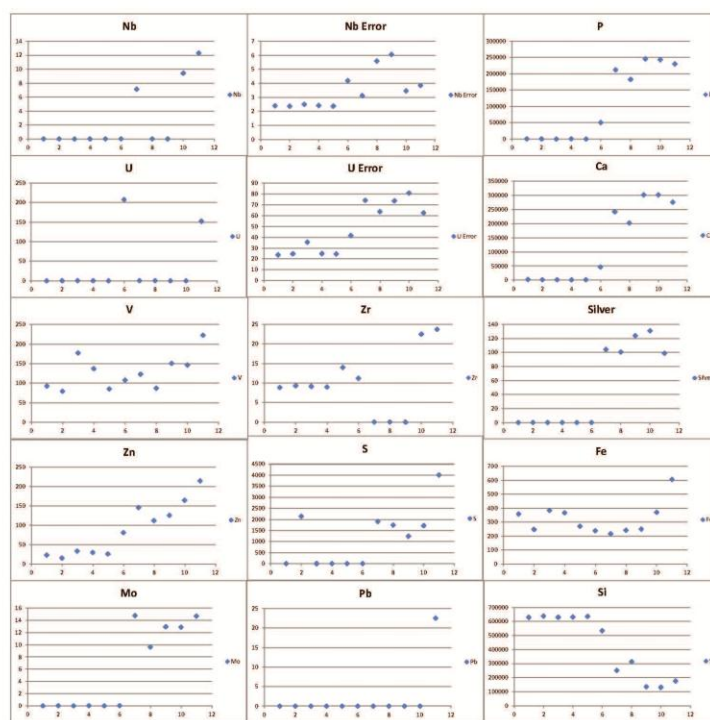


Figure C-19: Sample WSP 2. This sample was taken from two feet below the dolomite ledge in the WSP. The sample itself is host shale that is still attached to a phosphate nodule.

1' Below Dolomite

Sample	S	Cl	Si	P	Ca	Ti	V	Cr	Mn	Fe	Zn	Pb	U Error	U	Zr	Nb Error	Ni	Mo	Ag
1	1541.3	1922.4	56123.42	267182.4	325506	150.45	167	<L	<LOD	551.06	575.9	<LOD	98.96	<LOD	54.2	3.68	9	10.93	<LOD
2	2228.5	2289.9	21680.7	271203.5	340474.1	114.74	145.8	<L	<LOD	404.39	261	<LOD	88.45	<LOD	39.1	3.59	8	<LOD	<LOD
3	2064.5	1835	65619.56	257705.2	316330.1	161.37	171.6	<L	<LOD	545.27	879.2	<LOD	136.52	461.6	50.4	5.48	23	<LOD	<LOD
4	<LOD	<LOD	604167.9	5896.51	1705.88	418.5	223.9	<L	<LOD	849.55	80.32	<LOD	29.78	<LOD	12.9	2.71	<L	<LOD	<LOD
5	<LOD	<LOD	590700.3	5622.19	1894.72	407.56	223	<L	<LOD	842.26	74.19	<LOD	27.77	<LOD	13.1	2.72	<L	<LOD	<LOD
6	<LOD	<LOD	576577.4	6649.44	3263.22	404.84	215.9	<L	<LOD	819.49	72.5	<LOD	32.14	<LOD	12.3	2.76	<L	<LOD	<LOD
7	<LOD	<LOD	586941.9	4374.73	730.27	307.59	96.86	<L	<LOD	360	25.59	<LOD	25.93	<LOD	12	2.72	<L	<LOD	<LOD

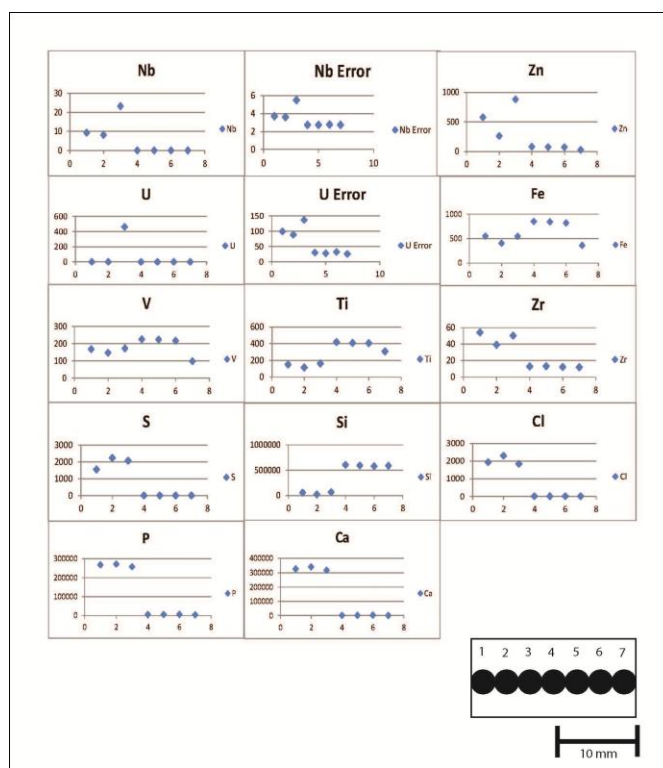


Figure C-20: Sampled from 1 foot below the dolomite bed. This is a nodule insitu with host shale.

Bed Above Dolomite

S	Cl	Si	P	Ca	Ti	V	Cr	Mn	Fe	Zn	Pb	U Error	U	Zr	Nb Error	Nb	Mo	Ag
11030.2	5669.24	335217.6	133780	168191	542.5	613	< LOD	< LOD	6315	420.4	21.84	711.31	2796.7	22.8	8.51	< LOD	< LOD	< LOD
6992.88	10169.4	286459.1	157417	208689	444.5	500	< LOD	< LOD	3953	286.6	< LOD	631.53	2433.4	33	5.02	15.4	< LOD	93.7
7051.82	10915.8	306360.3	159403	202666	590.9	634	< LOD	< LOD	4226	289.6	< LOD	549.85	2064	33.9	4.66	12.4	< LOD	< LOD
5079.32	10583.1	234106.4	209151	247809	219.2	266	< LOD	< LOD	2575	209.4	< LOD	321.88	1213.1	34.4	6.45	31.5	10.7	102
4741.29	5414.83	216738.3	216865	267658	230.5	241	< LOD	< LOD	1908	196.1	< LOD	271.38	1012.5	40	6.66	33.1	10.1	111
3502.9	4123.3	278439.4	198204	231153	271	232	< LOD	< LOD	2328	188	17.26	420.25	1543.2	38.8	5.53	22.4	< LOD	94.8
2810.29	3237.51	284618	200097	228664	281.3	363	75.4	< LOD	3009	195.7	23.35	561.34	2125.6	38.8	4.65	9.92	< LOD	< LOD
3074.17	4552.66	243766.2	217408	249400	269.9	290	< LOD	< LOD	2271	171.3	15.36	418.54	1572.8	40	7.68	39.6	< LOD	122
8077.67	5019.95	218669.1	214542	257979	275.2	248	< LOD	< LOD	2219	176.3	16.84	304.62	1157.1	48.4	7.23	37.9	< LOD	< LOD
4485.13	5114.2	242354	215161	250572	250.7	264	< LOD	< LOD	1952	160	< LOD	260.59	990.16	38.2	6.06	29.6	11.8	105
2417.75	3745.22	117396.9	224411	312517	309.8	266	< LOD	< LOD	2514	212.2	16.14	336.6	1322.6	37.2	6.73	33.3	< LOD	109
2222.6	3445.13	116183.2	226557	311947	306.5	260	< LOD	< LOD	2301	240.9	< LOD	368.03	1387.3	41	6.57	30.3	< LOD	99.6
2731.87	3745.49	145966.2	216593	305640	408	302	< LOD	< LOD	2477	237.1	21.25	366.54	1374.8	43.8	6.92	33.1	< LOD	121
4423.11	4411.48	117908.5	226753	318126	303.7	269	< LOD	< LOD	2355	244.6	16.18	360.69	1393.9	39.6	6.39	29.8	< LOD	101
3446.77	6478.08	169200.9	210238	304872	349.9	351	< LOD	< LOD	2686	278.5	17.32	369.23	1416	32.8	5.75	24.1	< LOD	117
4144.25	7814.97	206891.4	193720	291529	453.7	388	< LOD	< LOD	2599	262.2	19.41	361.23	1378.6	40.9	6.05	26.8	< LOD	103
3788.84	7056.6	161299.7	208740	297269	275.7	287	< LOD	< LOD	2398	251.2	15.61	248.37	1339	34.5	5.37	28.3	< LOD	120

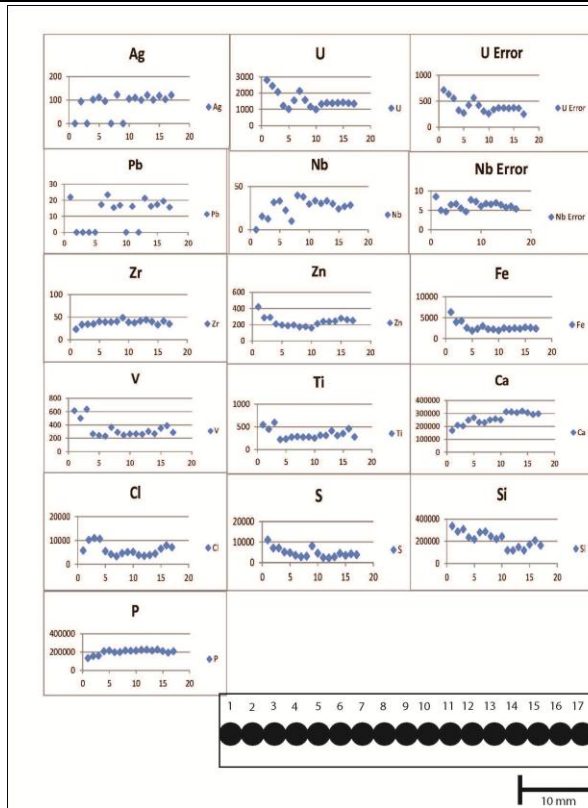


Figure C-21: Sample WSP 4. This is a laminar nodule that was found directly above the dolomite bed within the WSP.

6" Above Dolomite Bed

S	Cl	Si	P	Ca	Ti	V	Cr	Mn	Fe	Zn	Pb	U Error	U	Zr	Nb Error	Nb	Mo	Ag
< LOD	< LOD	598174.8	9270.1	1554.8	2059	1996	168	< LOD	7334	478.3	< LOD	58.54	171.21	48.5	2.98	< LOD	< LOD	< LOD
< LOD	< LOD	587395.5	11912	2699.3	1961	1930	128	< LOD	7552	495.5	< LOD	50.31	144.29	44.4	4.22	< LOD	< LOD	< LOD
< LOD	< LOD	593003.5	14942	3693.2	2019	1935	113	< LOD	6836	466.9	< LOD	48.72	135.45	40.6	4.35	< LOD	< LOD	< LOD
< LOD	< LOD	574779.4	16971	4885.2	2342	1967	116	< LOD	6171	433.4	< LOD	51.1	139.54	32.9	3.06	< LOD	< LOD	< LOD
2177	1842.9	153913.9	225666	307280	582.4	604	< LOD	199.7	2761	421.7	< LOD	425.08	1645.6	61.6	7.28	36.7	< LOD	107
2146.1	2721.2	58553.31	260284	340517	255	285	< LOD	578.9	2249	729	< LOD	409.83	1605	26.9	6.49	30.5	< LOD	157
3258.3	2961.1	44692.75	268721	348324	173	189	< LOD	216.5	1153	435.4	< LOD	247.28	946.62	35.6	8.3	46.7	< LOD	150
2631	3174.9	31407.76	273813	352946	140.5	170	< LOD	< LOD	1220	403.6	< LOD	191.71	735.19	20	6.84	36.7	< LOD	86.4
2125.2	3120.1	35840.91	271634	349227	215.6	254	< LOD	< LOD	1410	417.9	< LOD	212.46	808.51	41	5.49	24.9	10.1	102
2869.3	3404.4	27850.81	273220	348725	187.5	216	< LOD	482.6	1631	547.9	< LOD	217.01	845.92	26.9	6.98	38	< LOD	123
2410.2	2736.7	58560.86	263709	346329	190.8	200	< LOD	< LOD	974	389.7	< LOD	184.1	947.54	34.8	6.29	41	< LOD	102
2919	2037.8	115534.2	232689	322333	398.6	447	< LOD	634.7	2800	785.2	< LOD	378.18	1441.4	37.4	6.12	26.4	< LOD	< LOD

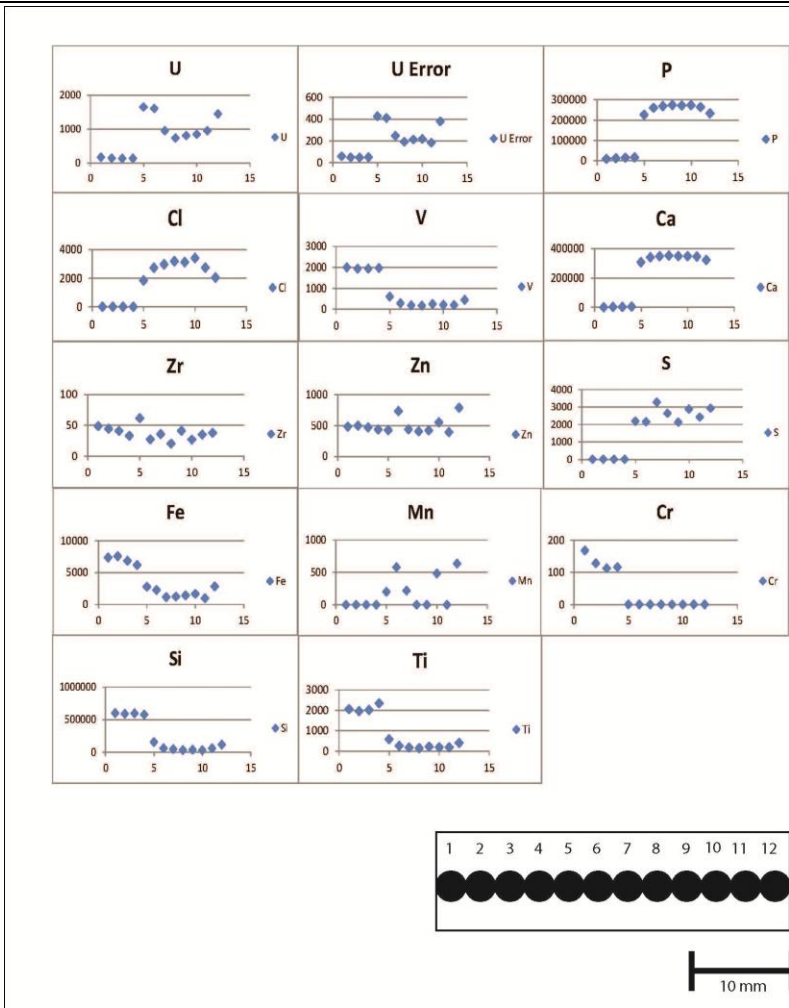


Figure C-22: Sample WSP 12. This was taken six inches from the top of the dolomite bed in the WSP. Here, there is the parent shale attached to a phosphate nodule. The readings of higher phosphorous levels graphically show where the phosphate nodule occurs in the sample. This sample is part one of two.

6" Above Dolomite Bed 1-7

S	Cl	Si	P	Ca	Ti	V	Cr	Mn	Fe	Zn	Pb	U Error	U	Zr	Nb Error	Nb	Mo	Ag
< LOD	< LOD	576796.8	9714.5	967.6	2173	2051	144	< LOD	9052	556.7	< LOD	53.43	172.7	58.6	2.87	< LOD	< LOD	< LOD
< LOD	< LOD	607489.1	7587.7	774.59	2333	2077	147	< LOD	8007	525.4	< LOD	48.92	143.1	53.9	2.96	< LOD	< LOD	< LOD
< LOD	< LOD	615538.3	7989.6	792.5	1615	1703	83.8	< LOD	5336	368.3	< LOD	46.08	128.8	40.6	2.9	< LOD	< LOD	< LOD
< LOD	< LOD	600845.5	7604.3	656.26	1945	1940	118	< LOD	6997	461.4	< LOD	47.07	132	47.8	3.41	< LOD	< LOD	< LOD
< LOD	< LOD	606682	8317.1	814.3	2044	1868	136	< LOD	6762	435.8	< LOD	53.55	154.7	45.8	3.9	< LOD	< LOD	< LOD
< LOD	< LOD	598710.9	7326.2	777.65	2034	1838	133	< LOD	6973	439.2	< LOD	49.5	144.8	51.7	4.24	< LOD	< LOD	< LOD
< LOD	< LOD	597604.9	7820.6	1111	2559	2254	164	< LOD	8131	480.7	< LOD	56.11	157	55.7	3.03	< LOD	< LOD	< LOD

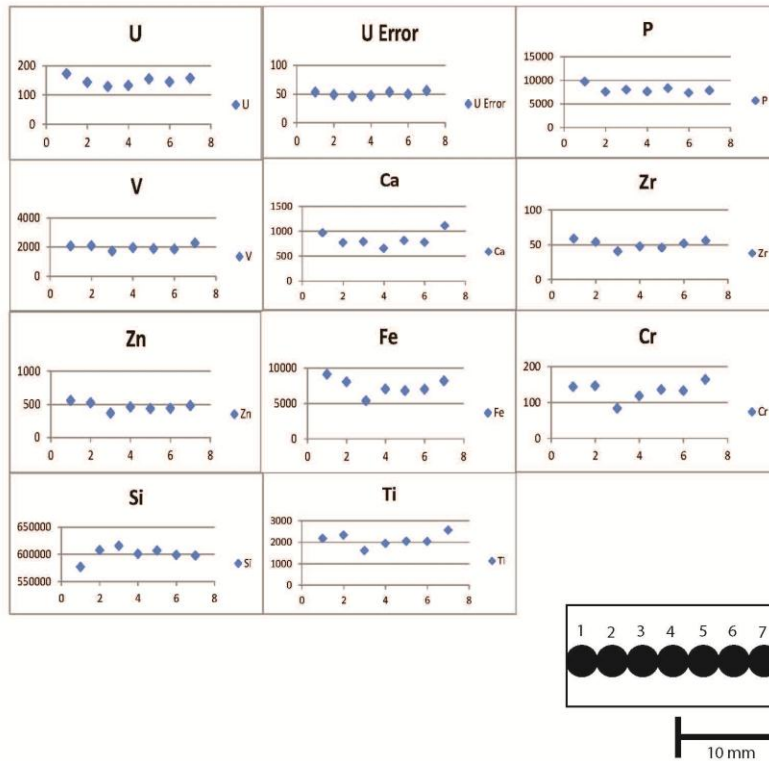


Figure C-23: Sample WSP 12. This is the same sample as Figure 34. However, the XRF measurements went across two separate directions perpendicular to each other. This figure transects across the shorter length compared to Figure 34.

VITA

Darwin Rice Boardman III

Candidate for the Degree of

Master of Science

Thesis: PRELIMINARY ANALYSIS OF PHOSPHATE NODULES IN THE WOODFORD
SHALE, LATE DEVONIAN – EARLY MISSISSIPPIAN, SOUTHERN OKLAHOMA

Major Field: Geology

Biographical:

Education:

Completed the requirements for the Master of Science in Geology at Oklahoma State University, Stillwater, Oklahoma in May, 2012.

Completed the requirements for the Bachelor of Science in Geology at Oklahoma State University, Stillwater, Oklahoma in 2009.

Experience: Summer internship and part-time geologist at EOG Resources from May, 2010 to August, 2011

Professional Memberships: American Association of Petroleum Geologists,
Geological Society of America, Oklahoma Geological Society,
Oklahoma State University Geological Society.

Name: Darwin R. Boardman III

Date of Degree: May, 2012

Institution: Oklahoma State University

Location: Stillwater, Oklahoma

Title of Study: PRELIMINARY ANALYSIS OF PHOSPHATE NODULES IN THE
WOODFORD SHALE, LATE DEVONIAN – EARLY MISSISSIPPIAN,
SOUTHERN OKLAHOMA

Pages in Study: 77

Candidate for the Degree of Master of Science

Major Field: Geology

Scope and Method of Study: Phosphate nodules from selected outcrops of the Woodford Shale in southern Oklahoma were sampled for analyses including thin section microscopy, x-ray fluorescence, x-ray diffraction and coulometric titration. Nodules were selected based on their external morphology and internal structure. In addition, host shale was analyzed to compare the composition of nodules with the encasing beds.

Findings and Conclusions: Five morphologies of phosphate nodules were categorized: Type A, circular and highly ordered; Type B, elongate with high internal structure; Type C, elongate with poorly defined internal structure; Type D, elongate with no obvious internal structure, and Type E, round with no obvious internal structure. Highly structured nodules that are laminar or circular have a higher concentration of metals with abundance increasing in darker bands. Distribution of metals is symmetrical in highly ordered nodules and predictable. Metals distribution is more random in unstructured nodules that lack symmetrical banding. TOC is reduced in phosphate-bearing shale compared to beds without nodules lower in the section. The decrease of certain metals and loss of structure in nodules is interpreted as representing less favorable conditions for phosphate growth. Radiolarians are especially well preserved in structured phosphate nodules. Geochemical signatures of phosphate nodules can be used to infer environmental conditions. Total organic carbon is lower in phosphate nodule-bearing zones compared to underlying non phosphate-nodule bearing zones. Phosphate nodules formed at the water-sediment boundary and grew faster than or equal to the sedimentation rate of the encasing shale.

ADVISER'S APPROVAL: Dr. James Puckette
